TLITI

TECHNISCHE UNIVERSITÄT MÜNCHEN

Institut für Wasserchemie und Chemische Balneologie

Lehrstuhl für Analytische Chemie

Development of Immunological Methods for the Detection of Micropollutants in Fresh Water Samples

Maria Hübner

Vollständiger Abdruck der von der Fakultät für Chemie der Technischen Universität München zur Erlangung des akademischen Grads eines

Doktors der Naturwissenschaft

genehmigten Dissertation.

Vorsitzender: Univ.-Prof. Dr. Michael Groll

Prüfer der Dissertation: 1. Univ.- Prof. Dr. Reinhard Nießner

                        2. apl. Prof. Dr. Dietmar Knopp

Die Dissertation wurde am 04.09.2015 bei der Technischen Universität München eingereicht und durch die Fakultät für Chemie am 18.11.2015 angenommen.

Acknowledgements

I want to address a special thank to Prof. Dr. Reinhard Nießner for the friendly reception at the institute and for giving me the trust necessary to accomplish my thesis.

Further, I want to thank Prof. Dr. Dietmar Knopp for his academic supervision and faithful guidance throughout my work. I appreciate his kind and patient way in leading the Bioanalytics group. Thank you for always taking time for discussion.

Warmly, I want to thank Prof. Dr. Souhir Boujday from the University Pierre et Marie Curie in Paris (France). Her input made this work more versatile in an academic and personal way, bacause I could spend several weeks in 2013 and 2014 in her laboratory in Ivry-sur-Seine. I apreciate her efforts to supervise me and my experiences in Paris very much.

I thank Joachim Langer for the analysis of water samples, Helmut Krause for the measurements of MALDI-TOF mass spectra and Christophe Méthivier for XPS measurements. I adress special thanks to Susanna Mahler for the support with LC-FLD measurements and the friendly atmosphere in the laboratory. My fellow student Maroua Ben Haddada, and Master student Verena Fink, as well as the Bachelor students Jan Berger and Alexander Urstöger for their high interest in the project and their help in the laboratory.

For proof-reading this thesis, I want to thank Verena Meyer, Maroua Ben Haddada and Prof. Dr. Souhir Boujday.

I thank all my colleagues at the IWC for their constant helpfulness. A special thanks to my collaborates in the Bioanalytic group: Anna-Catherine Neumann, Xu Wang, Dr. Susanna Oswald and Dr. Michael Pschenitza. I want to express my gratefulness towards my dear collegues Verena Meyer and Anika Wunderlich for their good mood and support during my time at the institue. At last but not at least, I want to thank my family for their absolute belief in me and my skills.

Publications

Parts of this thesis have been published in the following scientific journals:

Huebner M., Weber E., Boujday S., Niessner R., Knopp D., Rapid analysis of diclofenac in fresh water and wastewater by a monoclonal antibody-based highly sensitive ELISA. *Anal. Bioanal. Chem*. **2015**, *407*, 8873-8882.

Huebner M., Ben Haddada M., Méthivier C., Niessner R., Knopp D., Boujday S., Layer-by-layer generation of PEG-based regenerable immunosensing surfaces for small-sized analytes. *Biosens. Bioelectron.* **2015**, *67*, 334-341.

Mercier D., Ben Haddada M., **Huebner** M., Knopp D., Niessner R., Salmain M., Proust A., Boujday S., Polyoxometalate nanostructured gold surfaces for sensitive biosensing of benzo[a]pyrene. *Sens. Actuators B,* **2015**, *209,* 770-774.

"Inmitten der Schwierigkeiten liegt die Möglichkeit."

Albert Einstein

Contents

Contents

I Introduction

Many chemicals are released to the environment and are potentially toxic to the surrounding wildlife. In Europe, the water-related environmental legislation defines a growing need for regular monitoring of emerging micropollutants (EC Directive 2000/60/EC). These pollutants have different origins. For example, they are emitted by microorganisms like algae or bacteria. Pollutants from anthropogenic sources can stem from fuel combustion, pharmaceuticals in wastewater or pesticides in agricultural runoff. The challenge is to separate these pollutants at very low concentrations from complex matrices. The detection methods should be rapid, low-cost and reliable in order to handle increasing sample loads.

Immunoassays provide inherent features for such economical screening methods. They can be selective, sensitive and fast screening methods for environmental samples. These features are exploited in enzyme-linked immunosorbent assays (ELISA) on microtiter plates. Within 3 - 4 h, the determination of 24 samples is possible in triplicate including a 8-point calibration of the immunoassay. However, highly selective and highly affine antibodies have to be available. Currently, immunoassays based on monoclonal antibodies (mAbs) allow the rapid and sensitive detection of micropollutants. MAbs are developed by using the hybridoma technology. The generated hybridoma cells can be resurrected to produce the same mAbs over and over again. Subsequently, mAbs allow reproducible and robust screening methods. For this reason, mAbs against the priority pollutant diclofenac are prepared in this work. Diclofenac has recently been added to the First Watch List in the Water Framework Directive (2013/39/EU), because of its ubiquitary occurrence in fresh water all over Europe.

Moreover, a microarray-based automated flow-through ELISA with chemiluminescence detection is developed that allows the parallel detection of different micropollutants. The micropollutants diclofenac, microcystin-LR and benzo[a]pyrene are relevant analytes for the elaboration of sensitive and selective biosensor for the multiplex analysis of water samples. The selected pollutants cover a broad spectrum of molecular structures and molecular weight. On the one hand, they represent the variety of micropollutants present in surface water samples. On the other hand, they exemplify the broad applicability of immunoassays, because antibodies are available for all of these target analytes.

Considering the small molecular weight of micropollutants (100 – 1000 Da), an indirect competitive format for immunoassays and immunosensors is chosen in this work. Each

pollutant has to be immobilized on the immunoassay or immunosensor substrate. This task is challenging, because the micropollutants stem from different chemical classes and highly differ in their hydrophilicity. For each pollutant a convenient immobilization strategy must be developed. This challenge begins when the immunization with the hapten is planned: a strategy for coupling the micropollutant to a protein for immunization in mammals must be found. Usually, the hapten is coupled directly or *via* a linker to amino groups of the lysine residues of the protein. For conventional ELISA on microtiter plates, this coupling chemistry is then applied to construct a carrier protein in order to create a coating antigen. For immunosensor development, it is favorable to have amino groups available, which allow the use of the same coupling chemistry that was used for immunization.

In this work, an immunosensor surface chemistry based on amino groups is developed for the three model analytes. The immobilization steps should not require extensive synthesis of target analyte derivatives and should be easily reproducible. Finally, the robustness of this attachment and reproducibility of the sensor preparation will be crucial for the analysis of water by immunosensors. Subsequently, the sensor surface is tested regarding regeneration of the antibody binding and analyzed in detail by surface analytical methods. The developed microarray is tested concerning reproducibility of calibration experiments and recovery of the analytes in fresh water samples.

II Fundamentals

1 Micropollutants in fresh water

Industrial and natural chemical compounds contaminate freshwater systems. (Schwarzenbach, 2006) They occur in low concentrations down to a few micrograms per liter and are therefore called micropollutants. However, some of them cause toxicological problems within the water cycle at these low concentrations already. For several micropollutants, the removal efficiency in wastewater treatment plants (WWTPs) is ranging between 12.5 to 100%. (Luo, 2014) Subsequently, micropollutants usually enter the water cycle by discharges from WWTPs. To enable a sustainable water management, their emission and fate in fresh water must be monitored.

Chemical pollution of fresh water is addressed by European Union legislation in terms of the "Directive 2000/60/EC of the European Parliament and of the Council establishing a framework for the Community action in the field of water policy" which is also called the EU Water Framework Directive (WFD). It became effective at the end of the year 2000. Main objectives of this directive are the protection of fresh water and sustainability regarding water use by achieving good fresh water chemical statues in the European Union (EU). In terms of the WFD, fresh waters are rivers, lakes, costal and transitional waters. The directive deals with the selection and regulation of harmful substances with Union-wide concern in order to define the priority substances (PS) for control of fresh water pollution. The relevant PS significantly threaten the aqueous environment in the EU. Especially priority hazardous substances (PHS) should be identified whose occurrence in fresh water should be phased-out completely.

In order to define priority substances for the Annex X of the WFD, environmental quality standards were set in the Directive on Environmental Quality Standards (EQSD, Directive 2008/105/EC). This directive is also known as the Priority Substance Directive, which designated 33 compounds as PS or PHS. For example, 5 PAHs, the pesticides atrazine and diruone as well as surfactants like nonylphenol are listed as PS and possible PHS.

In the most recent Directive 2013/39/EU amending the WFD and the EQSD, it is once again stated, "causes of pollution should be identified and emissions of pollutants should be dealt with at source, in the most economically and environmentally effective manner". In the updated directive, the list of PS in Annex X has been extended to 45 substances. 20 of them are listed as PHS, which must be phased-out from discharges and alternatives for them

should be employed. This phasing-out will be problematic for some of the pollutants for which the availability of alternatives is not feasible, for examples for PAHs (see also Chapter 1.1).

The directive also expresses the challenges in the field of development of monitoring methods. The current methods are often labor-intensive and time consuming. Consequently, there is a need of developments of new monitoring strategies and analytical methods. In general, the emission controls have to be more stringent. The monitoring of EQS should be carried out using best available techniques "not entailing excessive costs".

The directive defines the quest for PS as a process that goes on by analysis and monitoring of the fresh water. Every 4 to 6 years, the Commission has to review the Annex X. Therefore, a watch list for the review of Annex X to the WFD is established. Guidelines for facilitating the monitoring in the watch list and coordination of such monitoring have to be established. On the first watch list, the pharmaceuticals diclofenac, 17-beta-estradiol and 17-alpha-ethinylestradiol are named. For these pharmaceuticals and steroid hormones, the directive defines a need for a strategic approach to monitor the pollution of water. In addition to the PS listed in the WFD, several other harmful micropollutants are emerging in fresh water. (Lou, 2014; Kunz, 2015; Petrie, 2014) Other emerging pollutants are antibiotics, β-blocker, disinfectants and industrial chemicals.

The list of more than 45 PS according the WFD comprises small molecules from anthropogenic sources. In addition, natural sources like cyanobacteria are another origin of freshwater poisoning. Cyanobacteria grow in rivers, wastewater treatment plants and oceans. In several occasions on different continents, poisonings with cyanotoxins have caused fatal causalities of humans, domestic and wild animals. (Niessner, 2010)

Regarding priority substances according to the WFD and emerging cyanotoxins, the range of harmful substances in fresh water provides a vast variety of chemical composition and structures (Figure 1). For the analysis of fresh water in this work, three prominent pollutants and toxins were chosen, which represent this variety regarding molecular weight and polarity.
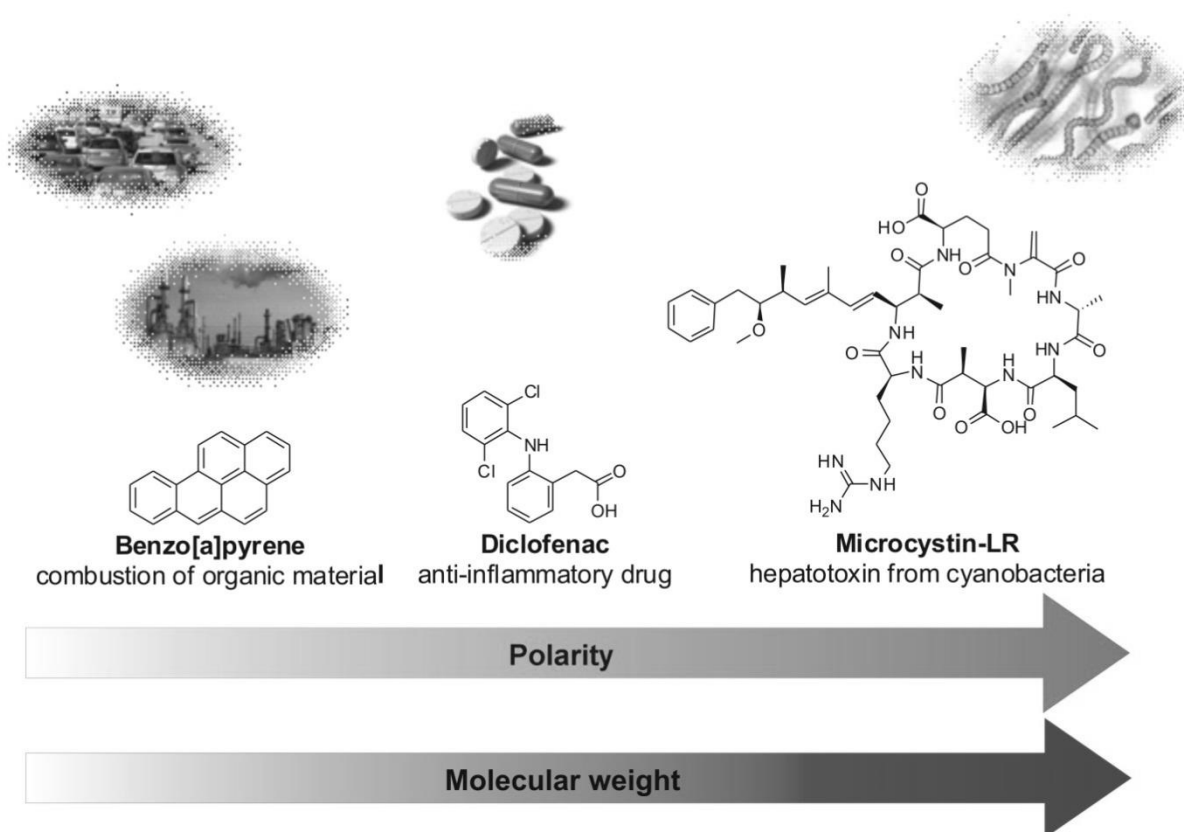
Figure 1: Selected micropollutants

1.1 Benzo[a]pyrene as an indicator for pollution by Polycyclic Aromatic Hydrocarbons (PAHs)

Polycyclic aromatic hydrocarbons (PAHs) are a huge class of compounds consisting of at least two rings of carbon and hydrogen atoms with delocalized π-systems. (Niessner, 2010; Vo-Dinh, 1998) They are formed during incomplete combustion or pyrolysis of organic matter at low temperature and lack of oxygen. PAHs are non-polar, neutral and constitute yellow or greenish crystals at room temperature. They are lipophil; accordingly, they are soluble in oil and fats, but are poorly soluble in water. They have low vapor pressures, and high melting and boiling points. (Ravirandra, 2008 a)

PAHs are ubiquitary in the environment because they stem from natural and anthropogenic sources. Examples for natural sources are smoldering fires and volcanic events. PAHs occur in structures of coal, turf or oil reservoirs bound. Anthropogenic sources are the combustions of fuels, coal and wood. In everyday life, a major source is also the use of softening agents in synthetics like shoes, tires, construction materials or paints for wood

7

preservation. (Umweltbundesamt, 2012) PAHs are released by these products and can be harmful to the user of these synthetics or surrounding biota.

The occurrence of PAHs in the environment is critical for water quality because they cause cancer. They are activated in the metabolism by oxidases to form DNA-binding diol-epoxides. (Niessner, 2010) The cancer is caused consequently at the organ exposed to the PAHs. For instance, they cause skin or lung cancer depending on the way of exposition. Some PAHs are mutagenic teratogenic and persistent. They tend to be bio-accumulative and toxic to humans and other living organisms. Consequently, they are classified as PBT substances. Like many 4 to 6 ring PAHs, benzo[a]pyrene (BaP) is highly carcinogen. Therefore, BaP is studied extensively. (Ravirandra, 2008 a) B[a]P contains 5 rings and is considered as an indicator compound for PAH pollution.

In the environment, PAHs bind to dust or soot particles and can consequently reach the atmosphere. The PBT substances travel by rain, fog or snow towards the earth's surface and settle on soil, plants or fresh water. (Ravindra, 2008 b) Due to their stability, PAHs are found in remote areas of the planet like mountain lakes, the Arctic (Ding, 2007) or the Antarctic (Piazza, 2013). Inputs to aquatic and marine environments come from urban (storm water) runoff, industrial runoff and atmospheric deposition. (Helfrich, 1986)

In Europe, the emission of PAHs from industrial facilities to the environment has to be recorded in the European Pollutant Release and Transfer Register[1]. According to this register, about 5.6 t/a PAHs were emitted into water by 43 facilities in the member states of the European Union in 2012. The majority of the emission stems from mineral oil or gas refineries (52 %) and production of pig iron or steel (23 %). Urban and industrial wastewater treatment plants released 8.7 % of the total industrial PAH emission to water.

However, the additional input of PAHs from industrial exhaust gases into fresh water cannot be determined exactly and must be estimated. The total amount of PAHs in fresh water from atmospheric deposition, runoff, industrial facilities and wastewater was calculated to be 20 t/a in 2005. (Goetz, 2009) About 75% of the PAHs in German fresh waters stem from urban surfaces, atmospheric depositions, surface run off, shipping and erosion.

---

[1] http://prtr.ec.europa.eu/PollutantReleases.aspx (02.01.2015)

In most fresh waters, PAH can be found at concentrations from 1 to 50 ng/L. (Niessner, 2010) In highly polluted samples, concentrations of up to 6 000 ng/L were measured. This high pollution by PAHs is caused by anthropogenic sources from industry, traffic and urban areas.

In the Directive 2013/39/EU amending the WFD and EQSD, 5 PAHs and Anthracene were identified as PHS. Fluoranthene and Naphtahlene were listed as priority substances. (Figure 2) Benzo[a]pyrene is regarded as an indicator substance for PAH contamination and has to be monitored.

Anthracene   Fluoranthene   Naphthalene   Benzo[g,h,i]perylene

Benzo[a]pyrene   Benzo[b]fluoranthene   Benzo[k]fluoranthene   Indeno(1,2,3- cd)-pyrene
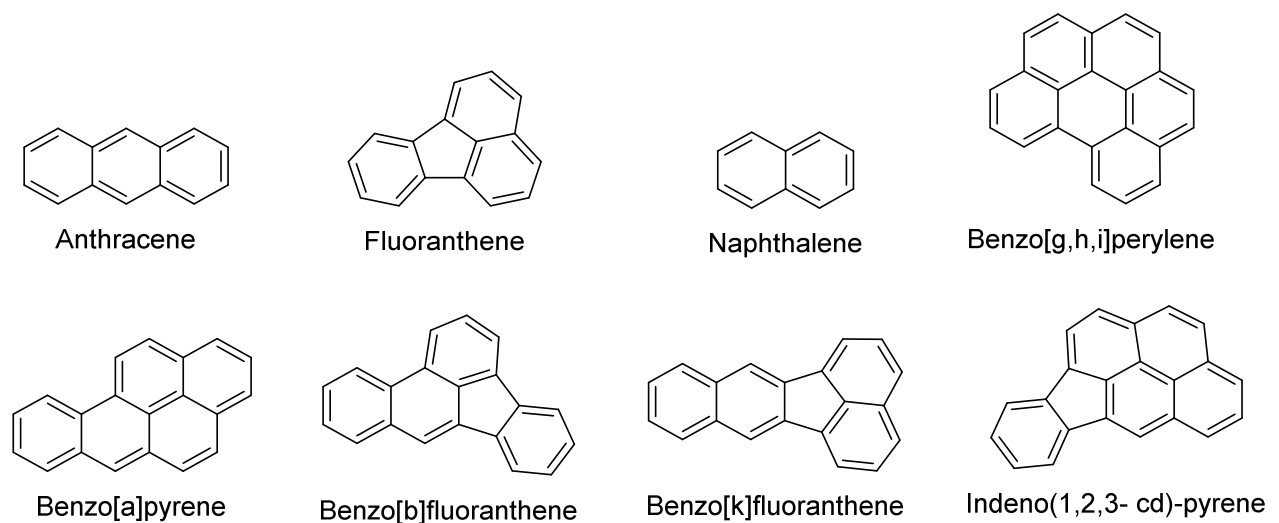
Figure 2: PAHs listed as priority substances in the Directive 2013/39/EU

High-performance liquid chromatography (HPLC) with fluorescence detectors (FLD) and gas chromatography with mass spectrometry (GC-MS) methods are usually applied for the detection of PAHs in water samples. (Barco-Bonilla, 2009; Pandey, 2003) In drinking water, the upper limit of B[a]P is 10 ng/L according to the European Drinking Water Directive (98/83/EC). In order to detect such low concentrations, enrichment of the analyte is necessary before analysis with HPHPLC-FLD or GC-MS. For example, a liquid-liquid extraction with cyclohexane can be performed. (Knopp, 2000) These validated methods can be time-consuming, labor-intensive and require advanced laboratory equipment.

In order to accelerate the PAH analysis of water samples, ELISA and immunosensors were developed. (Boujday, 2009 a; Boujday, 2010; Matschulat, 2005) Most recently, an electro-switchable biosurface was developed that allows the detection of 10 ng/L B[a]P in an assay

time below 1 h. (Lux, 2015) Consequently, the immunoassays and immunosensors are promising techniques for screening many water samples at low cost and time consumption.

1.2 Diclofenac as an example for pollution by pharmaceuticals

During the last two decades, pharmaceuticals and personal care products were found in the aquatic environment. About 100 of these substances, released through urban wastewater, are spreading in the water cycle reaching ground and drinking water (Benner, 2013; Huntscha, 2012; Kosma, 2014; Sachera, 2001; Ternes, 1998). One of the most frequently detected pharmaceutical is diclofenac (DCF), a non-steroidal anti-inflammatory drug. It is an over-the-counter drug with short dosing intervals. Therefore, DCF is consumed in large amounts and in the same time released to the aqueous environment. The EU Commission has included DCF together with 17-beta-estradiol (E2) and 17-alpha-ethinylestradiol (EE2) in the first watch list of priority hazardous substances in order to gather monitoring data (Directive 2013/39/EU). The most catastrophic observation has been reported from South Asia: the veterinary use of DCF is the main cause of population decline of three species of Gyps vultures since the mid-1990s. (Knopp, 2007; Oaks, 2004; Saini, 2012) Maybe, the diversity of raptors threatened by non-steroidal anti-inflamatory drugs misuse has to be widened to species outside the Gyps genus of vultures. (Sharma, 2014) However, animals were not exposed to water-borne DCF. Instead, they ate carcasses of domestic ungulates treated with this drug shortly before death.

DCF is detected in WWTP effluents in concentrations between 1 to 10 µg/L (Reemtsma, 2006), because the conventional activated sludge treatment allows only incomplete removal efficiencies. The concentrations in WWTP effluents seem to depend on the region. In the south, there is less DCF emitted than in the north of Europe. In WWTP effluents, concentrations as high as 0.3 µg/L in Greece (Kosma, 2014), 1.2 µg/L in Spain (Osorio, 2014), and 2.7 µg/L in Germany (Deng, 2003) and Ireland (McEneff, 2014) were detected. In fresh water, concentrations can be as high as 0.6 µg/L (Ternes, 1998; McEneff, 2014). It is subject of current research whether the DCF in fresh water affects wildlife in the aquatic environment. (Hoeger, 2005; Mehinto, 2010; Memmert, 2013; Petrie, 2014; Schwaiger, 2004; Triebskorn, 2004) Recently, the major human metabolites (Kenny, 2004; Figure 3) 4'OH-DCF, 5-OH-DCF and DCF-glucuronide (DCF-GLU) were quantified in WWTP effluents. The derivative 4'-OH-DCF is the major metabolite and can be detected in WWTP effluents in

even higher amounts than DCF itself. (Osorio, 2014) After emission to freshwater, the half-life of DCF is 8 days, because it can be degraded by photodegradation. (Bouissou-Schurtz, 2014) Consequently, DCF is not persistent, but can be regarded as a pseudo-persistent pollutant.

Currently, the first step towards the detection for monitoring DCF in WWTP effluents and fresh water is carried out by a solid phase extraction (SPE) of the substance with polymers. SPE can be coupled off-line (Gros, 2006) or on-line (Huntscha, 2012) to GC- or HPLC-MS to allow detection limits in the low ng/L-range. Mass spectrometers with high-resolution detectors allow the very sensitive and selective determination of characteristic ions. However, these coupling methods are costly, time- and labor-intensive.

For screening and monitoring measurements in-field or in small laboratories at WWTPs, immunoassays provide a suitable alternative. To monitor pollution and health issues, the number of immunosensors and immunoassays was increased for the detection of pesticides (Fang, 2011; Jiang, 2008; Xu, 2011) pharmaceuticals (Brennan, 2003; Deng, 2003; Tort, 2012) and other pollutants (Matschulat, 2005; Ramin, 2012; Zeck, 2001 a) in complex matrices like environmental, serum or food samples. Besides pesticides and other pollutants, the number of immunological assays reported for the determination of pharmaceuticals, e.g., E2 and EE2 (Kanso, 2013; Silva, 2013), carbamazepine (Farré, 2006), ibuprofen (Nagaraj, 2014), naproxen (Meulenberg, 2005), indomethacin (Li, 2009), sulphonamides (Tschmelak, 2004), caffeine, methamphetamine, benzoylecgonine, tetrahydrocannabinol (Smith, 2010) and cetirizine, (Bahlmann, 2012) in water samples increased steadily during the last years. These immunochemical techniques take advantage of the highly selective binding by antibodies. They allow detection limits down to the µg/L- to ng/L-range without sophisticated instrumentation needed. There exist various formats (Knopp, 2006) like test-strips (Gui, 2008; Xu, 2012), particle-based (Wang, 2014) or automated flow-through assays (Oswald, 2013). In microtiter plates, the so-called enzyme-linked immunosorbent assay (ELISA) is performed in parallel for several samples within a few hours time. For small analytes, the indirect competitive format is favorable, because these haptens have only one site for antibody binding.

For DCF, an ELISA based on polyclonal anti-DCF serum allows the detection of DCF in the low ng/L-range. (Deng, 2003) This antiserum is highly sensitive and specific. However, it is limited in quantity. Monoclonal anti-DCF antibodies (mAbs) can be produced by hybridoma

technology (Koehler, 1975). The antibody producing B-cell clone can be stored under liquid nitrogen and can be resurrected for antibody production. This means, that identical antibodies from one type of B-cell clone would be available for future applications in analytical laboratories (see also Chapter 2).
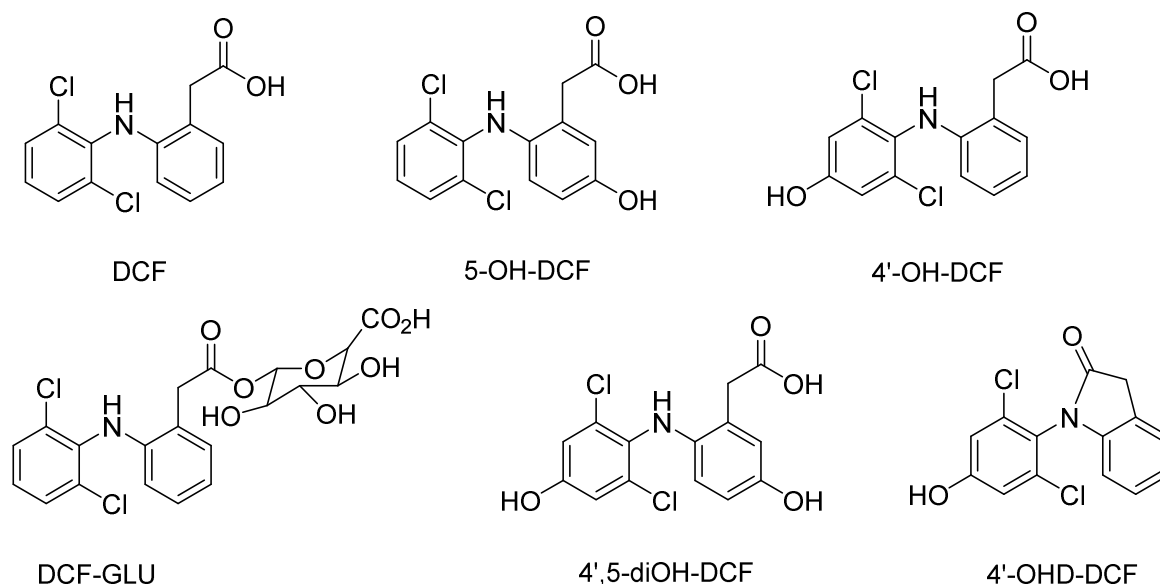
Figure 3: DCF and its major human metabolites that can be found in wastewater samples (Osorio, 2014)

1.3 Microcystin-LR: a cyanobacteria-born toxin

Cyanobacteria are bacteria that grow in the phytoplankton of fresh water. Stagnant or slowly running fresh water is rich of phytoplankton, which generates its biomass by photosynthesis. Cyanobacteria have no cell nucleus like bacteria, but are able to carry out photosynthesis and are also called blue algae. (Niessner, 2010) They use nutrients like atmospheric nitrogen, phosphor and trace metals. (Paerl, 2013) Therefore, they can live in diverse terrestrial and aquatic environments like alpine lakes and costal oceans. They are able to exploit anthropogenic influences like nutrient over-enrichment, fertilizers, air pollution and hydrologic alterations to ecosystems like water diversions, withdrawal or salinization. For example, wastewater causes eutrophication of fresh water. (Niessner, 2010; Shi, 2013) It is usually highly loaded with phosphates and nitrogen from feces, urine and washing agents. Consequently, wastewater treatment plants can be point sources of nutrition for cyanobacteria. They usually work by mechanic-biological cleaning of water and the nutrient phosphate is not removed from the wastewater. The detention capacity for phosphates could be implemented by soil filters. In practice, however, these filters are rarely used. Moreover, sunlight can stimulate the growth of cyanobacteria. (Pearl, 2013) So

12

cyanobacterial blooms occur predominantly in summer time. Some cyanobacteria have optimal growth rates at relatively high temperatures. Consequently, global warming promotes their growth, too.

The presence of algal blooms can be determined visually by loss of water clarity and green or brown algae islands in fresh water. (Pearl, 2013) Since they contain cyanobacteria, they negatively affect water quality and attack biota in aqueous environment. Dying blooms are decomposed by bacteria, which causes oxygen depletion and can lead to fish kills. Moreover, toxic secondary metabolites are released which can cause serious and acute intoxication of mammals by emission of a variety of bioactive or toxic substances. Not all of these bioactive substances were identified. (Niessner, 2010) They provide a huge diversity of oligopeptides, alkaloids, organophosphates or liposaccharides with toxic effects. Saxitoxin, anatoxin-a, microcystin-LR and nodularin are the most potent ones. Microcystins and nodularins inhibit protein phosphatase 1 and 2A in the liver. Consequently, the liver tissue is destroyed and inner bleedings can cause death. Nodularin is carcinogenic and microcystin-LR is classified as possibly carcinogenic to humans.

The molecular structure of microcystin-LR (MC-LR) is shown in Figure 4. It is a cyclic heptapeptide carrying 7 characteristic residues. Residues 2 and 4 are variable L-amino acids for microcystins. (Zeck, 2001a) Residue 5 is characteristic for microcystins and nodularins. It is the unusual C20 amino acid [(2S,3S,8S,9S)-3-amino-9-methoxy-2,6,8-trimethyl-10-phenyldeca-4,6-4,6E-dienoic acid] abbreviated as ADDA. It has a long hydrophobic side chain, with a phenyl group at the end.
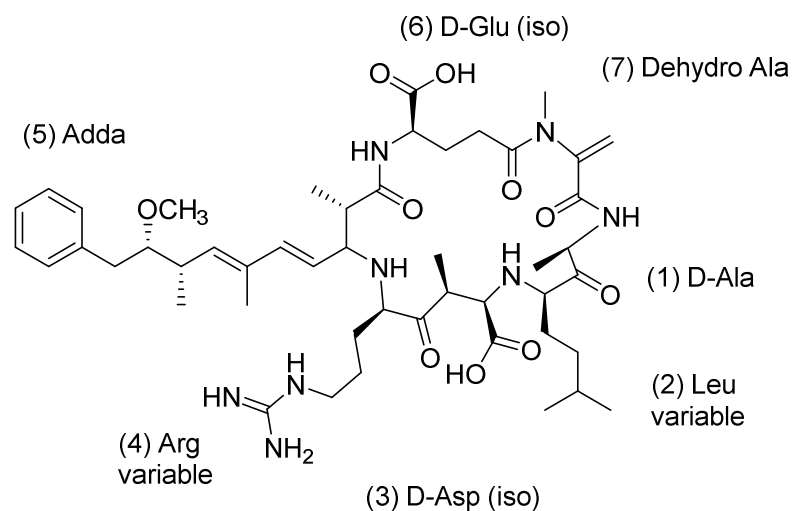
Figure 4: Microcystin-LR (MC-LR)

Microcystins are produced by different kinds of cyanobacteria like Microcystis, Planktothrix, Oscillatoria, Anabaena and Nostoc. (Zeck, 2001b) Microcystis and Planktothrix are the most frequent cyanobacteria in Germany. Microcystins are produced within the cells and are released during cell dieback and lysis into the surrounding water. (Niessner, 2010) Microcystins are degraded primarily by microbial activity and to a less extent by photochemical oxidation. Concentrations are at the highest where a high load cell material is present. In these so-called blossoms, the cell density and toxin concentration is thousand times higher than in the open water. Swallowing of such material can cause death as it has happened for animals like dogs or wild animal. Microcystins are constitutive components of cyanobacteria cells and are only poorly susceptible by environmental factors. Acute danger can arise from dense cell suspensions in fresh water. In drinking water, the guide value was set to 1 µg/L by the WHO regarding effects of chronic toxicity by MC-LR. Bathing should be restricted at a MC-LR concentration of 50 µg/L according to the WHO. In fresh water, cyanobacteria are usually monitored by microscopic investigations. To identify symptoms and to quantify toxicity effects, invertebrate bioassays in mice or rats are used. Moreover, microcystins and norularin can be detected by freshly isolated hepatocytes from rat. Biochemical methods like ELISA convince with their sensitivities that go down to the ng/L-range. In general, they lack specificity because similar structures to MC-LR are detected with high cross-reactivity. Protein phosphatase inhibition assays can reach similar sensitivities like ELISA and are in good agreement with liquid chromatography (LC) based methods.

Next to ELISA, the most frequently used analytical technique to measure cyanobacterial toxins is SPE combined with HPLC and UV detection. The detector is a photodiode array detector for UV detection at 238 nm corresponding to the maximum absorption for most microcystins. The threshold value of MC-LR by the WHO can be monitored by a standardized HPLC-UV method described in ISO 20179:2005. Normally, a gradient of acetonitrile in water is used to separate microcystins regarding their polarity. For the development of analytical methods, 6 out of over 60 microcystins are commercially available as standard solutions. These 6 microcystins can be quantified exactly. However, a co-elution of different microcystins is always possible. Furthermore, matrix interferences are frequent in the respective UV range. (Weller, 2013) Consequently, an overestimation of the toxic MC-LR of about 30% is possible.

LC coupled to mass spectrometry (MS) detectors is usually a very powerful method for environmental analysis. High-resolution MS allows more reliable identification of toxins. However, the variety of cyanotoxins is huge and many of them remain unknown. (Weller, 2013) Retention times and molecular masses or transitions of all potential toxins are not assignable.

In addition to the undefined number of chemical species, the variability of toxicity is causing difficulties for detecting and quantifying cyanotoxin in environmental samples. Effect-directed analysis should be used to avoid misleading conclusion results. One concept is the combination of chromatography with postcolumn antibody- and enzyme-based inhibition assays. (Zeck, 2001c)

However, in severe cases of toxin emission detection of cyanobacterial toxins must be quick. Moreover, there is a need to screen many samples to monitor toxin occurrence in fresh water, which is time dependent. For these fast and high-throughput screening measurements, immunoassays and biosensors are suitable. (Weller, 2013)

Immunoassay performance is highly dependent on the availability and on the quality of the antibody. Accordingly, mAbs are preferred for immunoassay development (see also Chapter 2). For the detection of MC-LR, several mAbs with high affinity and specificity towards different binding sites exist. For example, a mAb based on clone M8H5 shows broad cross-reactivity. Subsequently, it allows semi-quantitative detection of most microcystins. (Weller, 2001) The mAb from clone AD4G2 recognizes the rare amino acid ADDA. (Zeck,

2001b) It shows similar cross-reactivity for tested microcystins and allows the determination of a sum value. Another mAb based on clone MC10E7 recognizes all microcystins containing arginine (R) at position 4. (Zeck, 2001a) The most frequently occurring microcystins of this kind are MC-LR and MC-RR. Commercial immunoassays based on mAbs allow LODs of 0.1 µg/L for MC-LR.

Immunosensors are incorporating antibodies for automated detection of MC-LR. In 2013, an automated online biosensing system for the detection of MC-LR was published. (Shi, 2013) It is called automated online optical biosensing system (AOBS) with a LOD at 0.09 µg/L. During 1 year, between June 2011 and May 2012, it was used to measure MC-LR in Lake Tai which is one of the largest freshwater lakes in China. It was shown that MC-LR concentrations were the highest between August and October 2011. This observation corresponds to the light dependent photosynthesis and the warm water that should be present at that time of the year. These conditions are supporting the growth of cyanobacteria.

For the multiplex analysis of MC-LR next to Staphylococcal Enterotoxin enterotoxin B (SEB), a biosensor was reported which is based on a capillary ELISA technique in combination with a miniaturized fluidic system. (Lindner, 2009) Chemiluminescence was used for detection. Measurement time was 18 min and the LOD was 0.2 µg/L. A fiber-optic biosensor for multianalyte detection was reported for multiple analytes like MC-LR and TNT. (Long, 2010)

2 Immunoassays for the analysis of water samples

Micropollutants can be quickly and sensitively detected by immunoanalytical techniques. These methods are highly dependent on the prepared antibodies. In this chapter, the basic principles about antibodies, their preparation and immunoassays are presented.

2.1 Antibodies

In vertebrates, an adaptive immune system evolves steadily while they are exposed to a huge variety of viruses and bacteria. This immune system expresses more than 108 different antibodies, which recognize the specific structures of extrinsic organisms. (Berg, 2010) In this way, antibodies recognize pathogens and neutralize toxins in blood sera. (Renneberg, 2009)

A compound that induces the production of antibodies is called immunogen. An immunogen possesses antibody binding sites which are described as antigens. The recognition of antigens by antibodies is crucial in the evolution of the adaptive immune system. However,

16

II Fundamentals

not all antigens are immunogenic. Low molecular weight compounds (MW < 5000 Da) are not immunogenic, but they can be recognized as antigens. (Cammann, 2000) These small molecules are called haptens. For the generation of anti-hapten antibodies, conjugates with carrier proteins like albumin or thyreoglobulins are prepared. The binding site for antibodies on antigens is called epitope. The binding site on antibodies recognizing the epitope is called paratope.

Antibodies are immune globulins (Ig). The most abundant antibody in blood serum is the IgG, which is built up by 3 different fragments (Figure 5). These fragments are connected by disulfide bridges, which are cleaved by proteolytic activity of papain. The molecular weight of the resulting fragments is 50 kDa. Two of them are called F_{ab} fragments, because they carry antigen binding sites. The third fragment is an F_c fragment, because it readily crystallizes. The F_c terminus has an effect or function. For IgG, it induces a complement cascade that will end with the lysis of the target cells.

A whole IgG molecule has a molecular weight of about 150 kDa. It is built up from 2 different polypeptide chains: one light chain (L-chain, 25 kDa) and one heavy chain (H-chain, 50 kDa). These subunits are combined to a L2H2 structure by disulfide bridges. The overall conformation of an IgG molecule is described as a Y-shap. The F_c fragment is the root and the F_{ab} fragments are the arms of the letter Y. The center of the Y is built by a stretched part of the H-chains, so this so-called hinge region is flexible. Subsequently, the epitopes of the target structure do not have to be at fixed distance.

In blood sera, other Ig classes next to IgG occur. The heavy chains of IgG are named γ. The heavy chains of classes Ig A, M, D and E are α, μ, δ and ε. The light chains are either κ or λ for all Ig classes. The IgG, IgM, IgA, IgD and IgE classes differ in their heavy chain structure. Subsequently, they differ in their effect or functions.

The different IgG antibodies from one species are very similar. Each L- and H- chain carries a domain that is very different for different antibodies (V_H and V_L). These variable domains build up the paratopes of the antibody. In these chains, there are sections of 7 to 12 amino acids, which are hypervariable. The remaining domains are very similar for antibodies with different paratopes and are called constant regions (C_L1, C_H1, C_H2, C_H3).
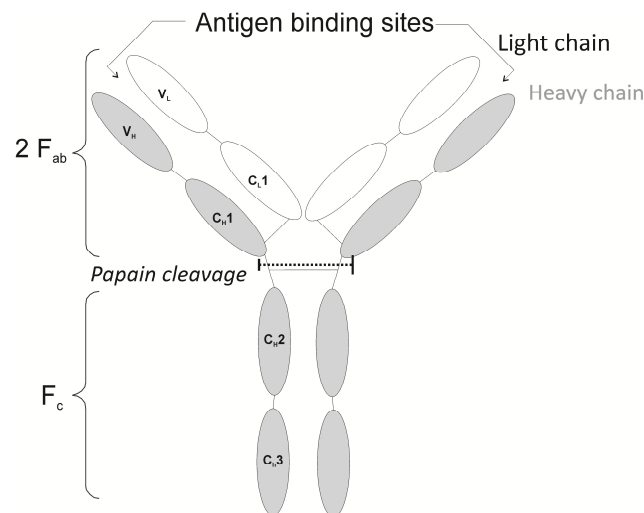
Figure 5: Schematic drawing of an IgG

2.2 Preparation of monoclonal and polyclonal antibodies

The first step of antibody generation is the immunization of a vertebrate (Figure 6). The antigen has to be chosen regarding the target analyte:

− for protein antigens, the antigen can be used directly,

− for toxins and microorganisms, inactivated derivatives of the target structure are used,

− for haptens, conjugates with carrier proteins are used.

For the hapten-carrier conjugation, different coupling strategies can be used. The carrier proteins like albumin have carboxy, carbonyl, amino or thiol groups to react with the low molecular weight compound of interest.

The antigen for immunization is presented in combination with an adjuvant. (Cammann, 2000) The adjuvant activates the immune system and allows improved antigen presentation. Freund's adjuvant is often used for this purpose in multiple immunizations. For the first immunization, complete Freund's adjuvant is injected. It contains the immunogen in a water-in-oil emulsion, as well as heat inactivated *Mycobacterium tuberculosum*. The microbial structures are amplifying the primary immune response. The second immunization is also called boost injection. For the repeated immunization, incomplete Freund's adjuvant is prepared without the microbial adjuvant. During the immunization phase, the titer of antibodies is regularly measured to identify immune animals regarding the target antigen.

From the immune animals, either polyclonal or monoclonal antibodies can be isolated. Polyclonal antibodies are in the serum of the blood. The antiserum can be obtained directly after the immunization phase. A long term immunization allows the highest affinity towards the antigen. For analytical chemistry applications, however, a polyclonal antiserum is often disadvantageous. Its quantity is limited to some mL, the yield, specificity and affinity can vary for different serum samples.

Figure 6: Preparation of antibodies

Polyclonal antibodies (pAb) are called polyclonal because they stem from different lymphocytes. Monoclonal antibodies (mAbs) can be prepared by isolating and cloning these lymphocytes according to the hybridoma technology developed by Koehler and Milstein in 1984. Subsequently, this method is more cost- and labor-intensive than the preparation of polyclonal antibodies. Nevertheless, it enables the preparation of mAbs for specific detection of single analytes in unlimited amounts of constant quality.

For the hybridoma technology, usually mice are immunized. After repeated immunization, the lymphocytes are isolated from the spleen of the mouse. In the cell fusion step, the lymphocytes are merged with lymphocyte cancer cells, which are also called myeloma cells.

The cell culture supernatants of the hybridoma cells are screened in indirect ELISAs regarding their binding towards the target antigen.

2.3 Characterization of monoclonal antibodies

The binding of antigens to antibodies is driven by non-covalent interaction forces. Dispersion forces, electrostatic interactions, hydrophobic interactions and hydrogen bond formations contribute to the assembly of an immune complex. The stability of the complex is influenced by the pH value, ionic strength and organic solvents. The immune complex formation is an equilibrium reaction and described by the Law of Mass Action (Equations 1 to 3):

$$Ab + Ag \underset{k_d}{\overset{k_a}{\rightleftharpoons}} AbAg$$
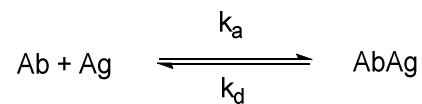
$$K_A = \frac{[AgAb]}{[Ag][Ab]} \qquad \text{(Equation 1)}$$

$$k_a[Ag][Ab] = k_d[AgAb] \qquad \text{(Equation 2)}$$

$$\Rightarrow K_A = \frac{k_a}{k_b} \qquad \text{(Equation 3)}$$

The equilibrium is time dependent and so, the incubation time plays a role for the immune complex formation. The affinity constant K_A for this equilibrium describes the strength of the binding between a paratope and an epitope. The affinity constant can be determined for monoclonal antibodies only where the concentration of binding antibody can be stated. For mAbs, K_A is in the range between 10^4 and 10^{12} [L/mol]. (Renneberg, 2009) It is usually determined in surface plasmon resonance (SPR) experiments based on an experimental setup as shown in Figure 7. In SPR experiments, the rate constants can be determined. The SPR sensors allow the observation of interaction between the immobilized molecule (ligand) and the binding partner (analyte) in real time and without labeling by measuring changes in refractive index (RI) close to the sensor surface. (Frostell, 2013) A commercial instrument for SPR measurements is the Biacore^{TM} by GE Healthcare, which was available for this work. For these experiments, the molecular mass of the mAb is determined by matrix-assisted laser desorption time of flight mass-spectrometry (MALDI-TOF-MS).
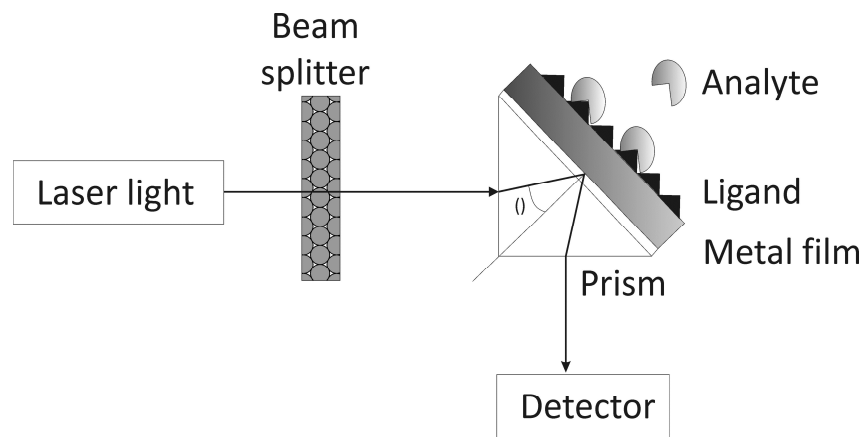
Figure 7: SPR setup

2.4 Competitive ELISA

The simplest immunochemical reaction is a precipitation test. (Cammann, 2000) The formation of an antigen-antibody network can be visually observed during the formation of an insoluble immune complex. However, this simple test is limited to antigens with several epitopes.

For low molecular weight compounds, the formation of the immune complex must be displayed by additional reactions. For this purpose, labels are used which evoke a signal depending on the analyte concentration. These labels can be fluorescent, radioactive, electrochemically or enzymatically active. Currently, the enzyme immunoassays (EIAs) have the highest impact in modern immunochemical analysis. They allow high conversion rates for indicator substances. Subsequently, high assay sensitivities and low limits of detection (LOD) are achieved by EIAs.

EIAs can be designed as heterogeneous or homogeneous immunoassays. In homogeneous immunoassays (HEIAs), the immune complex formation influences the substrate conversion directly. Washing steps, separation steps and a solid phase are not necessary. For example, an HEIA kit for the detection of synthetic cannabinoids in urine does not require sample pretreatment, has a high throughput and acceptable sensitivity for semi-quantitative analysis. (Barnes, 2014)

Heterogeneous immunoassays can be used, if no direct influence of the present immune complex on the test system can be observed. For heterogeneous enzyme immunoassays, the antigen or antibody is immobilized on a solid phase. Consequently, they are described as enzyme-linked immunosorbent assays (ELISAs). In general, they show higher assay sensitivity

than HEIA. The immobilization is usually performed on microtiter plates (MTP) with 96 wells. The MTP is made from polystyrene or polyvinyl for adsorption of protein. ELISAs require washing and separation steps to remove excess of enzyme conjugate.

From the immunological point of view, micropollutants in water samples are haptens (< 1000 Da). Subsequently, they have only one epitope for antibody binding. For their quantification, competitive ELISAs can be developed. This assay format allows high sample throughput and calibration in parallel. Specific antibodies are not labeled, so they maintain their full functionality.

For a direct competitive ELISA (Zeck, 2001a), the antibodies are captured on a MTP by antibodies against the F_c-region of the specific antibodies. These anti-Fc mAbs are coated on the MTP, then the anti-analyte mAb is captured and the analyte from the solution can be bound in the incubation step. Then, enzyme-labeled analyte is added to occupy free antibody binding sites. After addition of a substrate, the MTP is sent for photometric evaluation.

For an indirect competitive ELISA (Figure 8), the antigen is coupled to a protein which is not the same protein used for immunization. The antigen-protein conjugate is adsorbed on the MTP in a coating step. The free binding sites on the MTP are blocked, for example by casein. During the competition step, the sample and the antibody solution are added to the wells. The antibody binds either to the molecules in the sample or to the immobilized antigens. The bound antibody is labeled by a secondary antibody conjugated with an enzyme. After the substrate reaction, the MTP is sent to photometric evaluation. The secondary antibodies labeled with peroxidase are commercially available. Moreover, a low amount of antibody is needed.
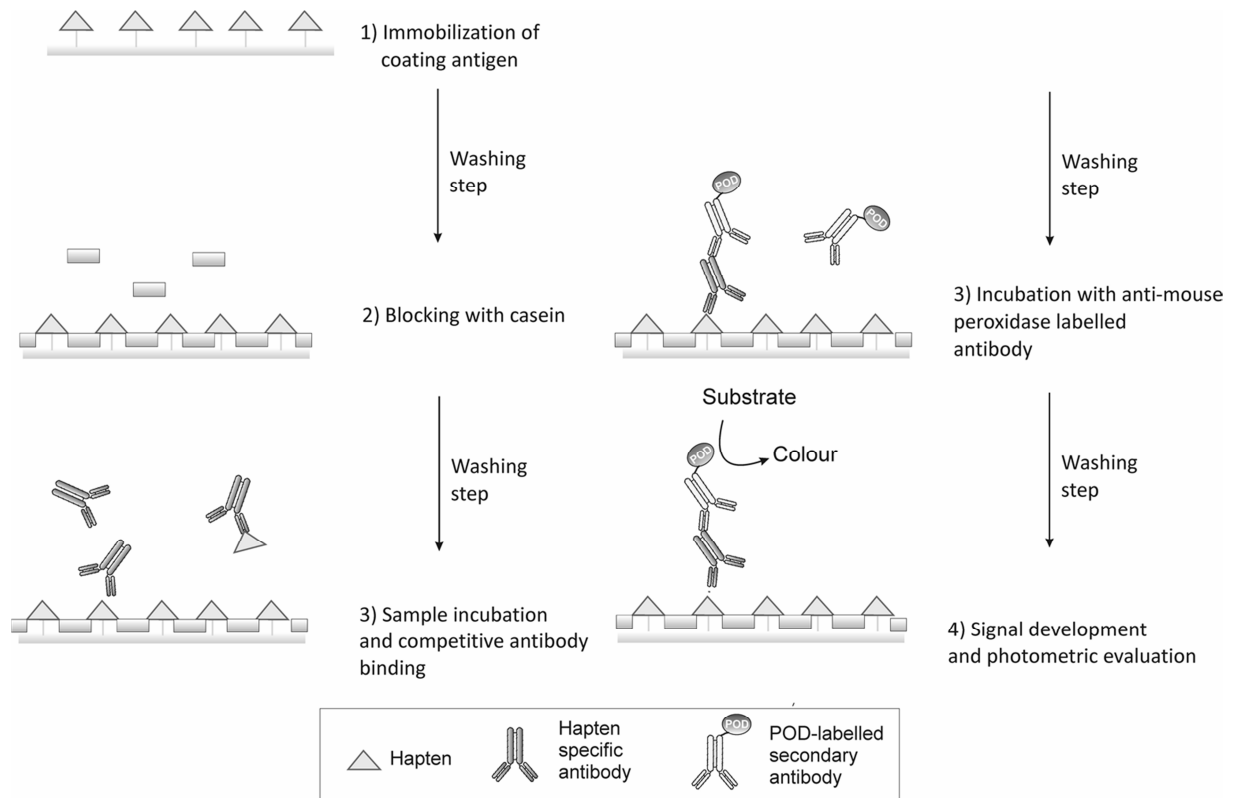
Figure 8: indirect competitive ELISA

2.5 Evaluation of immunoassays

An immunoassay is a ligand binding assay (LBA) with antibody as ligand. The receptor is a protein or hapten that was coupled to a protein for immunization. Generally, the response in LBA is a nonlinear function of analyte concentration. (Findlay, 2007) The characteristics of the dose-response relationship are direct or inverse depending on the format of the immunoassay. Moreover, the precision of an immunoassay is generally lower than a chromatographic assay. In ELISA, the assay sensitivity may be better than in a chromatographic assay. However, the assay range is often limited. Subsequently, samples must be diluted for quantification.

For calibration, a 4-parameter logistic (4-PL) model is the model of choice for LBAs in general and for ELISA in particular. It describes the typical sigmoidal shape of the calibration curve on a semilogarithmic scale (Figure 9). The 4-PL model is described by the following equation:

$$Y = D + \frac{(A-D)}{(1+\left(\frac{x}{C}\right)^{B})} \qquad \text{(Equation 4)}$$

Y   Response

D   Response at infinite analyte concentration

A   Response at zero analyte concentration

x   Analyte concentration

C   Inflection point of the calibration point (IC_{50})

B   Slope factor (>0)
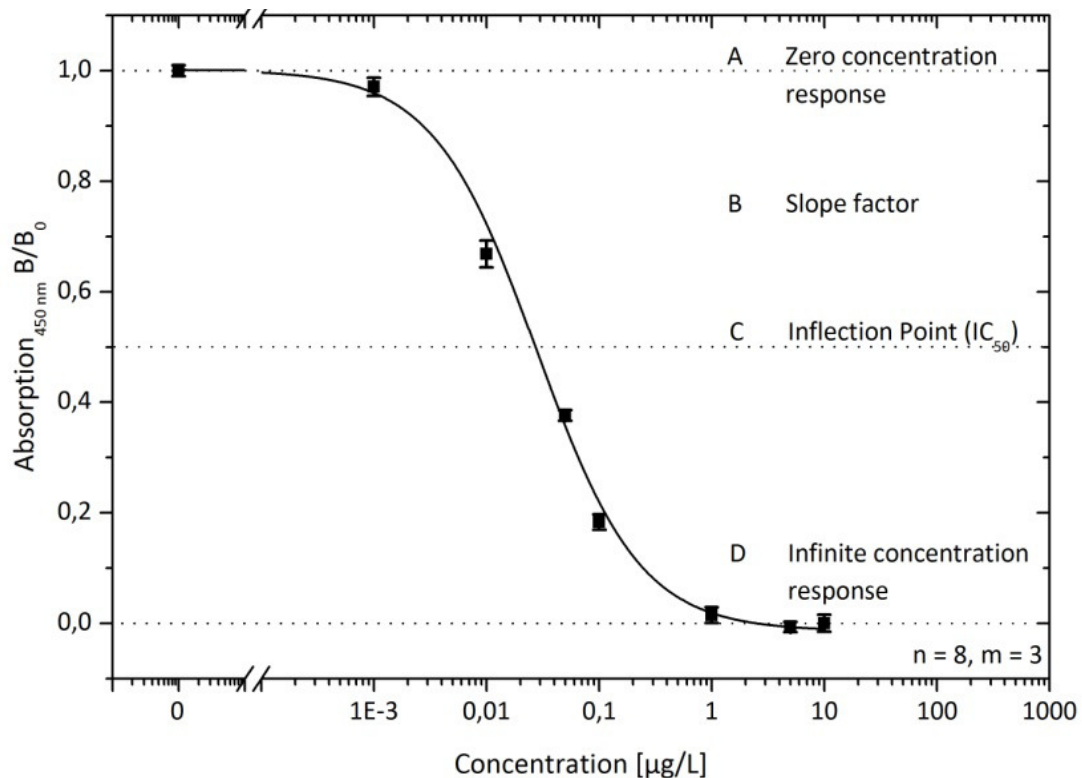
Figure 9: Typical 4-parameter logistic graph for an indirect competitive ELISA

It can be used for direct ELISA with A<D and for indirect ELISA with A>D. (Findlay, 2007) For best assay design, 5 to 8 calibration points should be used. Moreover, the calibration concentrations should be determined in duplicate or triplicate. The concentration progression of these standards should be logarithmic of the power of 2 or 3. The midpoint concentration should be somewhat above the IC_{50}. The maximum and minimum concentrations should meet the response at infinite and zero analyte concentration to optimize the 4-PL fit.

For the detection of micropollutants in water samples, recovery rates for spiked water samples are determined. The recovery rate is the percentage ratio of the measured concentration and the spiked concentration:

$$Recovery = \frac{c_{measured}}{c_{spiked}} \cdot 100\% \qquad \text{(Equation 5)}$$

In real water samples, cross reactivity (CR) between the analyte of interest and similar molecules can falsify the recovery of an immunoassay. For a given assay, cross reactivity can be measured by the ration between the IC_{50} values for the similar substitute to the analyte of interest (Equation 6). The lower the CR, the higher is the antibody specificity.

$$Cross\ reactivity = \frac{IC_{50(substitute)}}{IC_{50(analyte)}} \cdot 100\% \quad \text{(Equation 6)}$$

2.6 ELISAs for fresh water monitoring applications

For different micopollutants, competitive ELISAs have been developed (Table 1). They can be based on mAbs or pAbs. For BaP, DCF and MC-LR, assay sensitivities in the range of 60 to 65 ng/L can be accomplished.

In general, competitive ELISAs can be used for the detection of micropollutants. (Krämer, 2007) They reach the sensitivity needed for the WFD. In contrast to chromatography-based techniques, they do not need sample pre-concentration and extensive sample pretreatment. However, they lack acceptance in European laboratories, water works and water monitoring stations. Probably, inventors of ELISAs for environmental analysis have missed to show how broad the applicability is as displayed in Table 1 and Figure 1. Moreover, the ELISA based methods depend strongly on the antibodies used. Subsequently, there is a need for standardization of antibody production against haptens. MAbs allow reproducible IgG production. Subsequently, mAbs are wanted for priority pollutants to achieve a better acceptance of immunoassays for fresh water monitoring applications. Finally, the ELISAs should be automated for better inter-laboratory reproducibility. For this purpose, immunosensors can be developed in automated flow-through devices. The substrates for these sensors must be prepared in a universal and robust way to allow high acceptance and reproducibility.

Table 1: Indirect competitive ELISA results for selected micropollutants

Target	BaP	DCF	MC-LR
Available antibody	mAb clone 22F12 (mouse)	pAb (rabbit)	mAb clone MC10E7 (mouse)
Assay format	indirect	indirect	direct
Assay sensitivity, IC_{50}	65 ng/L	60 ng/L	60 ng/L
Source	Matschulat, 2005	Deng, 2003	Zeck, 2001a

3 Biosensors and microarrays for the analysis of fresh water samples

For the monitoring of fresh water samples, much effort has been made to develop automated biosensor systems. In general, a biosensor is "a device that uses specific biochemical reactions mediated by isolated enzymes, immunosystems, tissues, organelles or whole cells to detect chemical compounds usually by electrical, thermal or optical signals". (IUPAC, 1992)

3.1 Overview on existing biosensors

Biosensors for the detection of small molecules can be based on antibodies, aptamers or molecular imprinted polymers (MIPs). Aptamers are single-stranded DNA or RNA oligomers with individual sequences that bind to target analytes. They can reach high affinities and specificities. For DCF, a highly sensitive aptamer has been prepared (K_D = 42 nM; Joeng, 2009). Moreover, a highly affine aptamer (K_D = 50 nM) binding to MC-LR has been developed (Ng, 2012). Aptamers are produced in several rounds of enrichment out of large random libraries in a SELEX screening. Subsequently, the overall procedure requires several months. In comparison to antibodies, their advantages are that animal experiments are not necessary, their sequences are identified and consequently, their synthesis should be reproducible. On the contrary, they are not available for PAHs yet. The preparation of aptamers against PAHs is probably very challenging, because the essential condition for a successful generation of aptamers seems to be the hydrophilic character of the target.

MIPs are robust and low-cost in comparison to antibodies. (Weller, 2013) MIPs are polymerized around the analyte as a template molecule by several functional monomers and

a solvent. The template molecule is extracted and the remaining molecular cavities can be used for biosensing applications. However, they are difficult to reproduce because of batch synthesis approaches. A more promising approach for MIPs in analytical chemistry is to use them for selective solid phase extraction from complex matrices. (Pschenitza, 2014)

For highly selective and sensitive biosensors, antibodies are used. (Tschmelak, 2005 a) The resulting analytical devices are called immunosensors, which use antigen-specific immunoglobulin integrated within a physicochemical transducer. (Luppa, 2001) They are employed to automated immunoassays in microfluidic systems also known as lab-on-a-chip. (Han, 2013) These systems are sensitive analytical techniques for many applications in clinical diagnosis (Mohammed, 2011; Shiddiky, 2012), as well as food (Boujday, 2008; Rau, 2014; Salmain, 2012). There exist immunosensors for label-free and label-based competitive assay systems. In label-free assays, the antibody binding is detected directly by the transducer such as quartz crystal microbalance (QCM) sensors (Su, 2000), electrochemical or SPR sensors. For example, a piezoelectric immunosensor has been developed for the detection of individual antibiotics in milk and meat. (Karaseva, 2014) Furthermore, a portable multichannel SPR immunosensor was developed for the onsite analysis of antibiotics in milk samples. (Fernández, 2010)

In label-based assays, labels can be introduced via labeling of the detection antibody, tracers or secondary antibodies. The assays are designed according to competitive ELISA but in miniaturized versions. They allow the parallel detection of water pollutants from different compound classes in a single measurement. For example, a fully automated multiplex competitive immunoassay has been developed based on a microarray in MTP cavities. (Desmet, 2012) Five water pollutants can be measured in parallel on a 96-well MTP. For an indirect competitive ELISA, five antigens are spotted in a well and the samples are measured within 3 h with possible LODs of 0.01 µg/L.

For multiple analytes, a multiplexed microimmunoassay was developed in the indirect competitive format on a rotating disk substrate. (Morais, 2009) The total assay time was 30 min and LODs were in the range between 0.06 and 0.37 µg/L for 5 different pesticides, herbicides and pharmaceuticals. However, this assay format does not include a regeneration step of the disk used. Subsequently, each disk has to be replaced after one measurement. A regenerable biosensor was developed in a portable and fully automated system based on total-internal-reflection fluorescence. (Tschmelak, 2005 a; Tschmelak, 2005 b) It was used to

monitor priority pollutants in river water. For different pharmaceuticals and pesticides, LODs were in the low ng/L range. It was shown by the measurements with this system that for very low concentrations (1.0 – 3.0 ng/L) matrix effects from humic substances can disturb the recovery by the immunosensor. (Tschmelak, 2005 c) Other matrix effects like salts and pH are possible interference parameters. Despite the huge efforts that were made in the EU project to develop this measurement system (Tschmelak, 2005 a-c), the system was not integrated in water monitoring studies until now. Possible reasons are too high costs, problems with robustness or poor reproducibility of antibody preparation.

3.2 Setup for microarray-based micropollutant detection

For the multiplex detection of micropollutants, a microarray-based immunoassay is designed in this work by using the Microarray Chip Reader of the 3rd generation (MCR 3; Kloth, 2009 a). Regenerable microarrays were previously used for different applications in the MCR 3: antibiotics in milk (Kloth, 2009 b) and honey (Wutz, 2010), the plant toxin ricin *via* carbohydrate binding (Huebner, 2013), and mycotoxins in cereal extracts (Oswald, 2013).

The instrument setup is shown in Figure 10. It contains all antibodies, buffers and reagents for automated immunoassays with chemiluminescence detection (CL, see also Chapter 4). The samples, antibody solutions, buffers and reagents, are distributed by syringe pumps and valves in the instrument. The microarray chip is a glass slide modified as described in Chapter 3.3. It is integrated into a flow cell by a double side adhesive foil on a PMMA carrier. The detection unit is a charge coupled device (CCD) over the flow cell that takes images of the CL developed on the microarray.

(1) Syringe pump for sample injection (P2)
(2) Syringe pump for primary antibodies (P1)
(3) Syringe pump for secondary antibodies (P0)
(4) Syringe pump for luminol and hydrogenperoxide solutions (P3)
(5) and (6) Syringe pump for buffers(P4 and P5)
(7) Flasks for buffers and reagents
(8) CCD camera and microarray chip unit
(9) Flow channel for antibody detection
(10) Laptop computer for programming and assay evaluation

Figure 10: MCR 3 setup

For microarrays on planar chips and slides, the indirect competitive format is favorable, because a regenerable microarray surface can be prepared (Figure 11). The assay is carried out analogous to an indirect competitive ELISA on a MTP in the first steps 1 to 4. The analyte is immobilized on the microarray chip on distinct spots. The sample is pre-incubated with primary detection antibody and then directed into the flow cell, where the not bound antibodies are captured on the chip. The captured antibodies are labeled by a secondary antibody recognizing the F_c terminus of the primary antibody. For example, if monoclonal antibodies from mouse are used for analyte detection, the secondary antibody is anti-mouse labeled with peroxidase. Then, the substrate for chemiluminescence development is added and the CCD camera takes an image of the microarray surface. Finally, the bound protein is washed off the surface and the microarray surface can be used for the next measurement, if the analyte is immobilized covalently.
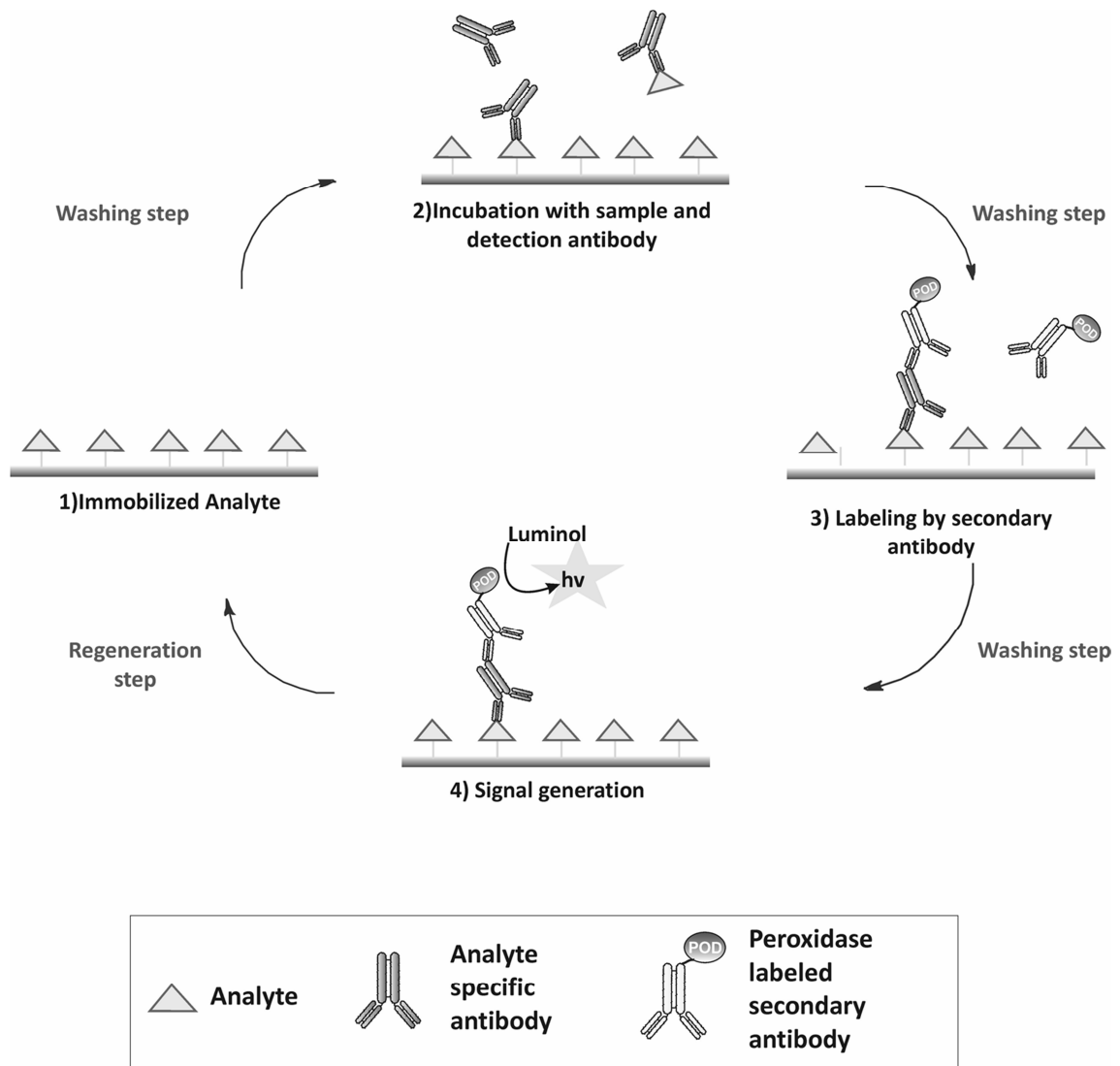
Figure 11: Concept of an indirect competitive immunoassay on a regenerable microarray surface

3.3 Preparation of regenerable immunosensors on glass-type surfaces

One of the greatest challenges in the field of immunosensors is the controlled and reliable surface functionalization. (Anderson, 2008; Piehler, 2000) This is particularly true in the case of hapten sensing, where the accessibility and reliability of the target molecules layer definitively impact the sensor response. (Boujday, 2010; Shankarana, 2007) On silica and silica-like surfaces, various strategies, mostly involving silane grafting on silanol groups, were described. (Gooding, 2011; Liebes, 2009; Ulmann, 1996) The control of this process is crucial, as the silane layer may be unstable in the aqueous media used for biological applications. (Dekeyser, 2008) However, for high throughput analysis the substrate should be stable and regenerable. In this way, the biosensing devices become economical, reproducible and cost-efficient. (Jiang, 2008; Su, 2000) In the present context, the term regeneration describes the

dissociation of the immune complex and liberation of the ligand on the silica surface. Such surface regeneration procedures are already described for a SPR (Shankarana 2007) and QCM (March, 2009) immunosensing, as well as for microarray-based chemiluminescence immunoassay (Oswald, 2013).

To immobilize the antigen on the transducer surface, a protein-hapten conjugate can be immobilized or the hapten can be coupled covalently direct to a shielding layer. The latter has been used successfully for reproducible mycotoxin determination in wheat extract. (Oswlad, 2013) For this application, a polyethylene glycol (PEG) based coating was attached to the silane layer on silica glass slides. The PEG allows a high surface coverage by the hapten and low non-specific binding what makes the surface quite resistant to biofouling. (Mehne, 2008; Piehler, 2000; Wolter, 2007)

The next step towards a reliable high throughput analysis with these silica glass slide modifications is the control and reproduction of the promising surface chemistry preparation. Moreover, it can be transferred to other silicate surfaces like silicon with native oxide layer and additional transduction techniques.

The first step for the silica surface modification (Figure 12) is the cleaning and oxidation of the silica surface in order to produce silanol groups. (Cras, 1999) Then, a 3-Glycidyloxypropyltrimethoxysilane (GOPTS) layer is grafted on the silica surface, followed by attachment of the diamino-poly(ethylene glycol) (DAPEG) with a molecular weight of ~ 2000 Da. The terminal amino groups are available to immobilize haptens or derivatives with appropriate chemical functions directly on the surface.

The haptens can be immobilized on the surface from a solution which is covering the whole surface (surface coverage) or by a microspotting method on distinct spots. The immobilization procedure depends on the sensor principle. For microarrays, a microspotting method has to be developed. The coupling chemistry has to be developed for each hapten. A usual approach is the coupling of active esters to amino groups. If this approach is not suitable, the coupling chemistry that was used for the antigen synthesis can be transferred to the immobilization on the chip.

In this work, the microspotting is performed by a contact printing method. The autmated microspotting device uses a needle to put droplets of the solution containing (activated)

hapten on the microarray substrate. The needle is touching the surface so it has direct contact with the substrate.

3-Glycidyloxypropyltrimethoxysilane
(GOPTS)

Diamino-PEG (DAPEG)
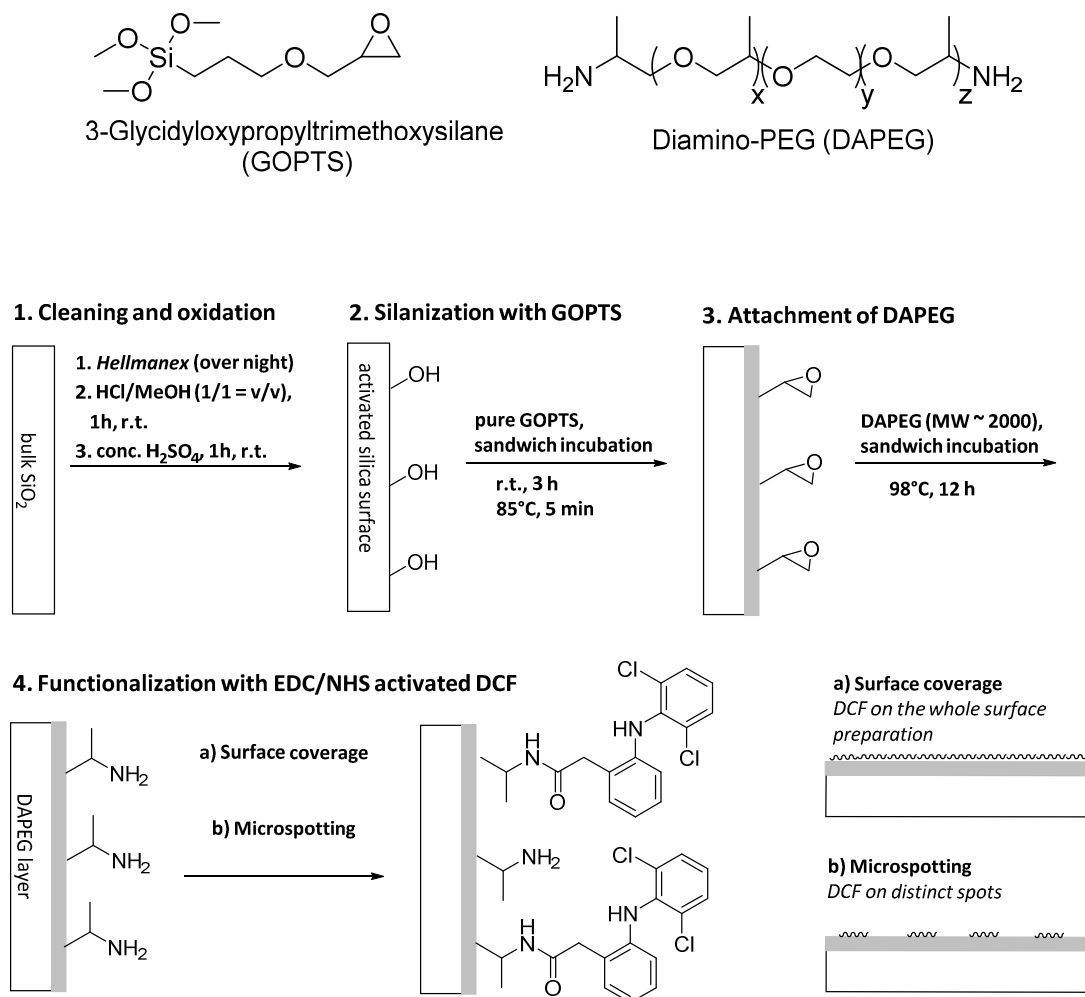
Figure 12: Surface functionalization for regenerable immunosensing

3.4 Methods for surface chemistry analysis during biosensors preparation

In order to allow robust and sensitive surface preparations for biosensing applications, different methods for surface chemistry analysis can be applied. (Aissaoui, 2012; Boujday, 2009 b) For the characterization of the modifications on silica surfaces, two substrates bearing terminal silanol groups can be utilized: glass slides and silicon wafers with a native silica layer on their polished surface. On both substrates, atomic force microscopy (AFM) is used to control the homogeneity. Water contact angle measurements allow to determine the interfacial properties of a biosensor surface. On Si wafers, grazing-angle attenuated total

reflection FT-IR spectroscopy (GA-ATR FT-IR) allows the sensitive detection of characteristic bands of monolayers on the biosensor surface. Furthermore, X-ray Photoelectron Spectroscopy (XPS) on Si wafers allows the ultimate analysis of the surface coating. In QCM measurements with silica coated quartz probes, the specificity and functionality of the immobilized ligand is checked.

3.4.1 Atomic force microscopy

For the investigation of the roughness and morphology on these two types of silica surface, atomic force microscopy (AFM) is used in the PeakForce Tapping^{TM} Mode (non-contact) under air provided by Bruker. AFM is a type of scanning probe microscopy (Figure 13). A sharp probe shaped as a tip of 2 nm in diameter is scanned across a surface. The deflection of the cantilever is detected by a laser beam sent towards a photodiode. The sample is moved in x and y direction to scan an area of the surface. The probe is controlled to move in z direction as well, to avoid the direct contact of the tip with the surface. The PeakForce Tapping^{TM} Mode enables to show nanostructuration of a planar surface. (Mercier, 2012; Spadavecchia, 2011) For instance, polyoxometalates or cubic nPEG-TiO$_2$ nanoparticles with diameters of about 20 nm and heights of about 5 nm can be identified by using this method. Moreover, weakly bound layers are removed by the cantilever resulting in irregular AFM images. (Aissaoui, 2012)
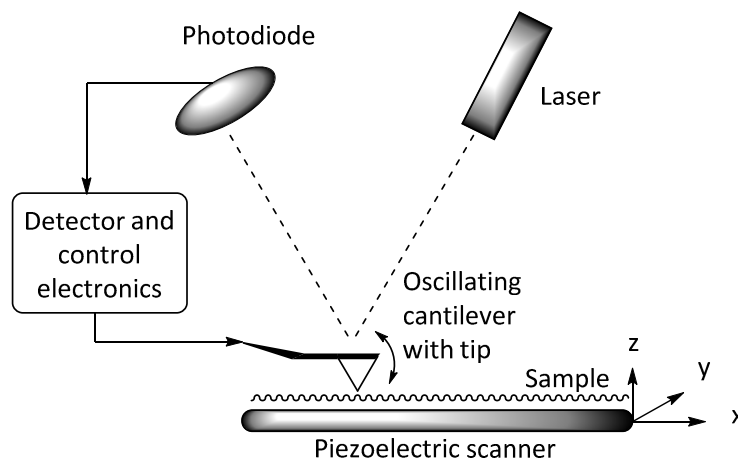
Figure 13: Principle setup of AFM in tapping mode

3.4.2 Water contact angle

Water contact angle measurements are carried out on both surface types (Si wafer and glass slides) to assess the interfacial properties of the resulting surface. The molecular

organization on the planar surface is represented by the hydrophilicity or hydrophobicity of the self-assembled monolayer. (Aissaoui, 2012) Organic layers and chains are contributing to a bulk interaction with the water drop that can be measured by the static contact angle measurement. For this measurement, a water drop is placed on the surface of interest and the angle between the surface is determined (Figure 14). This drop is called "sessile drop" and the solid surface tensions from contact angles can be calculated by referring to a relation, which has been recognized by Young in 1805. (Kwok, 1999) The contact angle of a liquid drop on a solid surface is defined by the mechanical equilibrium of the drop under the action of three interfacial tensions: solid/vapor γ_{vs}, solid/liquid γ_{sl} and liquid/vapor γ_{lv}. The relation in equilibrium of these three tensions is known as Young's Law:

$$\gamma_{lv} cos\theta = \gamma_{sv} - \gamma_{sl} \qquad \text{(Equation 7)}.$$

In practice, an image is taken like it is shown in Figure 14 by a CCD camera of the drop sitting on the surface of interest. Then, an algorithm is performed to fit a circle and to calculate the contact angle from the fitted curve.

The same instrument can be used to determine the interfacial tension (IFT) of a drop hanging from the capillary. For different solvents or mixtures of solvents, the IFT and the contact angle on a solid are different resulting in different wettability qualities. These qualities can be crucial for microspotting methods and surface properties in flow-through systems. For example, organic solvents must be used for increasing the wettability of the surface and in this way the interaction properties of the surface with an antibody or other biomolecules.
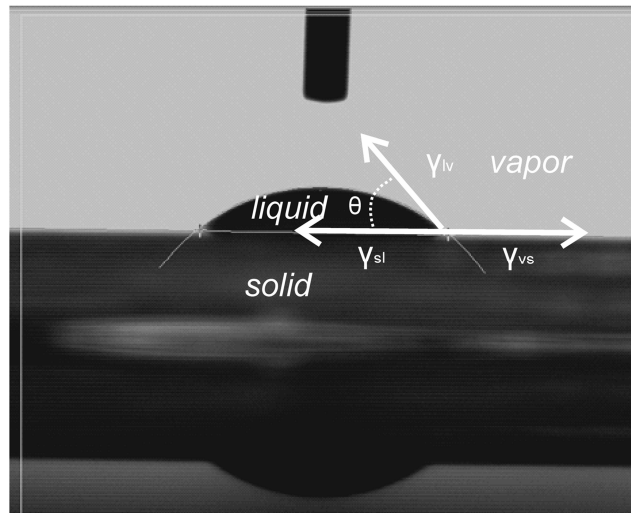
Figure 14: Image of a sessile drop contact angle system with tensions acting on the drop (white lines), the contact angle θ and the fitted circle (green)

3.4.3 Grazing-angle attenuated total reflection FT-IR

The chemical composition of the organic surface coating can be analyzed by grazing-angle attenuated total reflection FT-IR (GA-ATR FT-IR) on Si wafers. (Lummerstorfer, 2004) The wafer is pressed against a germanium crystal, which has a higher refractive index n than silicon for a total internal reflection at an angle above the critical angle of 59°. With this setup, internal reflection measurements can be performed. (Figure 15; Lummersdorfer, 2007) The mean square electric field $<E>^2$ is split into a E_x and E_z component perpendicular to the surface. Sandwiched between two media with high refractive index (n > 3), the E_z component within the organic layer (n ~ 1.5) experiences an enhancement of the electric field. In experimental setups, the angle of incidence is set to 65°, the sample thickness is 2 nm and the air gap between the sample and the germanium is minimal for maximum signal intensity.

The high intensity of the E_z component leads to another interesting information: the orientation of the organic layer molecules can be determined by observing the intensity of the bands around 2900 cm^{-1}. These bands correspond to C-H stretching bands. The intensities are proportional to the perpendicular dipole moment component of each vibration. Parallel vibrations are not enhanced. (Lummerstorfer, 2007) Subsequently, an arbitrary ordering of the chains corresponds to a high absorbance. On the contrary, a high ordering corresponds to a low absorbance, because the chains are almost perpendicularly oriented regarding the Si surface.
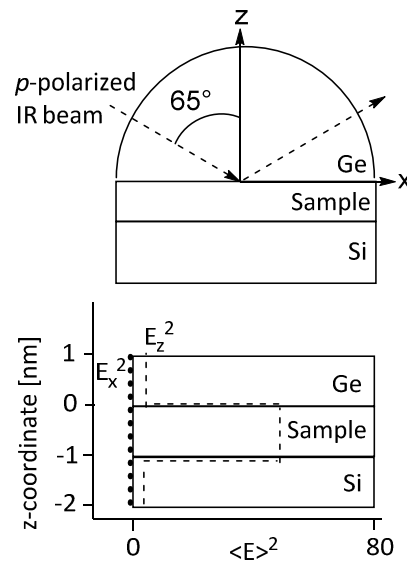
Figure 15: Electric field profiles for thin films sandwiched between two solids with IR radiation according to Lummerstorfer 2007

3.4.4 X-ray photoelectron spectroscopy

X-ray photoelectron spectroscopy (XPS) allows ultimate analysis of the surface coating with up to 3 nm layer thickness. It delivers signals from the kinetic energy of electrons with energy levels characteristic for the elements on the surface. In addition, a chemical shift can be measured due to chemical properties of the element of interest in the surface grafting. Subsequently, XPS is also known as Electron Spectroscopy for Chemical Analysis. (Fadley, 1974)

XPS enables estimating the layer thickness after each preparation step. The comparison of the intensity of the Si 2p peaks of a clean silicon substrate and the one with the layers allows the estimation of their thicknesses. Assuming a homogeneous layer, the thickness d is estimated using the following equation.

$$d = -\lambda_{Si2p}^{l} \cos\theta \ln\frac{I_{Si2p}(d)}{I_{Si2p}(\infty)} \quad \text{(Equation 8)}$$

θ is the photoelectron collection angle (45°). $I_{Si2p}(d)$ and $I_{Si2p}(\infty)$ are the intensities of the Si 2p peaks with the layer and without the layer respectively. λ_{Si2p}^{l} (3.5 nm) is the inelastic mean free path of electrons 2p of Si in the layer l. It can be calculated using the Quases program based on the TPP2M formula (Tanamua, 1994).

3.4.5 Quartz crystal microbalance with dissipation measurement

For studying the interaction of antibodies with surface preparations, label-free quartz crystal microbalance with dissipation measurement (QCM-D) is suitable. QCM-D is a piezoelectric sensor incorporating a quartz crystal. In Figure 17, a QCM setup is shown. On a quartz crystal, antibodies or antigens can be immobilized and the binding of another biomolecule is detected by the change of the resonant frequency of the quartz. According to the Sauerbrey equation (Sauerbrey, 1959), the measured frequency shifts ΔF are proportional to the mass uptake Δm:

$$\Delta F = -\frac{N\Delta m}{C_f} \quad \text{(Equation 9)}$$

with the mass sensitivity constant (C_f = 17.7 ng cm^{-2} Hz^{-1} at f = 5 MHz) and the overtone number (N = 5). The Sauerbrey's Equation is suitable for measurements under vacuum. ΔF is recorded by an oscilloscope. For the interpretation of the QCM-D data from liquid samples, the dissipation factor D must be observed. (Rodahl, 1995) As long as no dissipation by energy exchange with the liquid occurs, the adsorbed layer can be regarded as rigid. (Boujday, 2009 b) The total dissipation factor is the sum of all energy losses in the system. For example, internal friction in the quartz can cause energy losses in a QCM system. If the film on the quartz surface is viscous, energy is dissipated due to oscillatory motion within the film. (Rodahl, 1995) In the QCM instrument, the decay of oscillation of the quartz with the amplitude A is measured by switching off the driving voltage at t = 0.

$$A(t) = A_0 e^{-7/\tau} \sin(\omega t + \varphi) + constant, t \geq 0 \quad \text{(Equation 10)}$$

τ is the decay time constant, ω is the angularly frequency at resonance, φ is the phase and the constant is the offset. The decay constant is related to D_{tot} by

$$D_{tot} = \frac{2}{\omega\tau} \quad \text{(Equation 11).}$$

Measuring the amplitude A of the oscillation as a function of time t after switching of the driving power, the decay time constant τ and the angular frequency ω can be determined by using Equation 11.

ΔF measurements

ΔF acquisition

Flow cell

Flow →

→

Quartz crystal with
immobilized ligand

5 M Hz
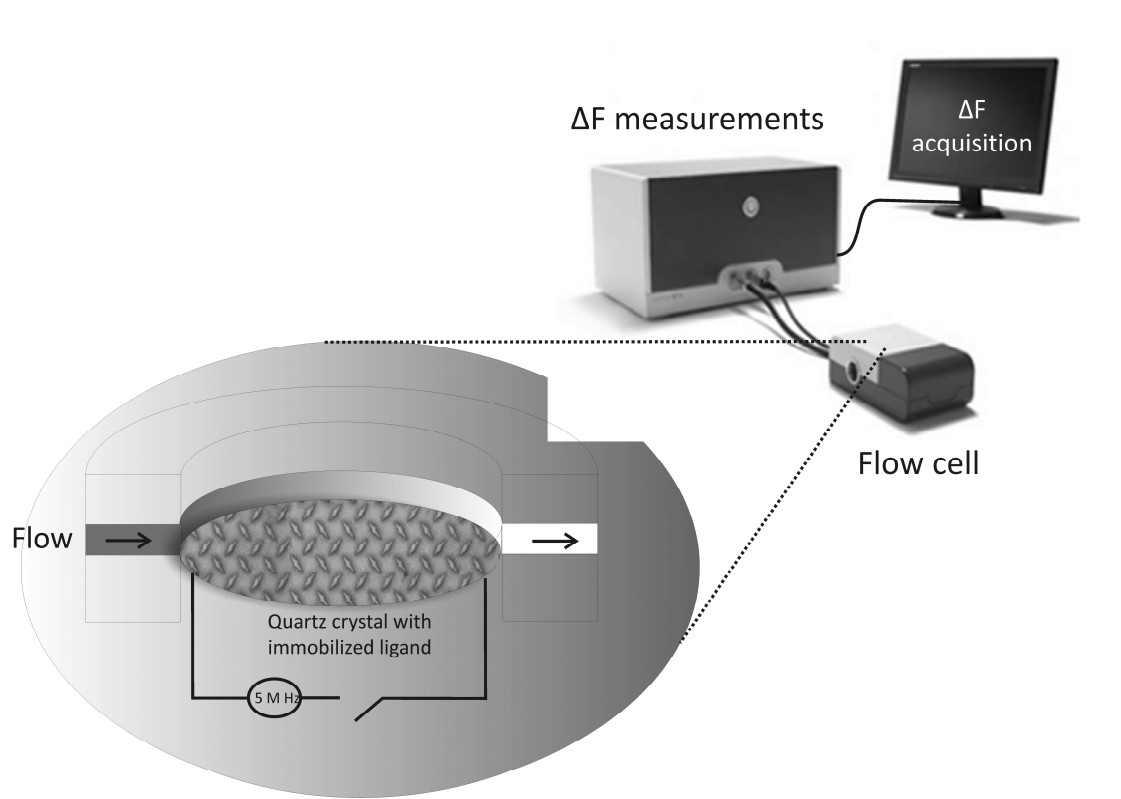
Figure 16 : QCM-D setup

4 Chemiluminesence as a detection principle for biosensors and immunoassays

The oxido-reduction of several hundred inorganic and organic compounds can cause chemiluminescence (Marquette, 2009). For immunoassay application, the oxidation of 5-amino-2,3-dihydrophthalazine-1,4-dione (luminol) in the liquid phase is exploited. The oxidation delivers an amino-phthalate ion in an excited state emitting light when returning to the ground state (Figure 17). Horseradish peroxidases (HRPs) are able to catalyze the CL reaction of luminol in the presence of hydrogen peroxide at pH values between 8 and 8.5. For biochemistry-based analytical systems like biosensors, immunosensors and microarrays, this CL production system is usually applied.
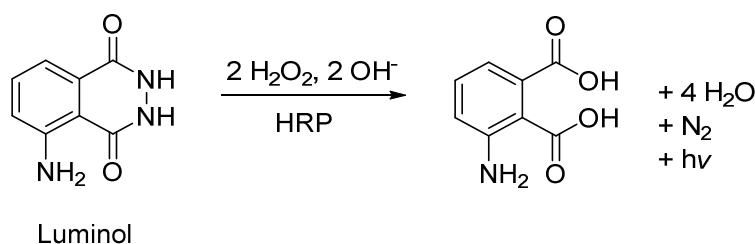
Figure 17: Oxidation of luminol biocatalyzed by HRP

Chemiluminescent enzymes have been exploited as labels for immunoassays for some years (Marquette, 2009). In microtiter plates, pathogens or disease markers can be detected. In the wells of the MTP, microarrays can be printed to allow multiplexed chemiluminescent immunoassays. Microarrays can be prepared on biochips, too. The detection of the chemiluminescence is usually based on imaging by a CCD camera. Chemiluminescent biochips are very sensitive detection methods. Some of the chemiluminescent biochip-based immunoassays were developed for analytical applications and the Evidence Investigator[TM] is commercialized. For example, it was used to screen sera regarding HIV infection. The other stand-alone platform called MCR 3 was already described in Section 3.2. Integrated immunoassay systems are usually for single use in point-of-care applications. The fluid handling and immobilization substrate are integrated in order to facilitate the detection of target molecules. In order to raise the sensitivity of a chemiluminescent biochip, gold nanostructured layers can be used. (Corigier, 2007; Lin, 2010; Marquette, 2009)

III Results and Discussion

1 Development of monoclonal anti-DCF antibodies for fresh water analysis

The production of monoclonal antibodies was performed by using the hybridoma technology according to Koehler and Milstein (Koehler, 1975). The immunogen was a conjugate of DCF to thyreoglobulin (TG). It was sent to Dr. Ekkehard Weber from the Institute of Physiological Chemistry at the University of Halle-Wittenberg. The conjugate was used to immunize mice of which hybridoma cells were isolated from the spleen. The resulting positive cell culture supernatants (CCS) of the B-cells were sent back to the IWC. They were screened in indirect competitive ELISA experiments in order to find highly affine anti-DCF antibodies for the analysis of fresh water samples.

1.1 Identification of monoclonal anti-DCF antibodies with high affinity by screening hybridoma cell culture supernatants

For the immunization of a mouse with the hapten DCF, a conjugate of DCF with thyreoglobulin (TG) was used. DCF was directly coupled to TG after activation of the carboxylic acid residue by the mixed anhydride method with isobutylchloroformiate. This method has already worked for the production of the polyclonal anti-DCF antiserum in rabbit (Deng, 2003). The IC_{50} value for this antiserum was 60 ng/L. The antigens for coating in ELISA were prepared with ovalbumin (OVA) and bovine serum albumin (BSA) by the active ester method with DCC and NHS.

Titer determinations showed that 4 immunized mice had positive immunoreactions towards DCF. They were further used for the fusion process. The resulting hybridoma cells were cultivated and their CCS were screened regarding their binding ability to OVA-DCF in an indirect ELISA. In total, 3000 clones were tested. 46 of them were identified to produce specific monoclonal antibodies against DCF during this first screening.

CCS of positive clones were sent to the IWC and analyzed regarding their sensitivity in an indirect competitive ELISA for the detection of DCF. They were used in different dilutions, because the concentration of mAbs may differ for different CCS. For higher concentration of antibody in a CCS, a higher dilution must be applied in order to obtain analyzable competition reactions in the indirect competitive ELISA on a microtiter plate (MTP). The optimal dilution allows an absorption of about 1.0 at 450 nm after 15 min of oxidation of

3,3',5,5'-tetramethylbenzidine (TMB) to a blue dye. The enzymatic reaction was stopped by the addition of diluted sulfuric acid to give a yellow color and the MTP were read out at 450 nm.

For the optimized dilutions, CCS were screened by an indirect ELISA regarding their ability to bind to DCF in solution by comparing the absorption values for 0 and 10 µg/L in a mixture of 10% MeOH in ultrapure water. The organic solvent was present in order to find highly robust antibodies for analytical applications where the use of an organic solvent might be necessary. For example, in microfluidic devices, organic solvents like methanol prevent the adsorption of analyte from solution to the wall material of the fluidics.

The most promising clones were identified by a signal loss due to a DCF concentration of 10 µg/L. They were further tested with dilution series between 0 to 100 µg/L DCF. 11 out of 46 CCS showed a high assay sensitivity with IC_{50} values below 50 µg/L (Table 2). They were stemming from mice 266, 267 and 268 as the first digits of the clone identification number expresses. Clones 268-5A3, 266-6D8, 266-6D10, 266-8B1, 266-10C9 and 266-12G5 were identified as the most sensitive clones with IC_{50} values ≤ 5 µg/L. CCS 266-6D10 turned out to be a false positive CCS, probably due to carryover from clone 266-6D8 during the primary screening stage. This assumption is also supported by the low dilution that was necessary for this clone. The positive B-cell clones from mouse 266-6D8, -8B1, -10C9 and -12G5 were highly productive compared to other CCS, because the CCS could be diluted up to 1/10 000.

Table 2: Positive CCS from hybridoma cells with sensitivities below 100 µg/L.

CCS identification number	Optimized dilution (v/v)	IC_{50} [µg/L]
267-1F7	1/100	20
267-1F3	1/100	15
267-2D3	1/400	16
267-7E3	1/10	9
267-9B7	1/10	11
268-5A3	1/20	5
266-6D8	*1/300*	*1*
266-6D10	1/10	4*

266-8B1	*1/600*	*0.2*
266-10C9	*1/2 000*	*4*
266-12G5	*1/10 000*	*0.5*

* false positive

1.2 Characterization of purified monoclonal antibodies

The most promising CCS were affinity purified and characterized by MALDI-TOF-MS, SPR affinity measurements and ELISA to determine molecular weight, dissociation constants, robustness and specificity for the analysis of fresh water samples.

1.2.1 MALDI-TOF-MS spectra

For the four most sensitive CCS, MALDI-TOF-MS spectra of the affinity purified antibodies were recorded (Figure 18). Peaks for $[M-H]^+$, $[M-H]^{2+}$ and $[M-H]^{3+}$ can be observed for every mAb. All peaks show shoulders like the peak at $[M-H]^{2+}$ (Figure 19). The peak at lower m/z ratio is the same for all antibody preparations. It can be attributed to IgG from fetal bovine serum (FBS) with a mass of 147 kDa as calculated from $[M-H]^+$, $[M-H]^{2+}$ and $[M-H]^{3+}$ peaks of all collected spectra. FBS is used to cultivate the hybridoma cells and therefore, the peak stemming from the IgG fraction of this serum must be equal for every final product.

The mass determination for the anti-DCF mAbs were calculated from $[M-H]^+$, $[M-H]^{2+}$ and $[M-H]^{3+}$ peaks in the MS spectra and are summarized in Table 3. In average, they have a mass of 151 kDa. However, the IC_{50} value of mAb 266-8B1 is below the other three analyzed mAbs. Its mass was determined as 150 kDa. It is the only mAb with a chain structure subtype IgG1 and a light chain with κ structure. The other three mAbs have IgG2b structures with κ subtype. Consequently, the lower mass of mAb 8B1 can be attributed to the different IgG subclass.
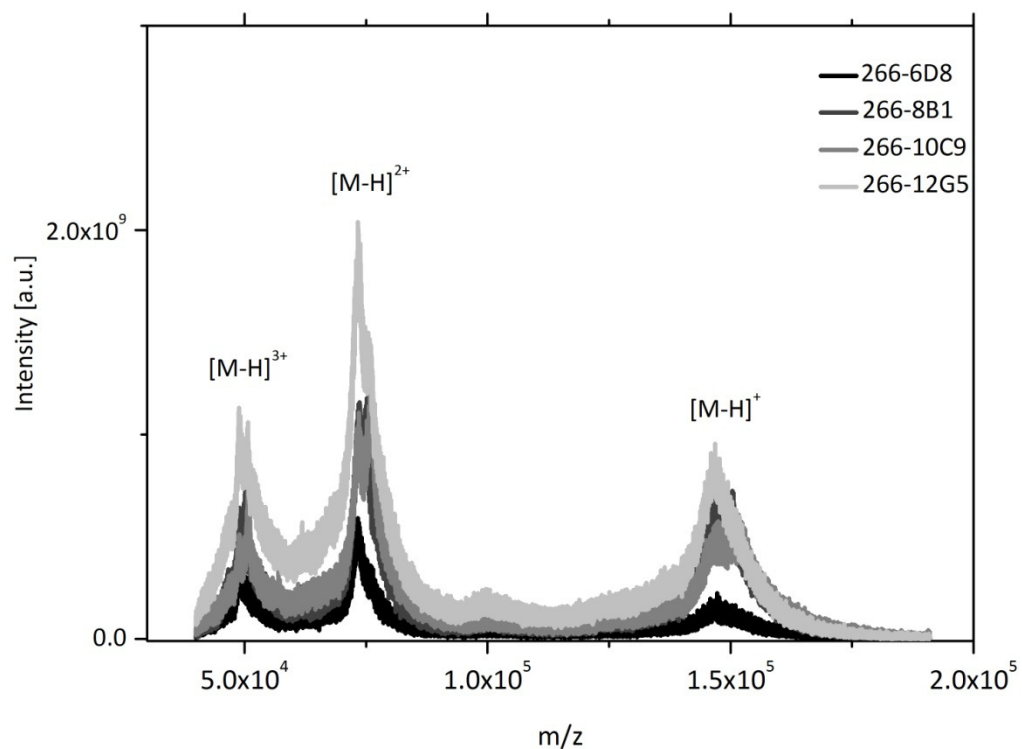
Figure 18: MALDI-TOF-MS spectra of affinity purified mAbs
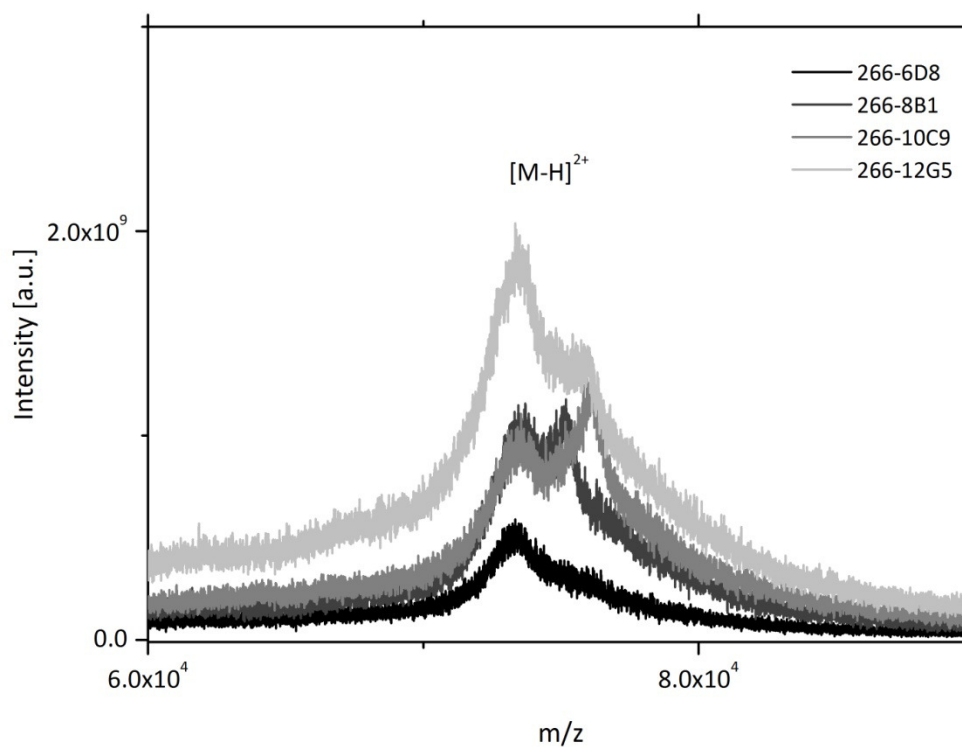
Figure 19: Excerpt from the MALDI-TOF-MS spectra of monoclonal antibodies

Table 3: Determined masses and chain structures for purified monoclonal antibodies

mAb	MW (average of [M-H]$^+$, [M-H]$_{2+}$ and [M-H]$^{3+}$)	Chain structure subtype for heavy chain and light chain
266-6D8	(151 ± 1.3) kDa	IgG2b, κ
266-8B1	(150 ± 0.2) kDa	IgG1, κ
266-10C9	(152 ± 0.4) kDa	IgG2b, κ
266-12G5	(151 ± 0.4) kDa	IgG2b, κ

1.2.2 SPR sensor surface design and binding curves

In order to carry out binding studies in the SPR device (Biacore X100), a DCF-OVA conjugate was immobilized on a CM5 gold chip provided by GE Healthcare. This sensor chip carries a matrix of carboxymethylated dextran which is covalently attached to the gold surface. The carboxy groups were activated by EDC/NHS to active esters which can react with free aminogroups of the DCF-OVA conjugate. For the interaction of the protein with the activated surface, the pH value of the immobilization buffer was optimized (Figure 20). It is crucial to find the pH value for optimal electrostatic pre-concentration for enabling the amide formation in the flow through device at flow rates of about 10 µL/min. The acid dissociation constant pK_a is 3.5 for the CM5 chip as stated by the manufacturer. For pH values below 3.5, the dextran surface is not negatively charged and electrostatic pre-concentration is not possible. Above this pH value, the surface is negatively charged and a positively charged protein can be attracted by electrostatic interaction. If the chosen pH value of the immobilization buffer exceeds the isoelectric point of the ligand, the protein is negatively charged and will be repelled by the dextran surface. For the OVA-DCF conjugate, the isoelectric point is unknown. Subsequently, several pH values between 3.3 and 5.5 for the 10 mM NaOAc buffer were tested (Figure 20). At pH = 3.3, an electrostatic pre-concentration was still possible in this experiment. With increasing pH, the pre-concentration decreases. At a pH value of 5.5, the signal even decreases in the course of protein injection. This indicates a repulsion of the injected protein conjugate.
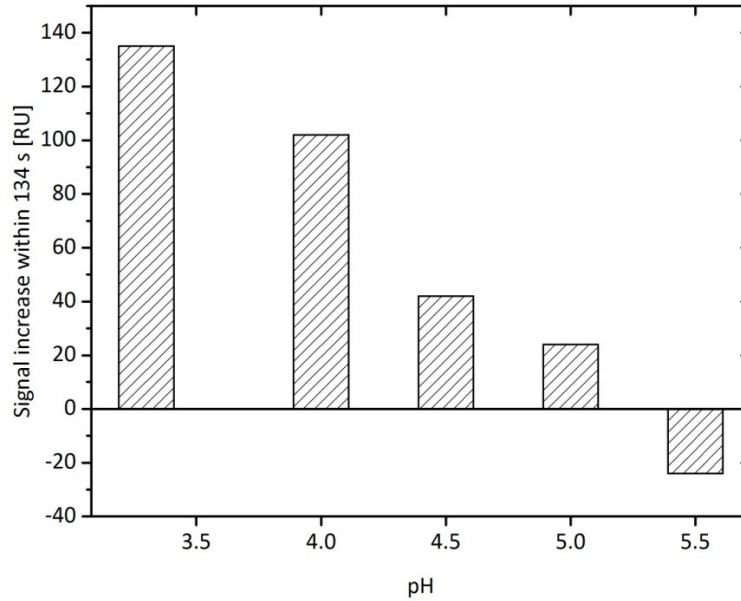
Figure 20: Electrostatic pre-concentration for DCF-OVA immobilization on a CM5 chip.

In Figure 20, it is shown for different pH values that different levels of electrostatic pre-concentration can be achieved. This is important in the design of a surface for kinetic measurements, where the maximum binding capacity should be optimal for analyzable binding curves (Frostell, 2013). For low immobilization levels, the binding kinetics is more pronounced and becomes easier to interpret. The ligand on the chip surface was a DCF-OVA conjugate with an approximate MW of 45 kDa. For a given analyte like a monoclonal antibody with a molecular weight of 150 kDa, the ligand immobilization level can be calculated according to Equation 11. For the calculation of the level of immobilized ligand, a value of 100 RU was used for the value of the maximum SPR response (R_{max}) on the prepared chip surface.

$$R_{max} = \frac{analyte\ MW}{ligand\ MW} \cdot immobilized\ ligand \qquad \text{(Equation 11)}$$

$$\Leftrightarrow immobilized\ ligand\ = \frac{R_{max}}{analyte\ MW} \cdot ligand\ MW$$

$$\Rightarrow immobilized\ ligand\ \approx \frac{100\ RU\ \cdot 150000\ Da}{45000\ Da}$$

$$\Rightarrow immobilized\ ligand \approx 330\ RU$$

Consequently, a level of immobilization of about 330 RU should not be exceeded in order to obtain kinetic data with the prepared surface. Therefore, a pH value of 4.5 is chosen for the

immobilization step and a total injection time of 840 s (14 min) is used in the immobilization cycle (Figure 21) to obtain a R_{max} below 100 RU. After the immobilization procedure, the immobilization level of ligand after the whole immobilization procedure is 504 RU. Thus, the reaction of analyte with the surface was higher than assumed from the pre-concentration experiments. However, it cannot be assumed that every immobilized DCF-OVA conjugate is a suitable ligand for a monoclonal antibody. The orientation of the DCF ligands cannot be influenced by this surface chemistry approach. Consequently, Equation 11 can be used as a hint for the experiment setup. However, it is not a way for bottom-up design of the chip for kinetic measurements. The final R_{max} for the surface preparation has to be determined by experiments for each surface preparation in particular. The R_{max} for each chip is carried out by repeated injections of antibody dilution until a saturation of signal is reached. For the 5 different antibodies characterized in this binding study, the maximum binding capacity was in average (72 ± 9.0) RU. So the signal intensity was comparably low and the prepared chip could be used for kinetic studies.
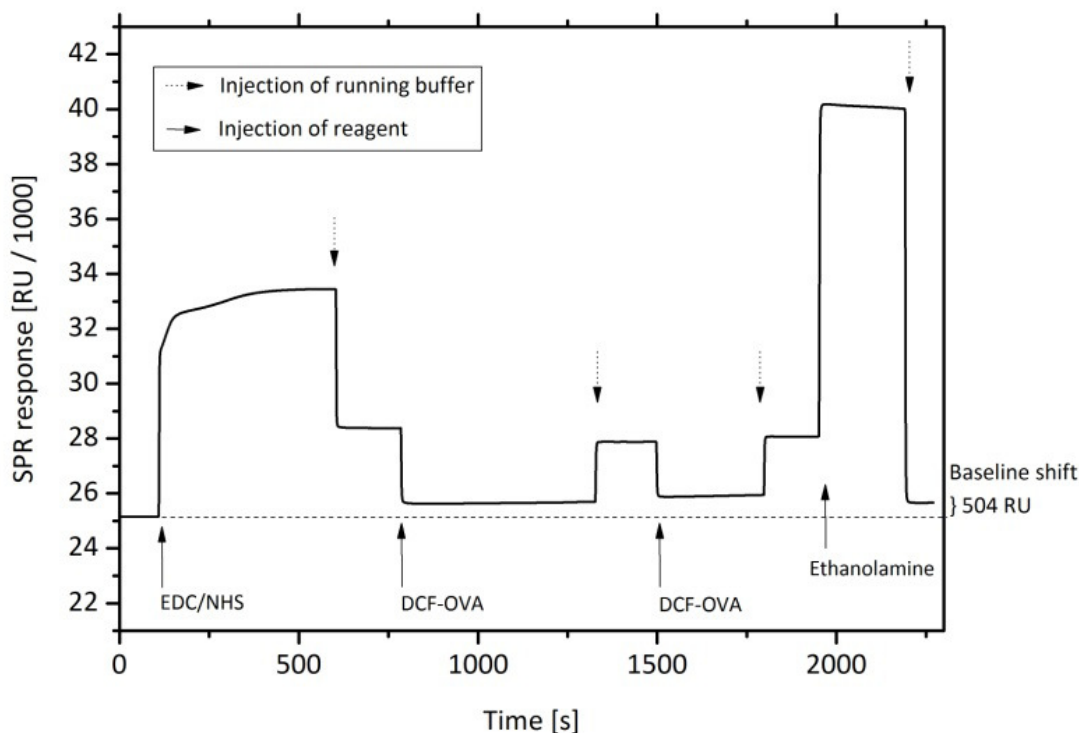

Figure 21: Cycle for the immobilization of DCF-OVA on a CM5 chip (Dextran surface)

The binding and dissociation rate constants were determined in single cycle kinetics (SCK) experiments (Frostell, 2013). This format eliminates the need of regeneration. Moreover, blank cycles can be run exactly as the ligand cycle with the same number of injections for

performing double reference subtraction in order to eliminate high contribution of bulk refractive index. Double referencing means that the blank cycle and the reference flow cell data are subtracted from the antibody binding sensorgrams.

In Figure 22, the sensorgram of the SCK experiment for antibody 268-5A3 is shown. Antibody concentrations of 0.057, 0.11, 0.23, 0.46 and 0.92 µM were injected consecutively. For each concentration step, 120 s were determined as interaction time. Then, running buffer was injected for 180 s to observe the dissociation behavior of the antibody. After the final injection, running buffer was injected for the observation of the dissociation process. Then, the regeneration and equilibration of the sensor chip surface was accomplished. The SCK curves were evaluated by the bivalent analyte model for kinetics analysis in the Biacore Evaluation software. The results are summarized in Table 4.

The same SCK experiment was carried out with antibody 266-12G5 with concentrations of 0.011, 0.033, 0.098, 0.29 and 0.88 µM (Figure 23). In comparison to antibody 268-5A3, dissociation is slower. The rate constants are calculated from the binding curves by the Biacore Evaluation software by using the binding model for a bivalent analyte. The ratio of the measured rate constants k_d and k_a yields the dissociation constant of the different antibodies (Table 4). Clone 268-5A3 showed the highest dissociation constant of 1.6×10^{-6}. For this antibody, the association rate constant k_a is $1.1 \cdot 10^{4}$ and in the range of the other mAbs. Subsequently, the high dissociation rate constant $k_d = 1.7 \cdot 10^{-2}$ is causing fast dissociation and a low affinity. The fast dissociation can be seen in the sensorgram in Figure 22 by the high slope during the dissociation phases, too.

For the remaining antibodies, 266-6D8, 8B1, 10C9 and 12G5, the dissociation is slower. The k_d values are in the range of 10^{-5} and are approaching the limits that can be measured with the Biacore instrument. They differ in the association rate and consequently in the dissociation constants. The highest affinity was measured for antibody 266-12G5 with K_D 1.5×10^{-10}. Its association is 10 times faster compared to the other antibodies. In a similar study with anti-steroid mAbs, similar values were measured by SPR. The affinity constants were in the range of 3×10^{-8} M. Dissociation was very slow for these highly affine mAbs and could not be observed in the sensorgrams (Kaiser, 2000). Consequently, the prepared mAbs for DCF are very high and their binding towards DCF is highly stable.

All of the highly affine mAbs were stemming from mouse 266. For this reason, they are from now on called mAb 6D8, 8B1, 10C9 and 12G5 in order to facilitate nomenclature.
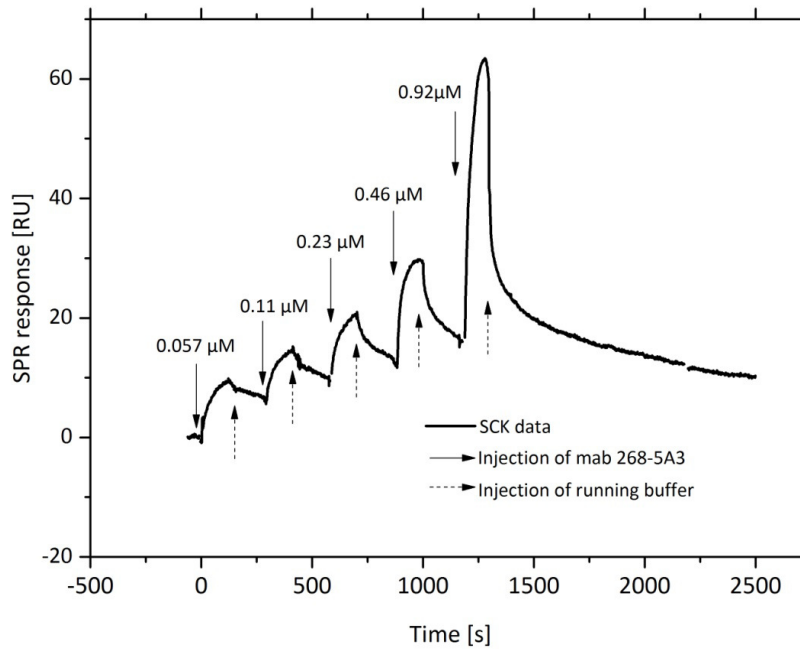

Figure 22: SCK curve for antibody 268-5A3
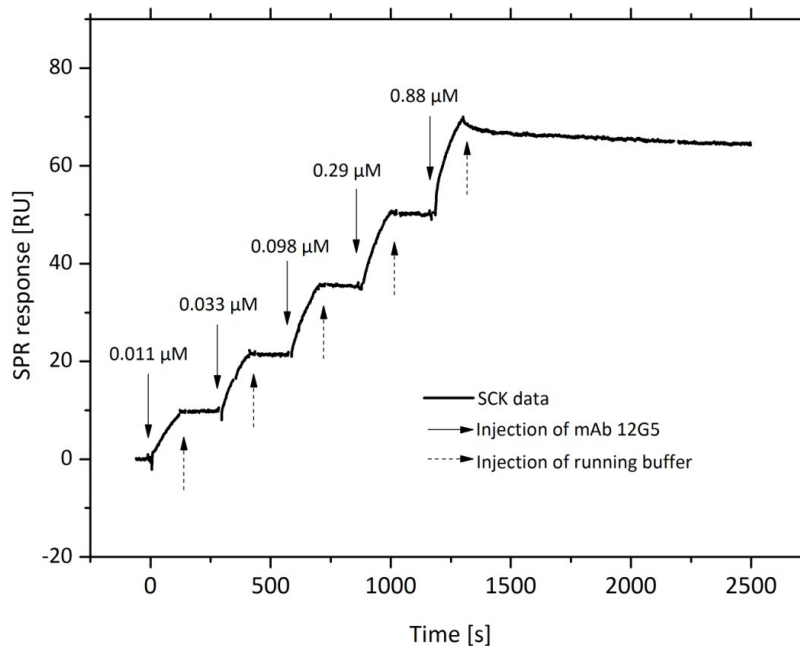
Figure 23: SCK curve for antibody 266-12G5

Table 4: Affinity constants determined by SPR measurements with 5 different concentration steps (n = 5)

mAb	k_a [1/Ms]	k_d [1/s]	K_D* [M]
268-5A3	$(1.1 \pm 0.025) \times 10^4$	$(1.7 \pm 0.53) \times 10^{-2}$	1.6×10^{-6}
266-6D8	$(0.65 \pm 0.026) \times 10^4$	$(2.3 \pm 0.53) \times 10^{-5}$	3.5×10^{-9}
266-8B1	$(1.2 \pm 0.016) \times 10^4$	$(2.4 \pm 0.064) \times 10^{-5}$	2.0×10^{-9}
266-10C9	$(0.98 \pm 0.042) \times 10^4$	$(6.2 \pm 0.75) \times 10^{-5}$	6.3×10^{-9}
266-12G5	$(23 \pm 1.0) \times 10^4$	$(3.5 \pm 0.063) \times 10^{-5}$	1.5×10^{-10}

* dissociation constant ($K_D = k_d/k_a$)
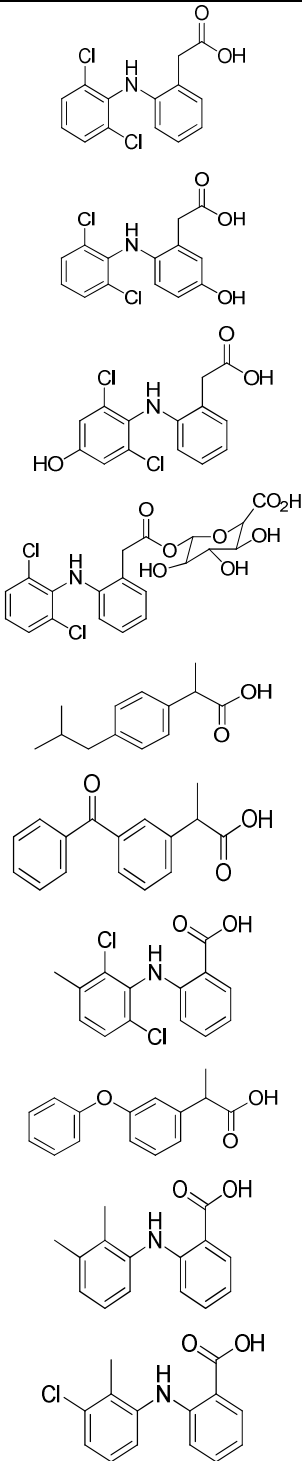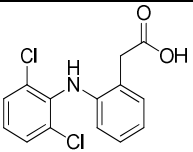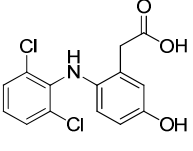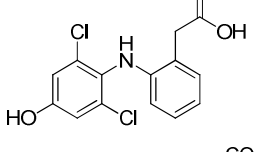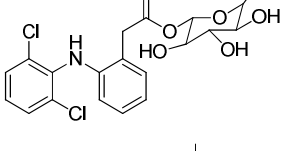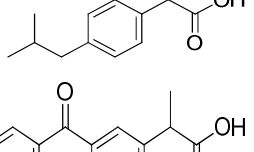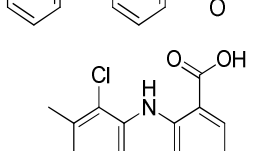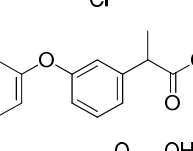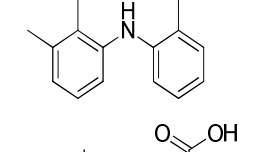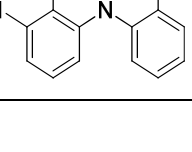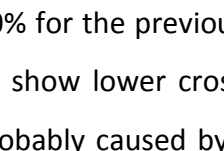
1.2.3 Cross reactivity

During the detection of DCF in surface and waste water, other human metabolites can cross react with the antibodies. The major human metabolites are the 5-OH-DCF, 4'-OH-DCF and DCF-GLU components (Table 5). The selsctivities of the mAbs were tested as reported for the polyclonal antiserum by determination of the cross reactivity (CR) with human DCF metabolites and other pharmaceuticals (Deng, 2003). CR is the ratio between the IC_{50} values for different compounds in % (Equation 6).

Predominantly, the 4'OH-DCF compound is found in wastewater treatment plant effluents (Osorio, 2014). The CR of the 4 mAbs with high affinity towards DCF were between 1.7 and 24%. This CR is comparably low and since the metabolites will occur in less amounts than DCF itself, the CR will not disturb the analytical method.

For antibody 6D8, the highest CR with the acyl glucuronide was detected with 24%. Its CR towards 5-OH- and 4'OH-DCF were relatively low with 3.5 and 6.2%. This observation indicates that mAb 6D8 binds predominantly to the part of the molecule that is opposite to the carboxyl group because the binding is less disturbed by a modification of the carboxyl group than by hydroxyl groups attached to the phenyl groups. MAb 8B1 cross reacts with DCF-GLU, 5-OH-DCF and 4'OH-DCF with 14, 9.6 and 1.7%, respectively. This indicates that the antibody recognizes the region of the chlorinated phenyl ring. For antibody 10C9 and 12G5 no specific binding region can be concluded from the CR with DCF metabolites. Since the CR is about 10% for the three metabolites tested, they might react in the region of the secondary amino group which is similar for the metabolites tested.

Table 5: Cross reactivity (CR) for mAbs with DCF metabolites and structurally similar pharmaceuticals

Compound		6D8	8B1	10C9	12G5
			CR (in %)		
DCF		100	100	100	100
5-OH-DCF		3.5	9.6	10	13
4'-OH-DCF		6.2	1.7	5.3	11
DCF-GLU		24	14	8.8	8.5
Ibuprofen		< 0.42	< 0.10	< 0.43	< 0.0069
Ketoprofen		< 0.42	< 0.10	< 0.43	< 0.069
Meclofenamic acid		< 0.42	< 0.10	< 0.43	0.35
Fenoprofen		< 0.25	< 0.06	< 0.43	< 0.25
Mefenamic acid		2.4	0.74	< 0.43	0.55
Tolfenamic acid		3.5	4.0	17	0.85

Compared to the CR of 100% for the previously reported polyclonal antiserum (Deng 2003), the monoclonal antibodies show lower cross reactivity towards the 5-OH-DCF metabolite. This higher specificity is probably caused by the separation of individual antibodies from a

complete antiserum by the hybridoma technique. In the polyclonal antiserum, all antibodies contribute to the final specificity. The mAbs represent single antibodies and therefore, the CR is lower towards this metabolite.

In addition to human metabolites of DCF, other pharmaceuticals can occur in WWTP effluents and fresh water samples. For this reason, the frequently consumed analgesics ibuprofen, ketoprofen, meclofenamic acid, fenoprofen, mefenamic acid and tolfenamic acid were also tested for CR with anti-DCF antibodies (Table 5). In comparison to the metabolites, CR was usually low. For ibuprofen, ketoprofen and fenoprofen, no CR was detected, because their assay sensitivities were above 1.0 mg/L with this compound. For instance, these three pharmaceuticals are not carrying a secondary amino group attached to phenyl rings. Probably, this amino group plays an important role for antibody binding probably by hydrogen bond formation. For mAbs 6D8, 8B1 and 10C9, the CR towards meclofenamic acid could not be detected. Only mAb 12G5 had a minor CR of 0.35% with this compound. The binding of the other mAbs were completely disturbed by the methyl group next to the chlorine. All antibodies could also react with mefenamic acid and tolfenamic acid with CR between 0.55 to 17%.

MAb 12G5 had the lowest CR with 0.55 and 0.85% indicating an important influence of the chlorine in α-position to the amino group for the interaction with the molecule.

MAb 10C9 did not cross-react with mefenamic acid, but with 17% the CR towards tolfenamic acid was relatively high. The non-covalent interaction is increased by the chlorine atom on the phenyl ring. This chlorine band seems to be important for the binding of mAb 8B1, too, because its CR towards tolfenamic acid is higher than for mefenamic acid with 4.0% and 0.74% respectively. The CR for mAb 6D8 is not influenced by the chlorine atoms, because it cross reacts to similar extent with mefenamic acid and tolfenamic acid (2.4 and 3.5%). As already mentioned above, it might react in opposite position of the carboxyl group as indicated in Figure 24. In summary, the CR of the mAbs towards other analgesics is well below 25%.
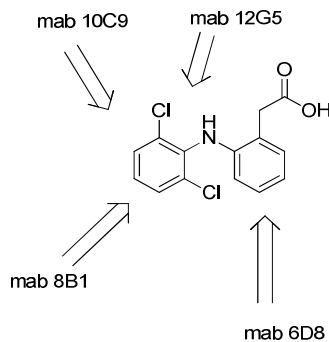
Figure 24: Molecular structure of DCF and possible major recognition sites for the developed mAbs

1.3 Effect of organic solvents on antibody affinity in ELISA

For immunosensing applications and flow-through assays, it will be an important feature of the developed antibodies to bind DCF in the presence of organic solvents like MeOH. Therefore, the CCS screening was carried out with DCF standard solutions containing 10% MeOH. However, for some applications more than 20% of final solvent concentrations may be necessary for example to avoid carry-over of analytes in the flow-through capillaries.

Consequently, the antibodies were tested regarding their stability in MeOH, ACN and EtOH. In these experiments, the standard solutions were prepared with different contents of organic solvent starting from 25% to 13%, 6.5% and finally 0%. In Figure 25, the corresponding calibration curves for mAb 8B1 are shown. The incubation time for the antibody competition step was 1 h. The IC_{50} values are increasing with increasing MeOH content. However, their coefficients of correlation were still high: $R^2 \geq 0.99$ (n=7, m=3). Subsequently, the interaction of DCF with the mAb is disturbed by the solvent. The non-covalent interactions like hydrogen bonds for the immune-recognition are influenced by the organic solvent. Nevertheless, the mAb can still bind to DCF in solution and to DCF-OVA absorbed on the MTP.

Similar observations were made with the other mAbs 6D8, 10C9 and 12G5. For methanol, all of the antibodies yielded an $IC_{50} < 10$ µg/L and good calibration curves with $R^2 \geq 0.99$ (n = 8, m = 3). For ACN and EtOH, the mAbs were not as robust as in MeOH. MAb 10C9 did not tolerate ACN at all and only 6% of EtOH. MAb 6D8 was stable in 6% ACN and 13% EtOH. Antibodies 8B1 and 12G5 accepted up to 13% of ACN and EtOH. In summary (Table 6), the developed mAbs can be used for calibration and measurements with organic solvent. It is best, to used MeOH. ACN and EtOH can also be used for mAbs 6D8, 8B1 and 12G5.
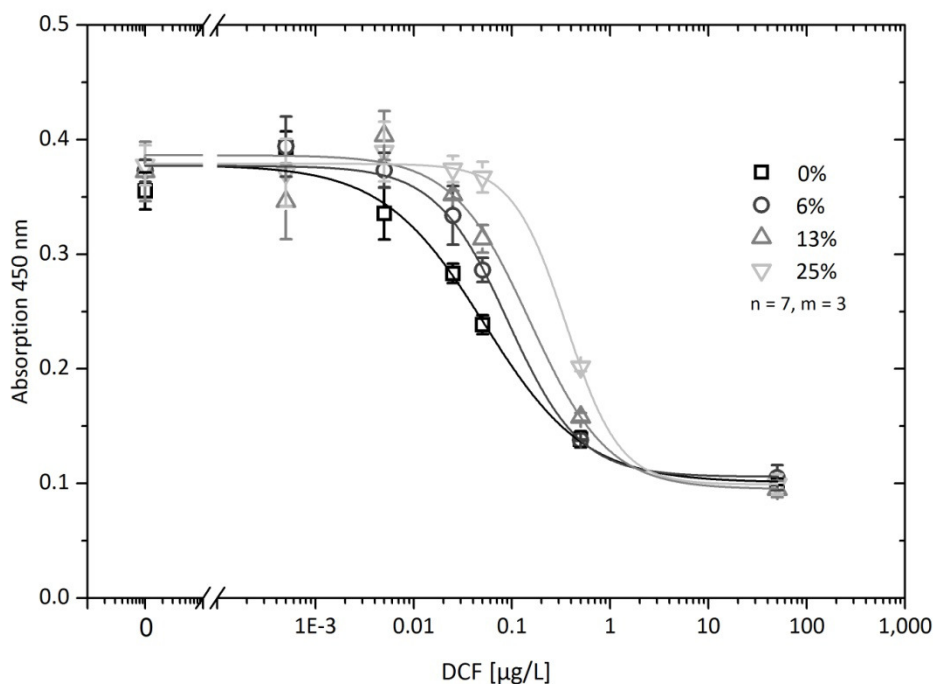
Figure 25: Dose-response curves for mAb 8B1 at different MeOH contents in DCF standard solutions

Table 6: Stability of mAbs in organic solvents in standard solutions for 1 h incubation time (IC$_{50}$ < 10 µg/L, R^2 ≥ 0.99)

mAb	MeOH	ACN	EtOH
		[%] (v/v)	
6D8	25	6	13
8B1	25	13	13
10C9	25	0	6
12G5	25	13	13

1.4 Protocol optimization

The purified mAbs presented in section 1.2 were all used for an indirect competitive ELISA for the detection of DCF. For antibody 268-5A3, no competition was observed in the calibration range between 0.001 to 100 µg/L. This observation is probably caused by the low affinity of this antibody as shown by SPR experiments. For this antibody, the protocol was not optimized any further.

The other mAbs 6D8, 8B1, 10C9 and 12G5 were used to optimize assay conditions for calibration in ultrapure water. The antibody concentration has to be low in order to achieve the highest assay sensitivity and lowest LOD. However, the signal intensity has to be high enough to obtain reasonable calibration curves. Consequently, the antibody dilution was optimized to give absorption at 450 nm of about 1.0 after 15 min of TMB reaction. The dilution factors were between 40,000 to 100,000 as shown in Table 7.

For the remaining 4 antibodies from mouse 266, an indirect competitive ELISA was developed based on the protocol used for CCS screening. In the beginning, the concentration of the DCF-OVA coating antigen was reduced from 1 µg/mL to 0.5 µg/mL resulting in lower IC_{50} values by a factor 2 for all antibodies. Moreover, it was necessary to prepare a new stock solution of coating antigen DCF-OVA in coating buffer every day. The coating antigen seemed to age and the reproducibility was bad if it was not prepared freshly.

In addition, the interaction time during the competitive incubation step was shortened from 1 h to 0.5 h for equal or better assay sensitivity. A reduction of the incubation time with anti-mouse-POD label from 1h to 0.5 h or 0.25 h resulted in lower assay sensitivity for mAbs 6D8, 8B1 and 10C9. Therefore, the labeling time remained at 1 h for all antibodies. In conclusion, the overall assay time was 3 h including the blocking, competition, labeling, substrate reaction and read-out of absorption.

In Figure 26, the curves for a typical calibration with the optimized ELISA protocol are shown. The calibration was carried out on one plate measured in triplicate for each antibody. The intra-assay RSD of the measured absorbance was lower than 5% in average (on a single MTP). Therefore, the LOD at a signal to noise ratio (S/N) of 3 was defined at 85% of the maximum signal intensity (Table 7). The analytical working range is defined as the quasi-linear part of the curve between 20% and 80% inhibition.
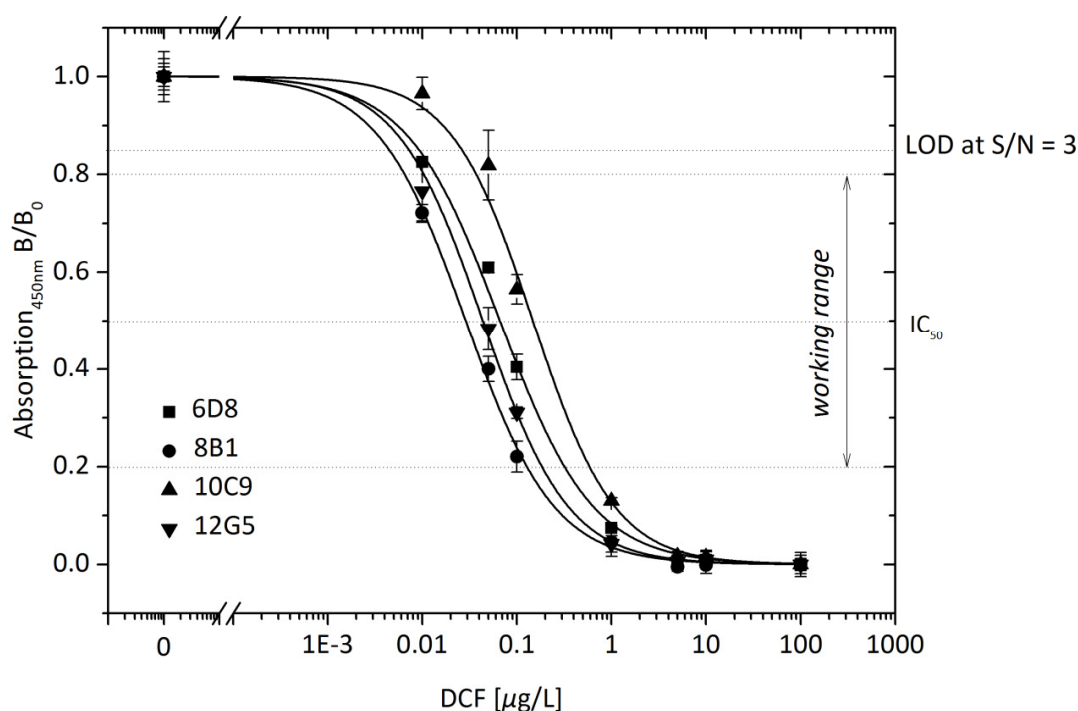
Figure 26: Calibration curves for purified monoclonal antibodies on one MTP (n = 8, m = 3).

Table 7: Sensitivity in ELISA and inter-assay variance on different MTPs on different days (n = 8, m = 3)

mAb	Dilution factor for ELISA	LOD [ng/L]	RSD in %	IC_{50} [ng/L]	RSD in %	Working range [µg/L]
6D8	40 000	8.9 ± 1.1	13	68 ± 2.4	4	0.013 – 0.35
8B1	60 000	4.5 ± 1.6	35	29 ± 2.9	10	0.0065 – 0.13
10C9	100 000	24 ± 5.0	21	142 ± 18	13	0.035 – 0.58
12G5	100 000	7.8 ± 1.8	23	44 ± 1.8	4	0.011 – 0.18

In the presented inter-assay study (Table 7), calibrations with 8 different DCF concentration between 0 to 100 µg/L DCF were carried out on different days (n = 8, m = 3). The correlation coefficient R^2 was ≥ 0.99 for the different calibrations for 4 different antibodies. The LOD for 10C9 is highest with 24 ng/L. The relative standard deviation (RSD) of this LOD for mAb 10C9 study was relatively high with 21%. Antibodies 6D8 and 8B1 allowed highly sensitive assay calibrations with LODs of 8.9 and 4.5 ng/L, respectively. The LOD for antibody 12G5 was 7.8 ng/L ± 23%. The total variation was less than 3 ng/L for mAbs 6D8, 8B1 and 12G5, so their reliability was comparable. The same observation is made for comparing the IC_{50} values of

these mAbs. The working range was wider for mAb 6D8, ranging from 0.013 to 0.35 µg/L. The three mAbs were highly sensitive and allowed reproducible calibration curves in ELISA experiments.

1.5 Matrix effects in fresh water

During the analysis of real samples like fresh water and wastewater matrix effects can occur. In general, a suppressed ELISA signal is generated and leading to overestimated target analyte concentrations. Beside interferences by structurally closely related chemicals (specificity) differences in the pH-value, ionic strength, existing pollutants like organic solvents and surfactants, between a sample and the solvent used for calibration (e.g., buffer or pure water) can have significant effect on antibody binding. Therefore, the effect of pH value, Ca^{2+} concentration and humic acid (sodium salt from Carl Roth) concentration was investigated in detail and results are illustrated in Figures 27-29. While antibodies 6D8, 8B1 and 10C9 were negatively influenced at pH 5.2 (a significant increase in the IC_{50} value was noticed) mAb 12G5 was not affected in the tested pH range. Furthermore, while antibodies 10C9 and 8B1 were sensitive only at highest humic acid concentration of 20 mg/L, mAb 6D8 was already influenced at 5 mg/L. Interestingly, mAb 12G5 was insensitive over the complete concentration range. In the same way, a Ca^{2+} concentration ≤ 75 mg/L was tolerated by this antibody. Concluding, based on its stability mAb 12G5 was selected to perform ELISA application to fresh water and wastewater analysis.
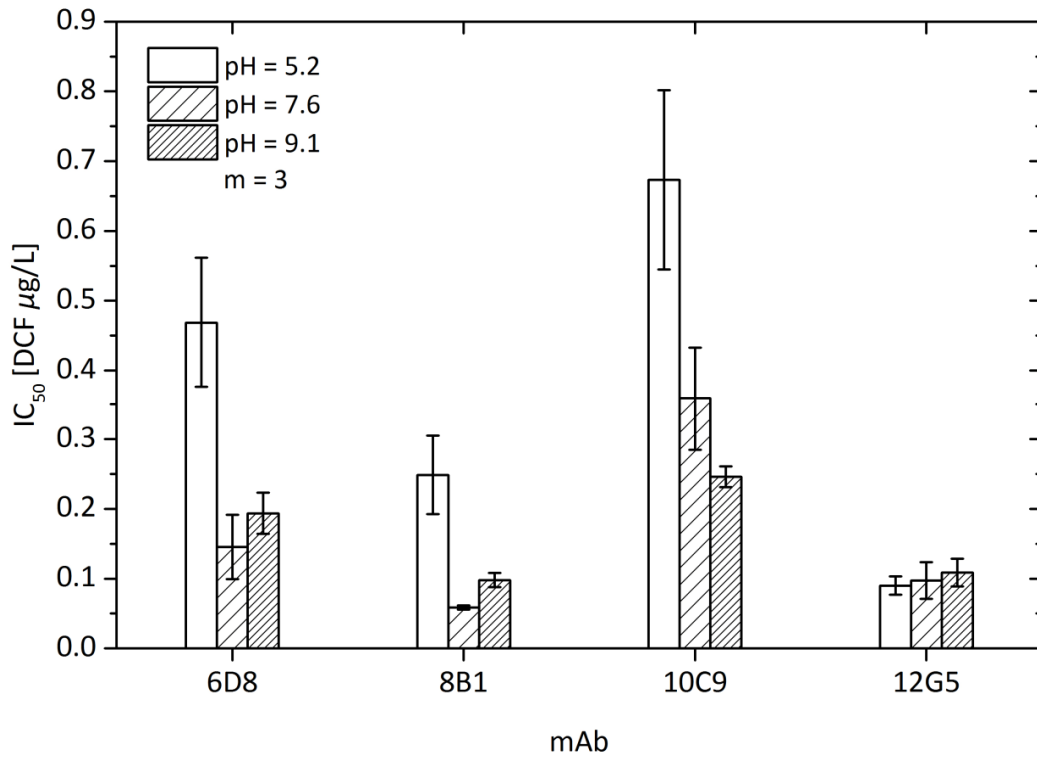
Figure 27: Effect of sample pH-value (5.2, 7.6, and 9.2) on the IC_{50} value (µg/L) of the DCF calibration curve established with four monoclonal antibodies.
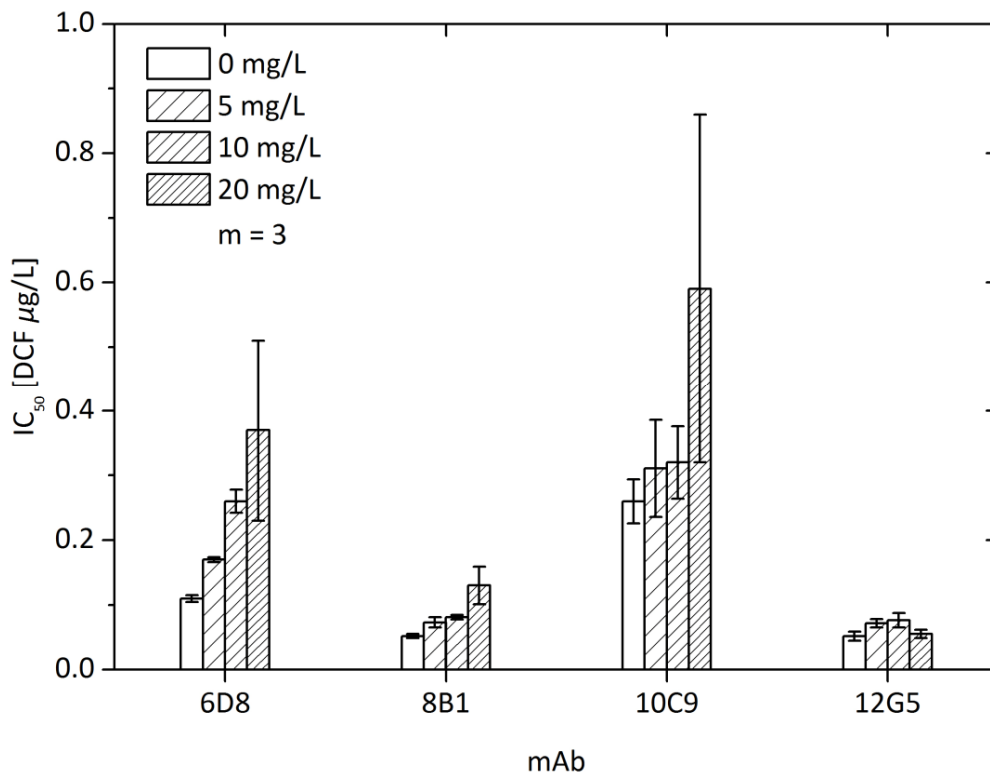
Figure 28: Effect of humic acid concentration (0, 5, 10, and 20 mg/L) on the IC_{50} value (µg/L) of the DCF calibration curve established with four monoclonal antibodies.
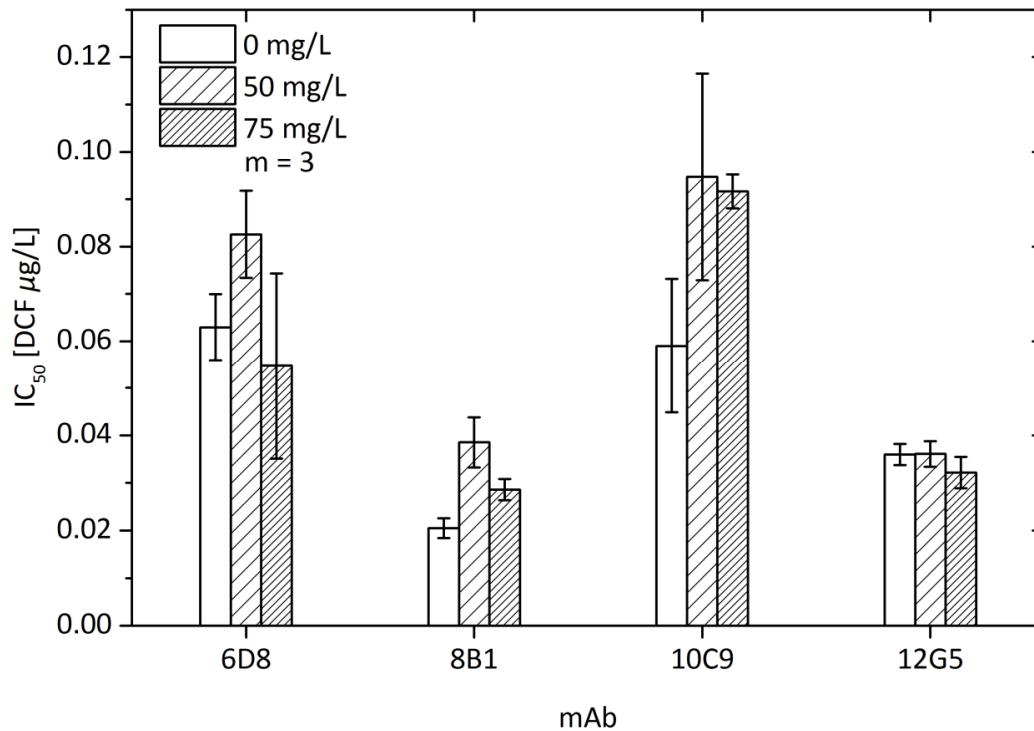
Figure 29: Effect of calcium ion concentration (0, 50, and 75 mg/L) on the IC_{50} value (µg/L) of the DCF calibration curve established with four monoclonal antibodies.

For the analytical method based mAb 12G5, recoveries were (114 ± 29)% for a spiked river (Isar) and a lake (Wörthsee) water sample at 0.2, 0.1 and 0.05 µg/L . Consequently, matrix effects influence the recovery in ELISA experiments. The influence of the matrix parameter on recovery rates was further investigated. In Figure 30, the influence of humic acids on the recovery rate is shown. To ultrapure water, humic acid sodium salt from Carl Roth was added in concentrations of 1 − 8 mg/L. These artificial samples were spiked with 50 ng/L DCF.

For concentrations of 1 to 4 mg/L, the recoveries are in between 92 to 97 % with deviations of up to ± 11%. For these concentrations, the antibody binds less reproducibly to the DCF in solution and on the plate surface compared to 0 mg/L humic acid concentration with a recovery of (100 ± 3)%. From 5 mg/L of humic acid, the recovery exceeds 100%. This observation shows that the recognition of DCF in solution is disturbed in an arbitrary way. Accordingly, the matrix effects cause an increased fluctuation of the recovery rate and shift the recovery for high loads of chaotropic ions or humic substances.
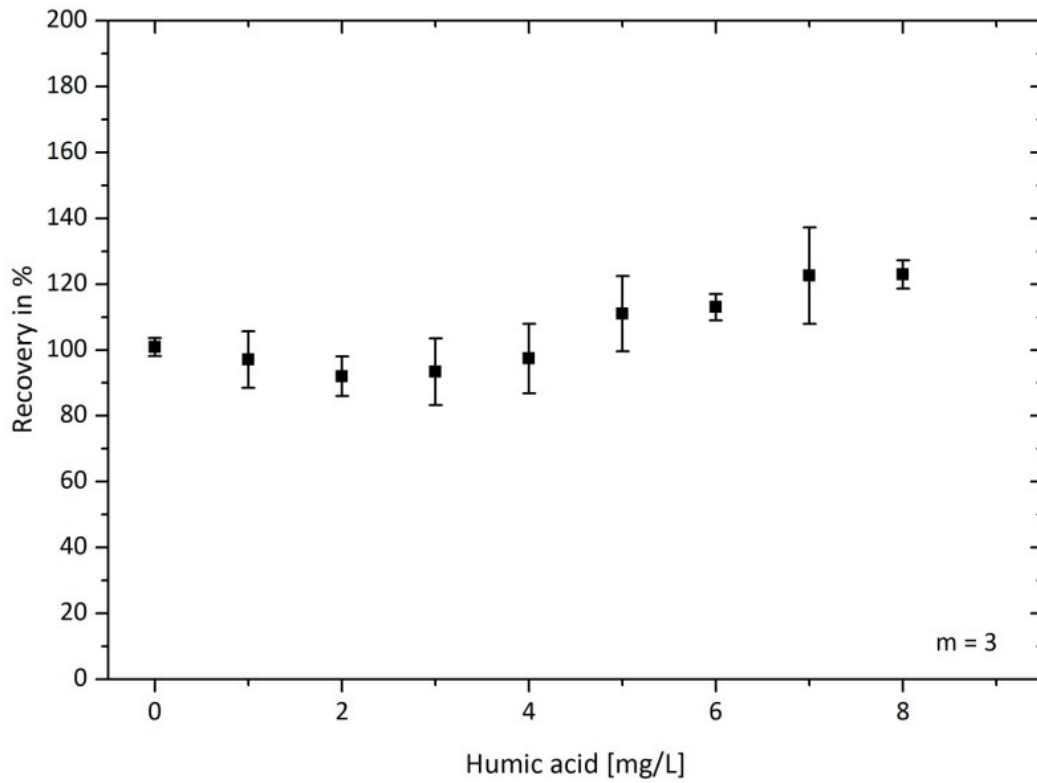
Figure 30: Influence of humic acid sodium salt on recoveries in ELISA with monoclonal antibody 12G5 at fortification level 50 ng/L DCF
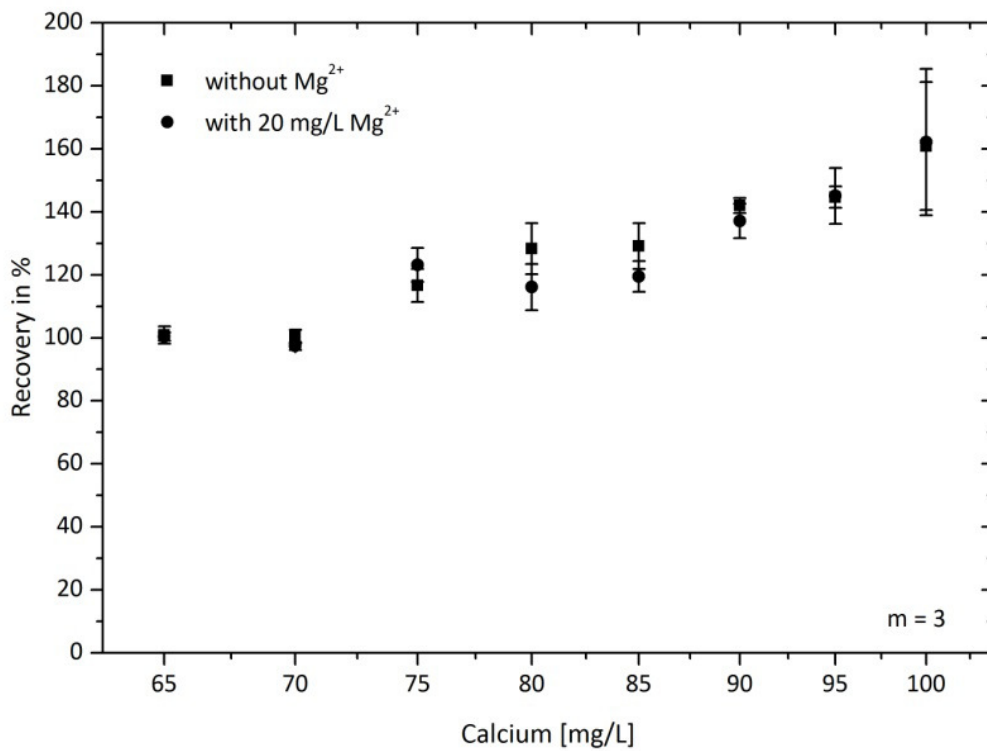
Figure 31: Influence of calcium or magnesium ions on recoveries in ELISA with monoclonal antibody 12G5 at fortification level 50 ng/L DCF

In Figure 31, the influence of Ca^{2+} on the recovery values for fortified ultrapure water (50 ng/L) is shown. The ion concentration was raised from 65 to 100 mg/L what exceeded the value for a typical concentration in Munich drinking water (see also Table 8). For this experiment, no EDTA was added.

At concentrations of up to 70 mg/L, the calcium is tolerated by antibody 12G5. With increasing ion concentration, the recovery becomes higher and less precise with standard deviations of up to ± 20%. Ca^{2+} is an ion agent that disrupts the non-covalent interactions by shielding charges and destabilizing hydrogen bonds. In this way, the binding sites for DCF can be disturbed. The effect of an increasing recovery with a higher Ca^{2+} concentration show that less antibody can be detected on the microtiter plate. Accordingly, the binding site for DCF is blocked and this simulates a higher DCF concentration than the sample is originally containing. The addition of Mg^{2+} at 20 mg/L like it can occur in drinking or fresh water samples, does not affect the recovery any further.

In the tested fresh water samples which were used to determine the recovery as stated above, calcium concentration was below 65 mg/L and magnesium was below 17 mg/L (see also Table 19 in the Experimental Section). Therefore, the fluctuations of recovery rate were probably caused by humic acids.

In surface and wastewater samples, other pharmaceuticals and human metabolites of DCF can occur beside DCF as described above. Antibodies bind to the analyte based on molecular structure of the target. Therefore, specificity of 266-12G5 was investigated by using the optimized protocol (Table 8). In comparison to Table 5, no MeOH was added to the standard for calibration, the coating procedure was optimized and the time for competitive mAb binding was reduced to 0.5 h. The results in Table 8 were achieved by using a 1 h competition step and organic solvents in the standard solutions. The human metabolites of DCF were tested. For the major metabolite 4'-OH-DCF, the cross reactivity was 5.0%. For two other human metabolites, 5-OH-DCF and for DCF-GLU it was 5.0 and 1.5 %. Pharmaceuticals with similar molecular structure showed low cross-reactivity with values between 0.0005 to 5.0 %. In comparison with Table 5, the optimized protocol allows lower CR for the metabolites tested by a factor 2. For the tested pharmaceuticals, the CR are still low. For mefenamic acid, a CR of 5% was measured instead of 0.55% in Table 5. The optimized assay conditions allow better antibody binding to mefenamic acid for mAb 12G5.

Table 8: Cross reactivity for human metabolites of DCF and similar pharmaceuticals for mAb 12G5 with the optimized ELISA protocol

Compound	IC_{50} [µg/L]	CR in %
DCF	0.05	100
5-OH-DCF	3	1.5
4'-OH-DCF	1	5.0
DCF-GLU	1	5.0
Meclofenamic acid	5	1.0
Tolfenacmic acid	15	0.3
Mefenamic acid	1	5.0
Ketoprofen	> 1000	< 0.005
Fenoprofen	> 1000	< 0.005
Ibuprofen	90	0.05

1.6 Analysis of fresh water

The indirect competitive ELISA was used to measure DCF in fresh water samples (Figure 32, Table 9). The samples were taken from the river Isar and the lake Wörthsee in Bavaria, Germany. For blank water samples, the average blank value was within the range of the blank values in ultrapure water. All samples were run at least in triplicate and HPLC-MS was used as a reference method with SPE.

In Scharnitz - a village close to the source of the river Isar - DCF was found neither by ELISA nor by the reference method. More downstream, a sample was taken from the river in Munich. DCF was detected with 9 ng/L by ELISA and 12 ng/L respectively by HPLC-MS. Similar values were found in the lake Wörthsee with 10 and 15 ng/L. These values were below the LOQ for both methods. Isar water samples from Freising and Marzling were more polluted with DCF at concentrations of 79 and 25 ng/L as determined by ELISA and 66 or 24 ng/L by HPLC-MS. This can be explained by the location of the sampling spots more downstream than the sampling sites in Munich after 3 or 4 more WWTPs respectively. In average, the ELISA values do not differ significantly from the reference values (p-level = 0.78 for paired t-test, m = 4, α = 0.05).
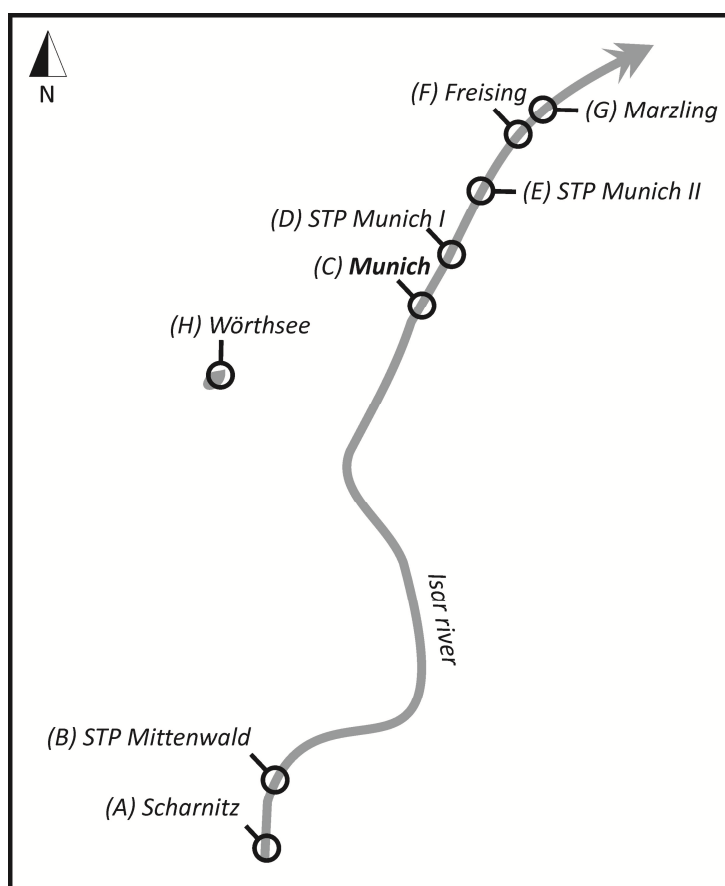
Figure 32: Sampling sites of fresh water (A, C, F, G, H) and wastewater (B, D, E) along the river *Isar* and at the Wörthsee

Table 9: Results for the analysis of fresh water samples

Fresh water	ELISA	HPLC-MS
	DCF [µg/L]	
Isar (A)	< LOD	< LOD
Isar (C)	0.009*	0.013*
Isar (F)	0.079	0.066
Isar (G)	0.025	0.025
Wörthsee (H)	0.010*	0.015*
Mean ± SD (m = 4)	0.031 ± 0.0011	0.030 ± 0.00062
p-level for paired t-test	0.78	
* < LOQ		

1.7 Analysis of wastewater

Monoclonal antibody 12G5 was used to analyze wastewater samples from wastewater treatment plant (WWTP) influents and effluents. The concentrations were high, so a

63

minimum dilution of 1/20 was necessary for quantification in ELISA. For ELISA, the influent sample preparation was carried out once with filtration and once without filtration before dilution (Figure 33). The values do not differ significantly with a p-level for a paired t-test of 0.31 (α = 0.05, m = 3). Consequently, the samples could be analyzed without a filtration step prior to dilution. For SPE, the samples were filtrated anyway and therefore, filtrated influent and effluent samples were used for comparison to HPLC-MS.

In average, ELISA found concentrations of (2.5 ± 0.72) µg/L and the reference method (2.2 ± 0.66) µg/L (Table 10) for wastewater samples. The results of both methods do not deviate significantly as determined by a paired t-test (p-level = 0.056, m = 6, α = 0.05). The trend for higher values in ELISA can be explained by possible losses of the analyte during SPE for HPLC-MS analysis and by CR for ELISA with 4'OH-DCF raising the recovery rate, too.

According to ELISA, the influent samples contained concentrations of 2.1 to 3.9 µg/L. The effluent samples contained 1.6 to 2.9 µg/L. The influent samples contained more DCF than the effluent samples. ELISA showed a degradation of DCF of 25-28% and HPLC-MS of 17-52%. This means, that in average 70% DCF is passing through the WWTPs. Consequently, DCF was found in fresh water, too, as described above (Table 9).
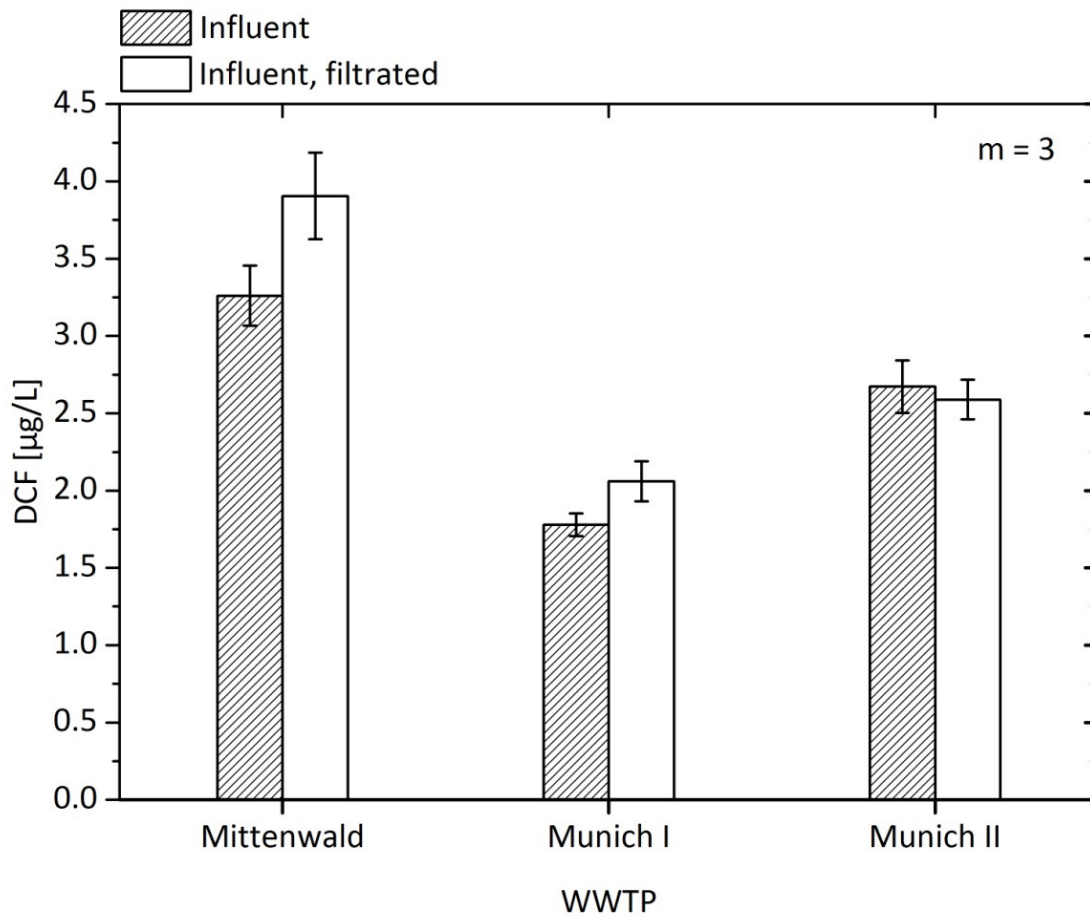
Figure 33: Results for wastewater analysis with and without filtration prior to dilution for ELISA analysis. Error bars represent standard deviations for measurements in triplicate ±s

Table 10: Assessment of ELISA results in comparison to HPLC-MS

WWTP	sample	ELISA		HPLC-MS	
		DCF [µg/L]	Degradation in %	DCF [µg/L]	Degradation in %
Mittenwald	influent	3.9		3.4	
	effluent	2.9	26	2.6	24
Munich I	influent	2.1		1.8	
	effluent	1.6	25	1.5	17
Munich II	influent	2.6		2.7	
	effluent	1.9	28	1.3	52
Mean ± SD (m = 6)		2.5 ± 0.72		2.2 ± 0.66	
p-level for from paired t-test:		0.056			

2 Surface chemistry aspects for sensitive immunosensing of small analytes

Antibodies can be used for automated sensing devices based on label-free and label-based sensing principles. The surface chemistry used for these immunosensors is crucial for reproducible and sensitive measurements. Accordingly, for the detection of emerging pollutants, a stable and robust surface chemistry was developed and characterized.

2.1 Stability and reversibility of antibody binding to haptens on PEG modified surface preparations in QCM-D experiments

By QCM-D, binding capacities and regeneration steps can be monitored in real time on surface preparations. The recognition properties of the PEG surface modified with DCF were assessed by QCM-D using injection of a diluted polyclonal anti-DCF antiserum (0.1%). For QCM-sensors, the PEG-ylated quartz surface was completely covered with DCF. The resulting measurement data for the frequency shift and the dissipation are shown in Figure 34a. Before the antiserum injection, the frequency was stabilized in degassed PBS/EtOH (9/1 = v/v). Accordingly, the antiserum injection led to a decrease in the frequency, indicating the binding of antibodies. Then, the degassed PBS/EtOH solution was injected again to remove weakly bound antibodies and to measure the frequency shift due to affinity bound anti-DCF antibodies. Meanwhile, the dissipation increased when the diluted serum solution was injected and returned to its value when the buffer solution was added. After the stabilization of the signal, the measured frequency shift was 12Hz. As the dissipation at this step was very low, the Sauerbrey equation (Equation 9) can be applied which leads to a surface coverage of 42 ng/cm^2. This protein density corresponds to a thickness less than a monolayer (Boujday, 2009 b). After successive washing the surface with regeneration buffer and degassed PBS solution, the frequency returned to the initial value. This indicates that the bound protein was completely removed. Non-specific binding of an anti-mouse IgG (2 µg/mL) was not observed. On another surface preparation without DCF on the PEG layer, no antibody binding was observed.

To evaluate the stability of the DAPEG surface and to investigate the reproducibility of the procedure, several regeneration cycles were carried out. The signal of the stabilization is averaged over 120s. The resulting values and their standard deviations (m = 120) are shown

in Figure 34b. They indicate that the bound protein can be removed from the surface for at least 9 times. The average values for the stabilization of the frequency shift after the injection stayed constant over the first three measurements at approximately 12Hz. Afterwards, the signal varies within a range of 72 Hz with the exception of the 10th measurement which allowed only a very low frequency shift. This signal decrease is probably due to the long time (9h) the piezoelectric device was running.

The label-free detection of the bound material can be distorted by non-specific binding of other proteins from the polyclonal antiserum or the samples. For this reason, the non-specific binding of other proteins was investigated for the DAPEG-DCF layer on the quartz carrier (Figure 35). For the comparison of a dilution of 1 µL anti-DCF serum in 999 µL PBS containing 10 % EtOH, 1 µg mL^{-1} BSA and 1 µg mL^{-1} anti-zeraleon (a mycotoxin) were used. For the signal evaluation, the zero value for the signal was subtracted from the stabilized signal. After the antibody injection, the specific interaction allowed a frequency shift of - (11.5 ± 0.16) Hz. For the BSA solution -(5.36 ± 0.35) Hz were observed. This corresponds to 47% of the signal intensity. Hence, the non-specific binding to the functionalized surface can be almost the half of the signal intensity. For the dilution of another monoclonal antibody, the non-specific binding is − (1.54 ± 1.09) Hz which corresponds to 13% of the specific antiserum. This shows that the non-specific binding events can falsify the observed binding events. In order to evaluate the binding capacity of the surface for anti-DCF serum, different dilutions were measured.

The anti-DCF mAbs were also used to study their binding on the PEG modified quartz surface with DCF attached (Figure 36). MAb 6D8 allowed a good reproducibility in 3 binding experiments. However, the amount of bound mAb 6D8 was low compared to the other mAbs. For mAb 12G5, a high signal and reproducibility was achieved. Consequently, it can be used for flow-through assays based on this surface chemistry for the detection of DCF.
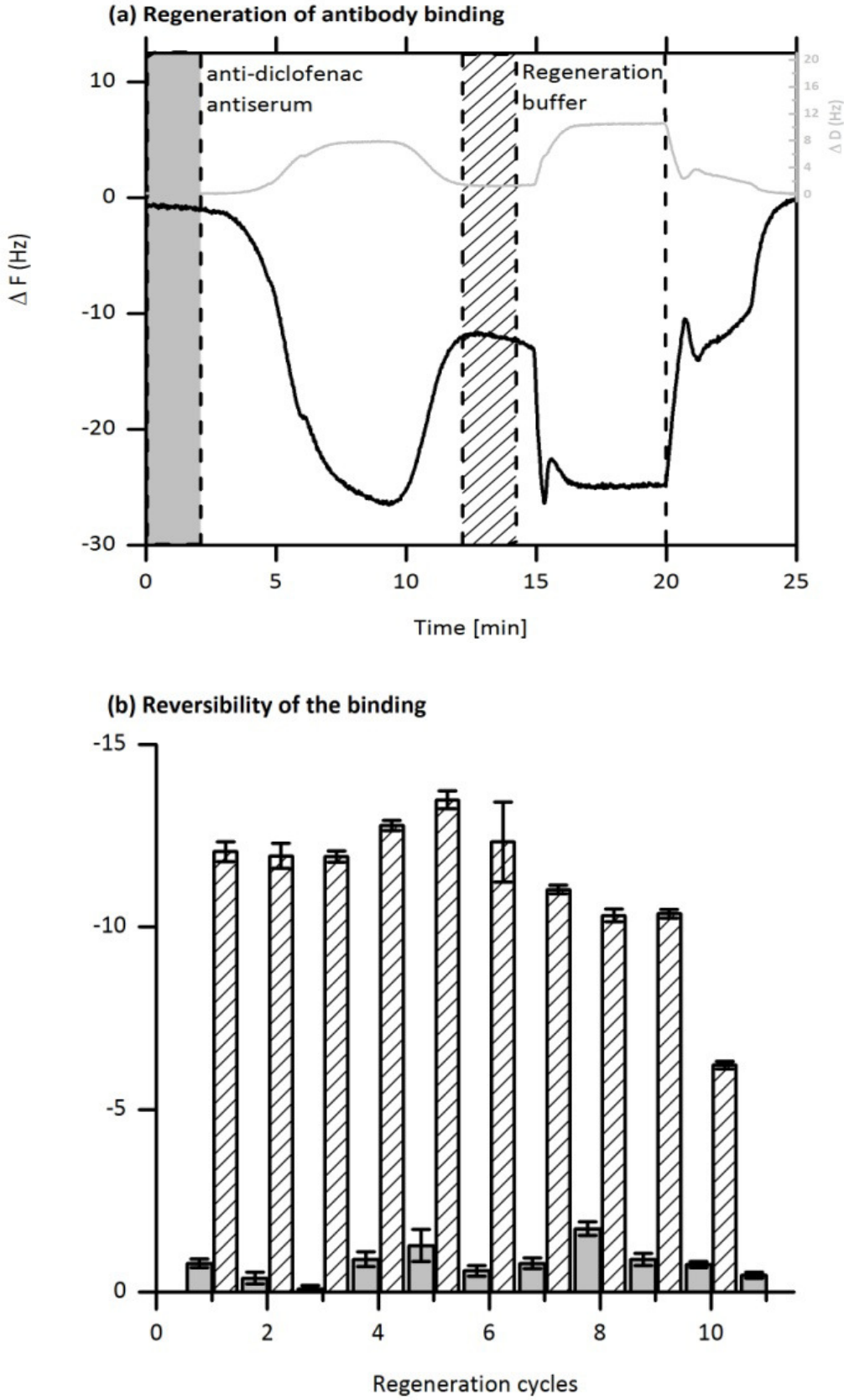
Figure 34: (a) Regeneration protocol and reversibility for anti-DCF antiserum binding to DCF immobilized on the DAPEG modified quartz surface. (b) The frequency shift was measured before and after the antiserum injection
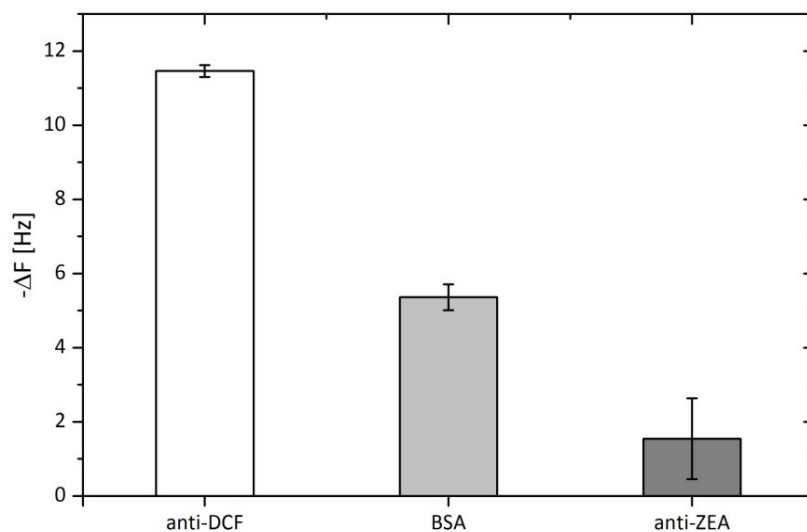
Figure 35: Frequency shift after the injection of different protein solutions (1 µg/mL)
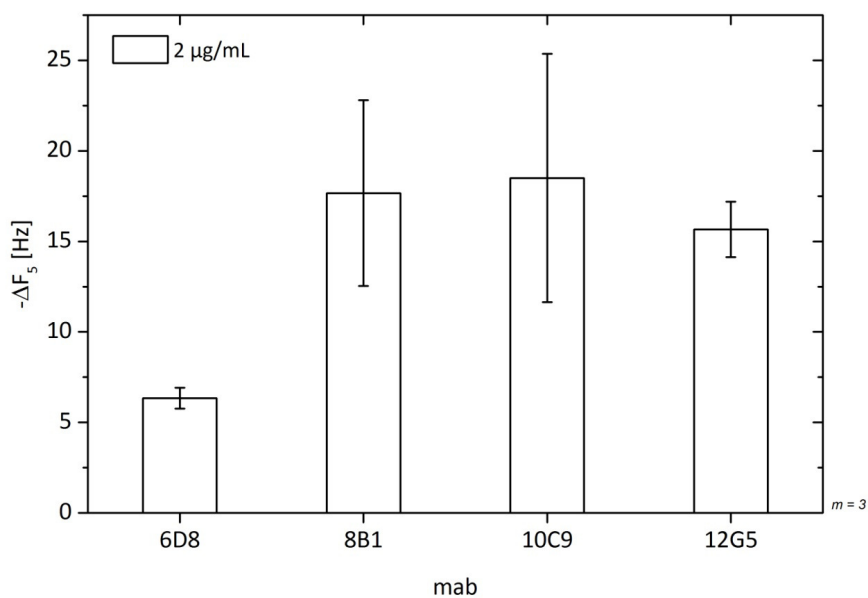
Figure 36: Binding of anti-DCF mAbs to DCF on PEG-ylated quartz surfaces in regeneration experiments

2.2 Microspotting of small molecules

In previous works (Sauceda-Friebe, 2011; Oswald, 2013), the analytes carrying a carboxylic acid function were activated by using hydroxybenzotriazole and 1-ethyl-3-(3-dimethylaminopropyl)carbodiimid (EDC) in carbonate buffer (0.30 g $NaHCO_3$ and 0.16 g Na_2CO_3 in 100 mL water, pH 8.5) containing 30% DMSO and 1% glycerol. This method was designed for a hapten concentration of 1 mg/mL in the spotting solution (about 1 to 3 mM).

2.2.1 A microspotting method for the immobilization of small molecules

The same method was applied for the microspotting of DCF and PBA (Figure 37). For DCF, the signal intensity was at 2800 a.u. for the polyclonal antiserum with a dilution of 1/5000. For PBA, no signal could be generated with this microspotting method. The high salt concentration in the microspotting buffer was probably reducing the solubility of PBA and prevented covalent immobilization on the surface.

For this reason, a new approach was carried out by eliminating any salts from the microspotting buffer and using organic solvents. In the beginning, the organic solvents were used exclusively. The solvent were chosen regarding their ability to activate primary amino groups as nucleophiles. In general, polar aprotic solvents are used for this purpose like DMSO, DMF or dioxane. The solvents were used to activate PBA by EDC and NHS and were used as described in Figure 38. By using this approach, PBA could be immobilized on the DAPEG surface by microcontact printing (Figure 39). The same method worked for DCF, too. The best coupling efficiency was achieved by using DMF or dioxane. For all solvents, 6 measurements were carried out successively on one chip (m = 6). The signal deviation was less than 2 % for the 6 measurements on one chip. Consequently, the microspotting method produces a regenerable microarray surface. For further experiments, dioxane was chosen because it is not toxic in contrast to DMF.

The spot size for this microspotting method can be influenced by using water in the spotting solution (Figure 40a). The supramolecular effects of adding the water to dioxane were investigated by contact angle measurements. In these measurements, single drops of about 10 µL are created and measured by a camera. The interfacial tension (IFT) of the drops can be measured for different ratios of water/dioxane (Figure 41). This magnitude describes the cohesive forces in the solvent drop. With an increasing amount of dioxane, the IFT of the pending water drop decreases. The hydrogen bonds between water molecules cause the high IFT of a water drop. By adding an organic solvent like dixoane, the molecular interactions become weaker and in this way, the IFT decreases. Subsequently. the volume of a drop is also decreasing.

The drops are deposited on a surface in order to measure the contact angle on a DAPEG surface preparation (Figure 42). The contact angle measurements show that the surface is covered on a larger area by adding more organic solvent. The pure dioxane spot has a lower

volume than the water drop. However, a higher dioxane content allows larger hapten spots on the surface. This observation indicates that the surface coverage is raised by more organic solvent due to supramolecular interactions of the binary water/dioxane system with the DAPEG surface. The maximum signal intensity is reached with 50 % dioxane in water Figure 40b) and the spots are more compact compared to 90% dioxane.
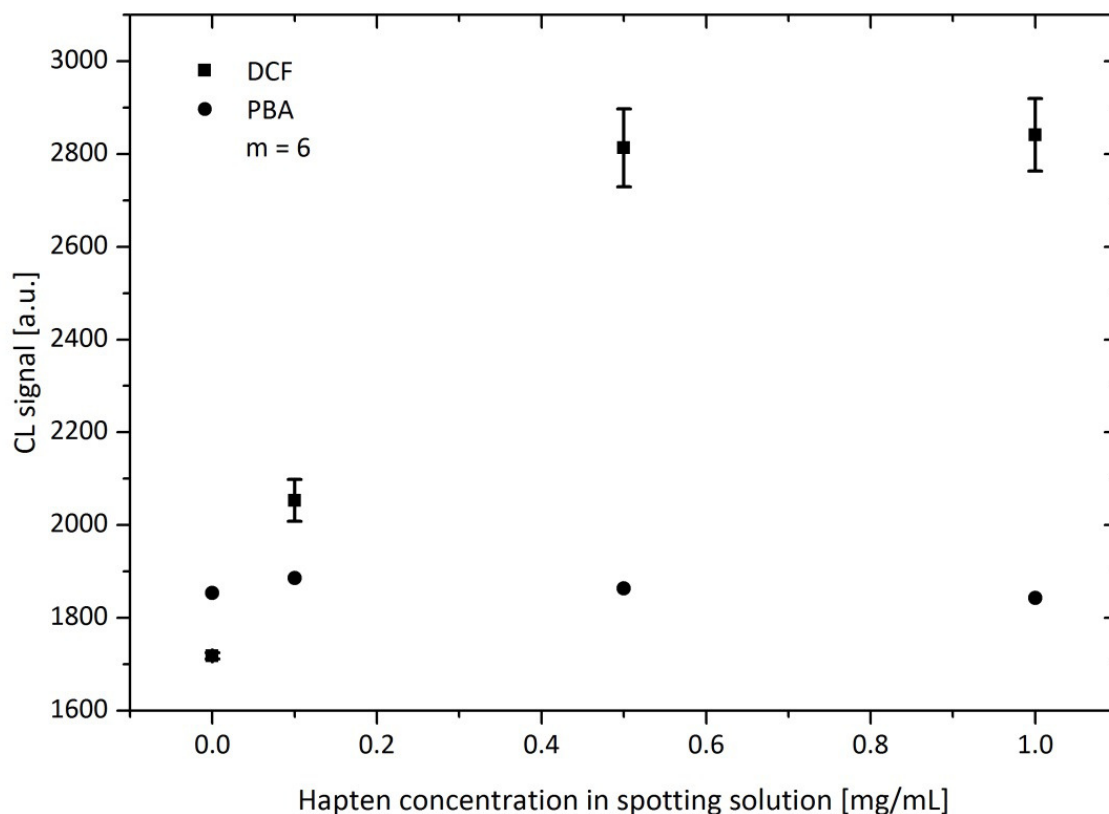
Figure 37: Microspotting by using the HOBt/EDC method
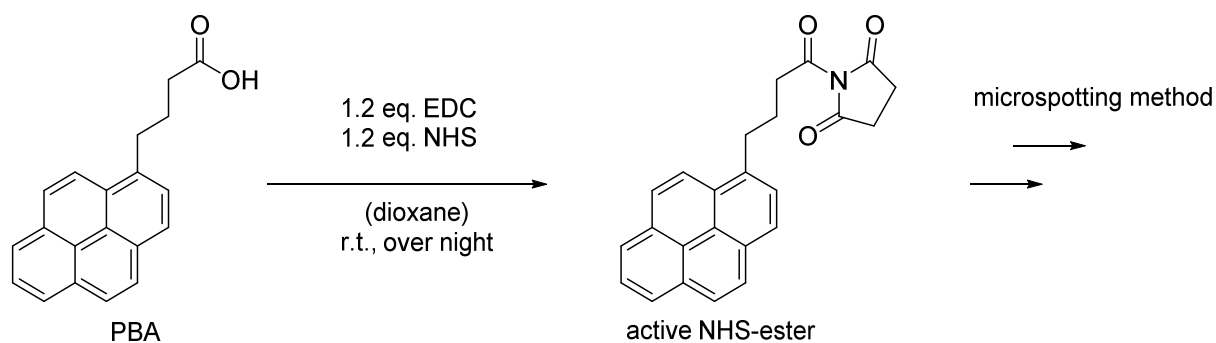
Figure 38: Active ester formation for PBA
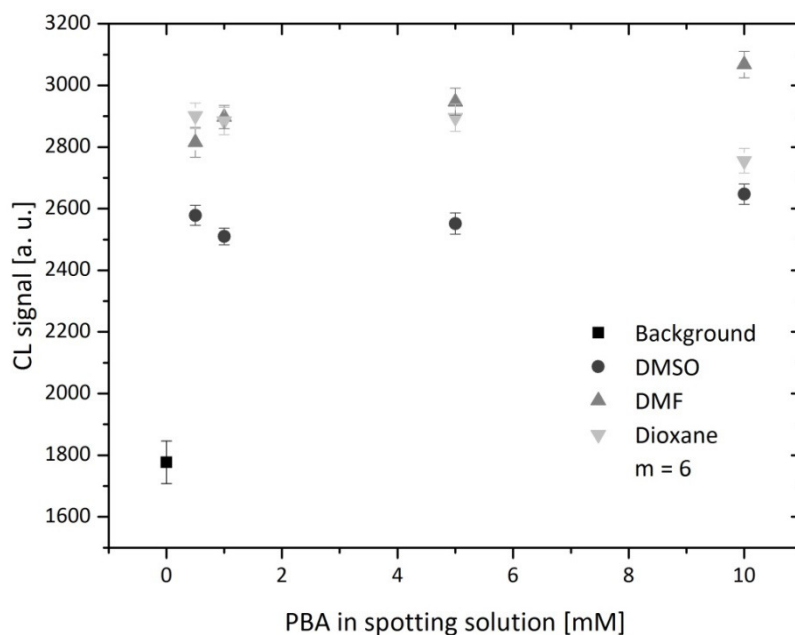
Figure 39: Activation of PBA by EDC/NHS and microspotting by using organic solvents
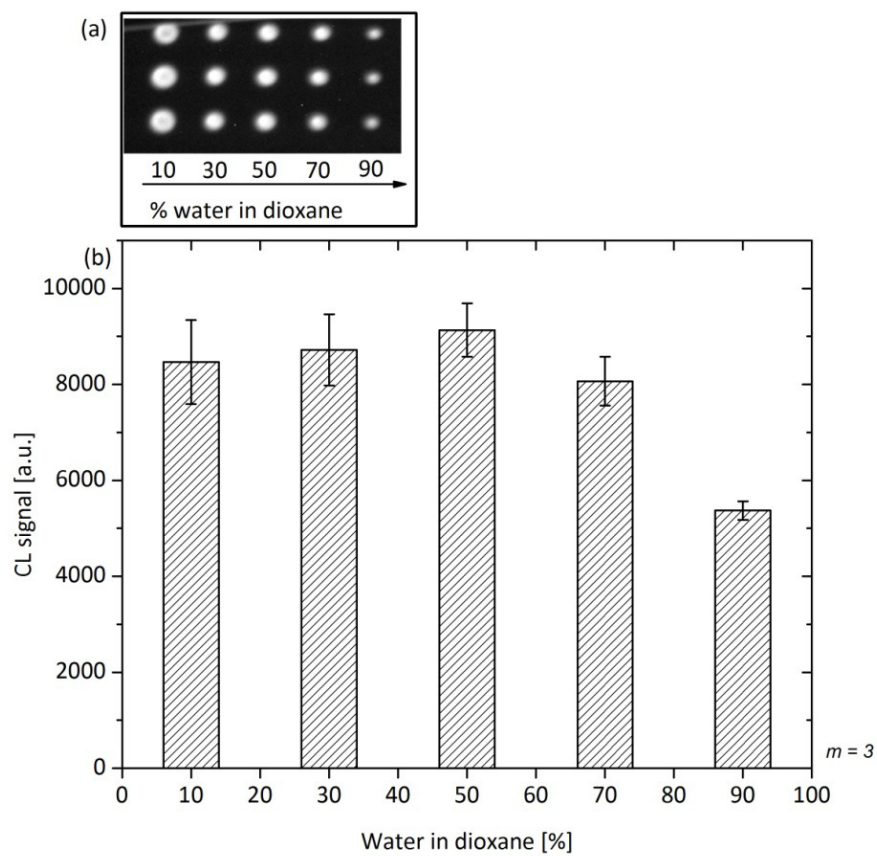
Figure 40: (a) Original image of anti-DCF captured by a surface with immobilized DCF (0.5 mM). (b) Average CL signal
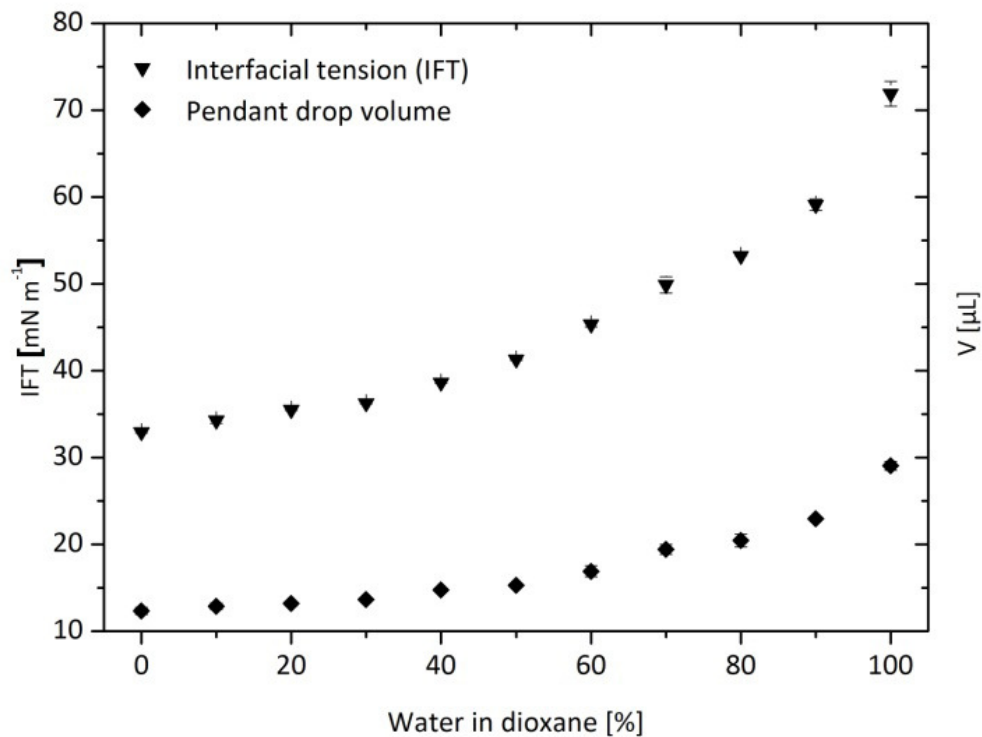
Figure 41: Interfacial tension and volumes of the pending drops for different water/dioxane compositions
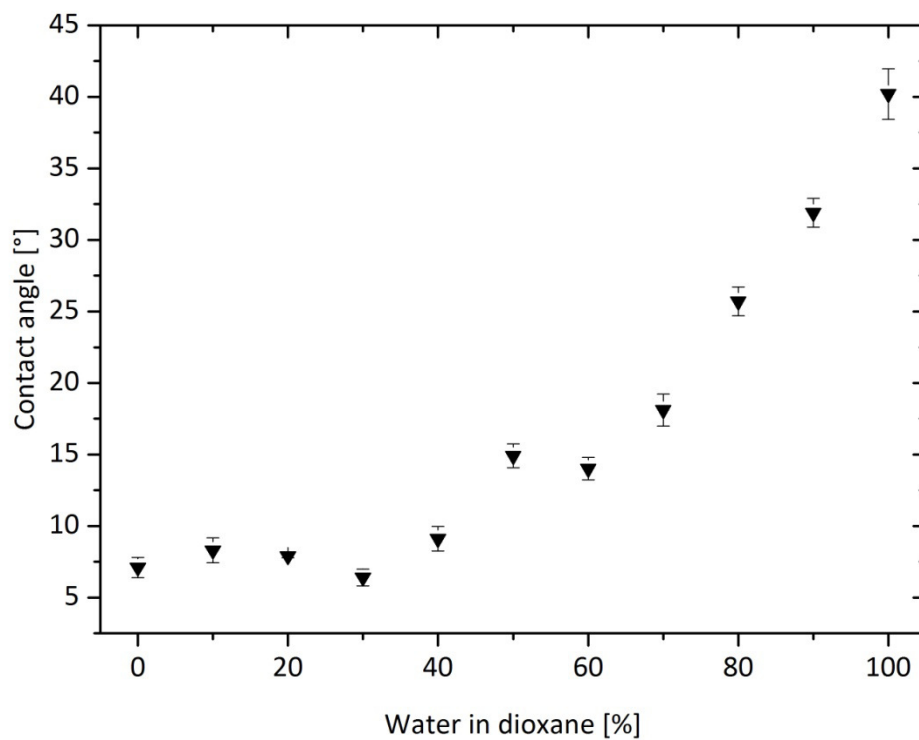
Figure 42: Contact angle on the DAPEG surface for different compositions of the binary system water/dioxane.

2.2.2 Optimization of the microspotting method and calibration of the flow-through ELISA for DCF

The amount of DCF in the spotting solution was optimized in regeneration measurements (Figure 43). The blank measurement was repeated 30 times with the polyclonal antiserum. During the first 3 measurements, the signal is increasing. Then, it can be observed that the signal is decreasing (Table 11). The decrease is smaller for 0.1 - 1 mM DCF compared to 5 - 10 mM: 87-89% compared to 80-85%. This observation can be explained by an access of DCF that is not bound covalently to the microarray surface and that is washed off during the regeneration cycles. For smaller amounts of DCF in the spotting solution, the access is smaller. In this way, the decrease is smaller. Consequently, the optimal spotting concentration of DCF is 0.5 mM or 1 mM. This concentration allows reasonable signal intensity and signal loss. For calculation of the LOD at SNR = 3, 23 regeneration measurements number (n = 21) are averaged for DCF = 0.5 mM and 1 mM in the spotting solution. The average standard deviation for the blank corrected maximum signal intensities is below 5%.

Figure 43: Regeneration of a microarray prepared with different amounts of DCF in the spotting solution. Error bars represent standard deviations for 5 different spots on one microarray.

Table 11: Signal intensity and decrease for different spotting concentrations of DCF.

	c (DCF)	0.1 mM	0.5 mM	1 mM	5 mM	10 mM
Measurements 4-6	Signal in the beginning	7974	8890	9749	10927	13965
Measurements 28-30	Signal at the end	7059	7868	8453	9297	11112
Signal decrease	100 % × (Signal at the end)/ (Signal in the beginning)	90%	90%	87%	85%	80%

The preparation of a DCF microarray on a DAPEG modified glass slide was performed in order to test the non-specific binding, reversibility and lifetime of the spotted chip in the used instrument. The background signal (0 mM) in Figure 43 shows that outside the DCF spots no antibodies were non-specifically adsorbed on the DAPEG surface.

For the investigation of long-term stability of the microarray on the glass slide in aqueous environment, a calibration experiment with aqueous DCF standards (0.001–100 mg/L) was performed on the same glass chip after 14 and 23 days (Figure 44). Between the measurements, the glass slide was stored in water at room temperature within the flow cell of the instrument. The sensitivity of the immunoassay can be indicated by the inflection point of the sigmoidal calibration curve (IC_{50}). The assay sensitivity did not change significantly for 15 days. However, after the 23 day-period, the sensitivity dropped by about 50%, i.e., the IC_{50} shifted from initially (0.237 ± 0.034) mg/L to (0.487 ± 0.094) mg/L. Hence, the shelf life of the prepared microarray chips can be estimated roughly 14 days under the aqueous conditions in the flow-through device. Consequently, the prepared microarray surface is highly stable.
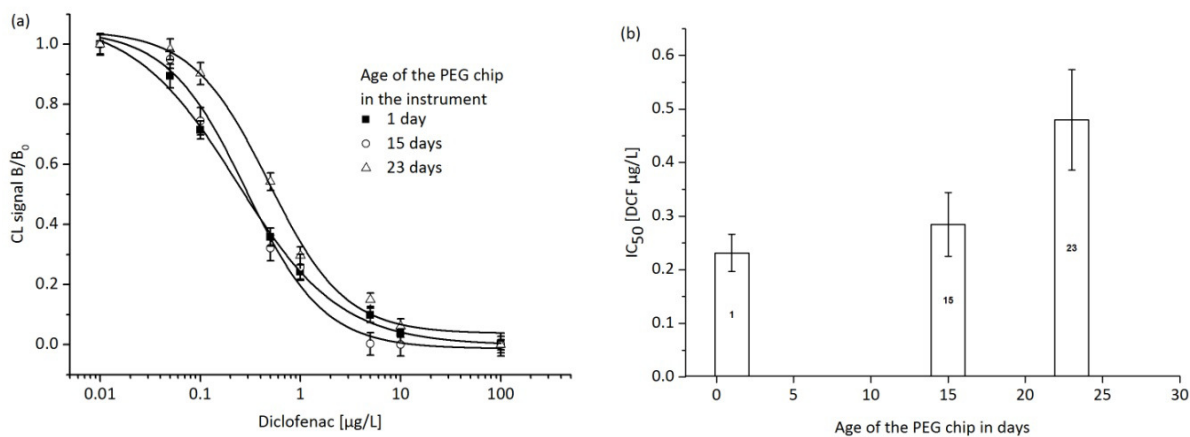
Figure 44: Microarray stability with DCF. Error bars represent standard deviations in of 5 spots on one.

The calibration was also performed by using the newly developed mAb 12G5 (Figure 45). The mAb allowed low intra-assay deviations (< 5%, m = 3) on one chip. The assay sensitivity IC_{50} was (0.20 ± 0.0078) µg/L and the LOQ (80% signal intensity) was (0.054 ± 0.0037) µg/L. Interestingly, the assay sensitivity was comparable to the measurements with the polyclonal antiserum on day 1 (Figure 44, 0.237 ± 0.034). The achieved assay sensitivity is reasonable for fresh water and wastewater samples. However, the combined method for the multiplex analysis was further optimized for MC-LR and BaP measurements in the MCR 3.
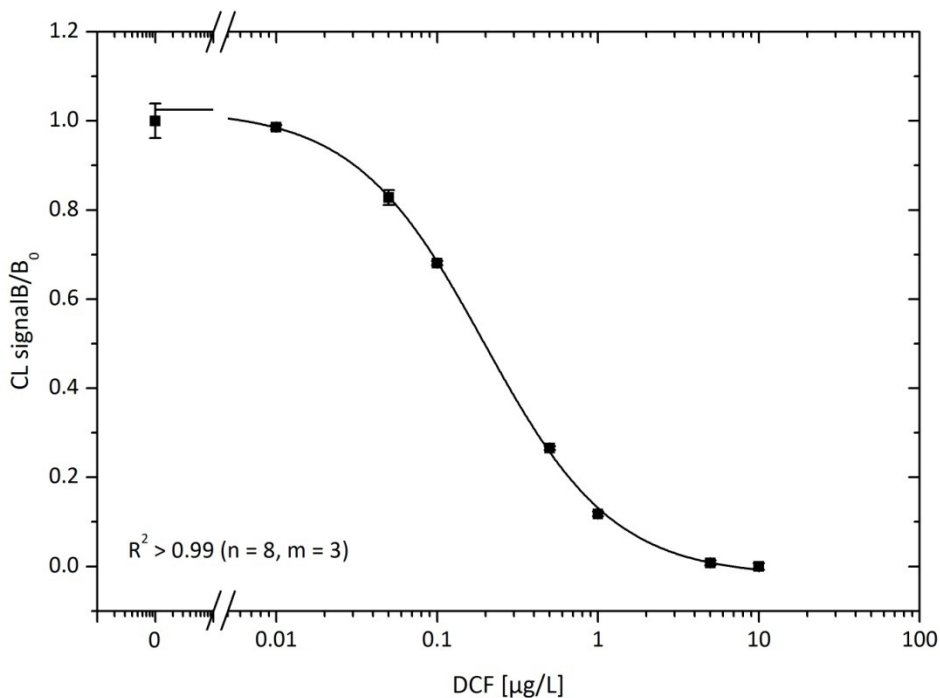
Figure 45: Intra-assay experiment on DCF on a microarray by using mAb 12G5

2.2.3 Development of a microspotting method for MC-LR

MC-LR carries two carboxylic acid groups. Moreover, it is very limited available and usually stored in stock solutions of a few μL. Consequently, the molecule cannot be activated like DCF in an economic way. It can be immobilized by using the Traut's reagent (Zeck, 2003) by taking advantage of a Michael reaction. The molecule carries a Michael acceptor that can react with thiol groups on the microarray surface as depicted in Figure 46.
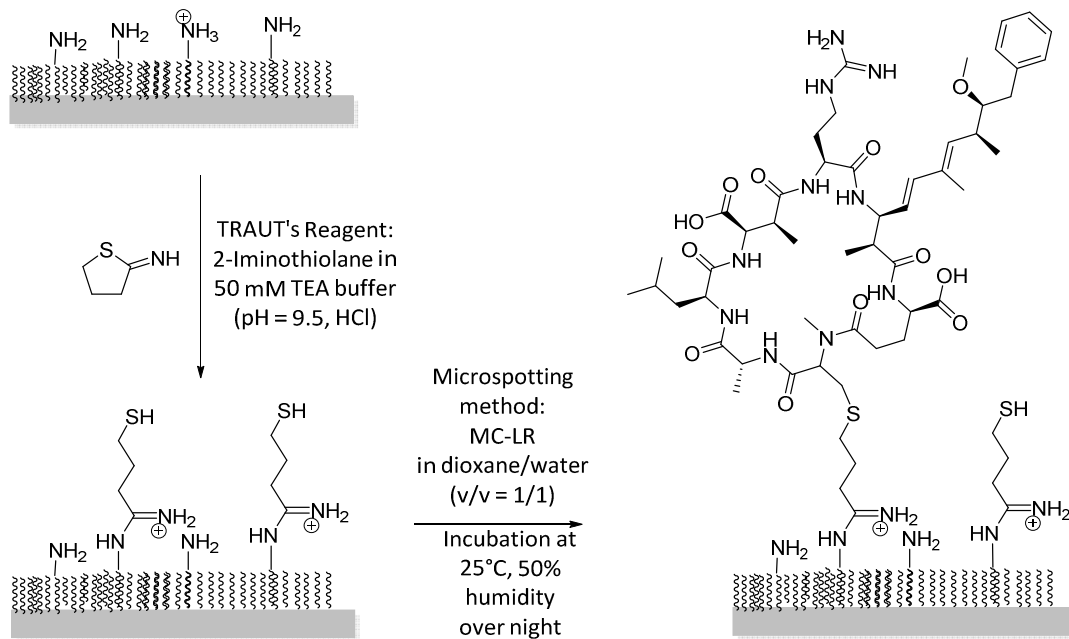
Figure 46: Microarray preparation for MC-LR

For the microspotting method, the dioxane, DMSO and glycerol content was optimized in order to have a high coupling density of MC-LR. Only in the spotting solution with dioxane, CL signals were obtained. The MC-LR concentration was optimized as shown in Figure 47. It can be seen that in general lower concentrations of MC-LR are immobilized compared to DCF: the maximum signal is reached at 0.02 mM. Raising the MC-LR concentration to 0.05 and 0.1 mM does not raise the signal any further. The signal is in general much lower than the DCF signal (Figure 43). This observation can be explained in different ways:

− The coupling density of MC-LR is lower, because the surface modification with thiol groups is lower compared to the density of amino groups on the DAPEG surface.

− MAb 10E7 was diluted 1/250 compared to the polyclonal antiserum which was diluted 1/10,000 for the measurements shown in Figure 43. Consequently the antibody concentration was too low for mAb 10E7 to have a high signal intensity.

The regenerability of the prepared surface was also tested in this experiment (Table 12). The signal was regenerable with a signal of 98% at the end of the measurement day (n = 23). Consequently, MC-LR is bound covalently to the PEG surface on the glass slide.

In an intra-assay study, a calibration was carried out (Figure 48). The measurements were highly reproducible and highly sensitive with a LOQ at (0.10 ± 0.022) µg/L and an IC_{50} at (0.33 ± 0.054) µg/L.
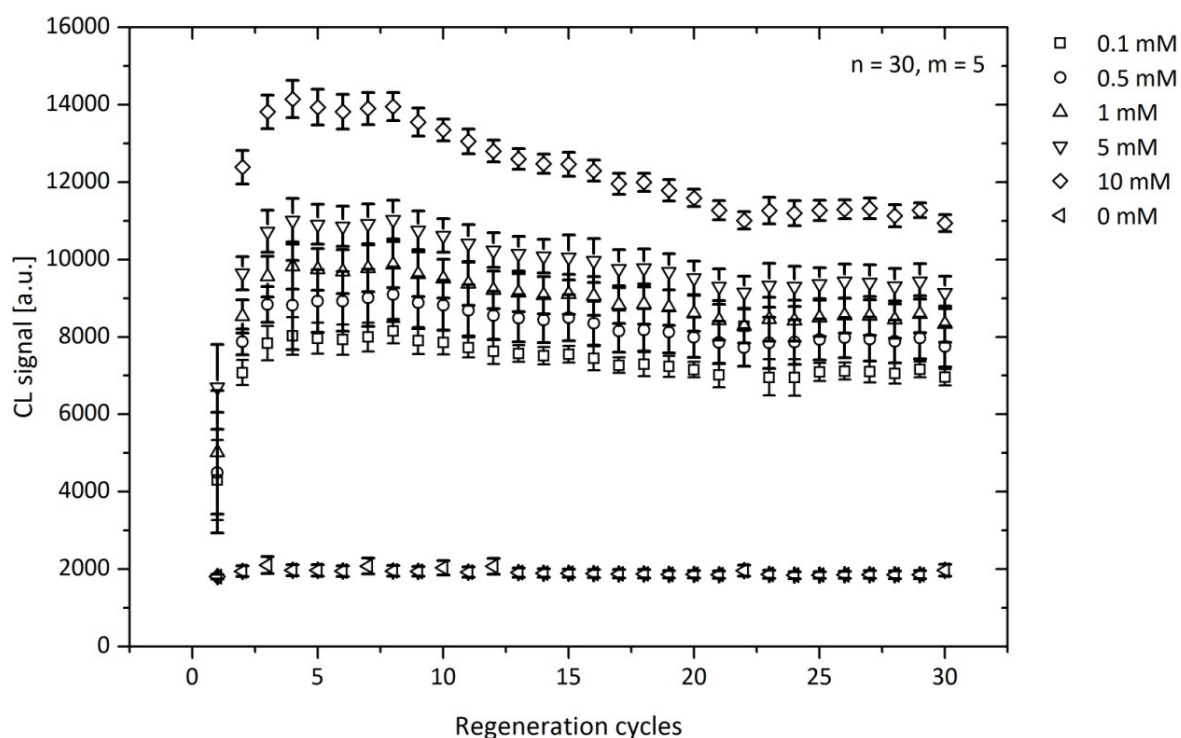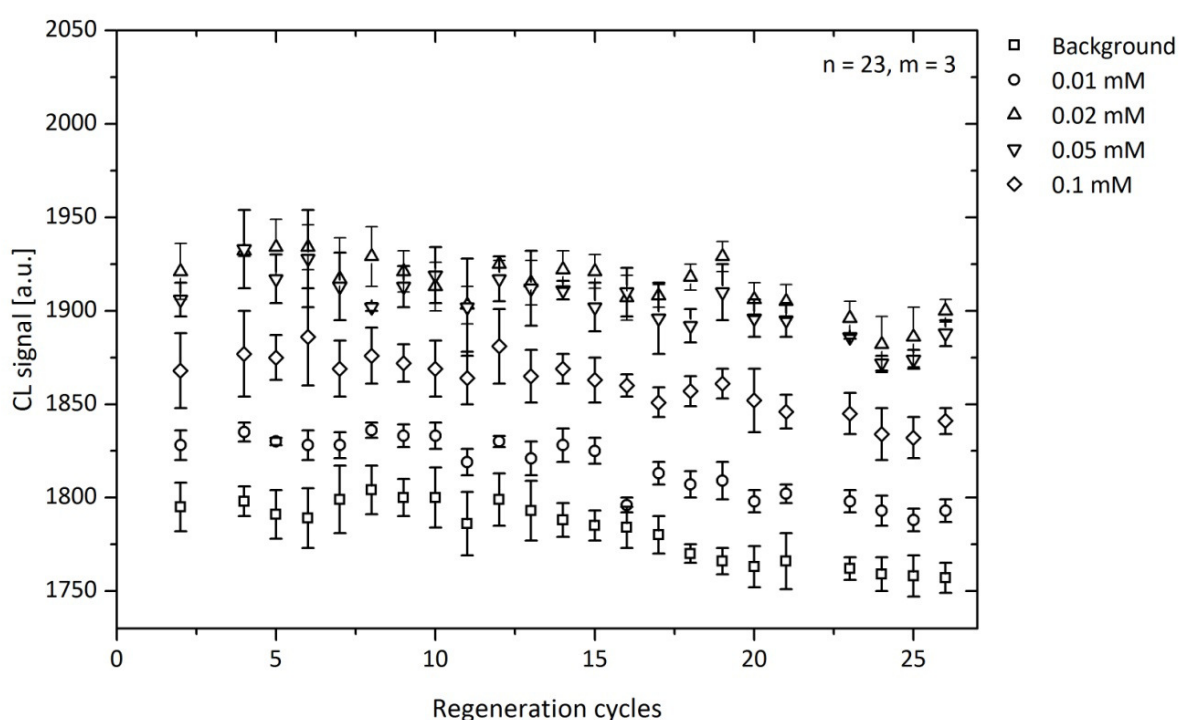

Figure 47: Regeneration of a microarray prepared with different amounts of MC-LR in the spotting solution. Error bars represent standard deviations for 5 different spots on one microarray.

Table 12: Signal intensities and decrease for different spotting concentrations of MC--LR

	c(MC-LR)	0.01 mM	0.02 mM	0.05 mM	0.1 mM
Measurements 4-6	Signal in the beginning	1831	1933	1926	1879
Measurements 28-30	Signal at the end	1791	1889	1878	1836
Signal decrease	100 % × (Signal at the end)/ (Signal in the beginning)	98 %	98 %	98 %	98 %
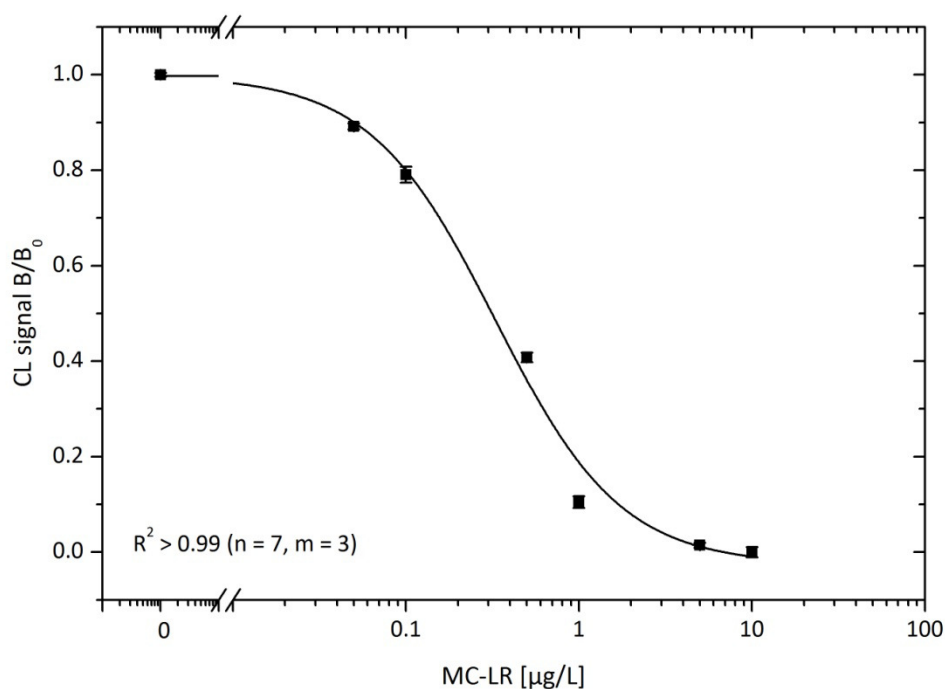
Figure 48: Intra-assay study on MC-LR on a microarray by using mAb 10E7

The figure shows a sigmoidal calibration curve with x-axis labeled "MC-LR [µg/L]" ranging from 0 to 100 and y-axis labeled "CL signal B/B_0" ranging from 0.0 to 1.0. The text "$R^2 > 0.99$ (n = 7, m = 3)" appears in the lower left.

2.2.4 Optimization of the microspotting method and calibration procedure for the detection of BaP

Benzo[a]pyrene cannot be immobilized like DCF, because it has no carboxylic acid group. It also lacks any other functional group that could be used for covalent immobilization on the DAPEG surface. Thus, derivatives of BaP carrying carboxylic acid groups can be used like it was done for the hapten coupling to the carrier protein for immunization (Matschulat, 2005). Some PAHs show cross reactivity for the reaction with mAb 22F12. This cross reactivity can also be used for the immobilization of PAH derivatives on the surface.

There are several PAH butyric acid derivatives available that were used for immobilization (Figure 49). The microspotting method was used as described above. The background corrected CL signal was the highest for 3-fluoranthenebutanoic acid and 1-pyrenebutanoic acid (PBA) at about 1800 a.u (Figure 50). Lower signals were found for 3-benzo[a]pyrenebutanoic acid and 8-benzo[a]anthracenebutanoic acid at about 400 and 700 a.u. No signals were measured for 6-chrysenebutanoic acid and 7-benzo[k]fluoranthenebutanoiuc acid. For the further optimization of the technique, PBA was used because it enables high signal and is available commercially.

79

3-Fluoranthenebutanoic acid   1-Pyrenebutanoic acid   8-Benz[a]anthracenebutanoic acid

6-Chrysenebutanoic acid   7-Benzo[k]fluoranthenebutanoic acid   3-Benzo[a]pyrenebutanoic acid
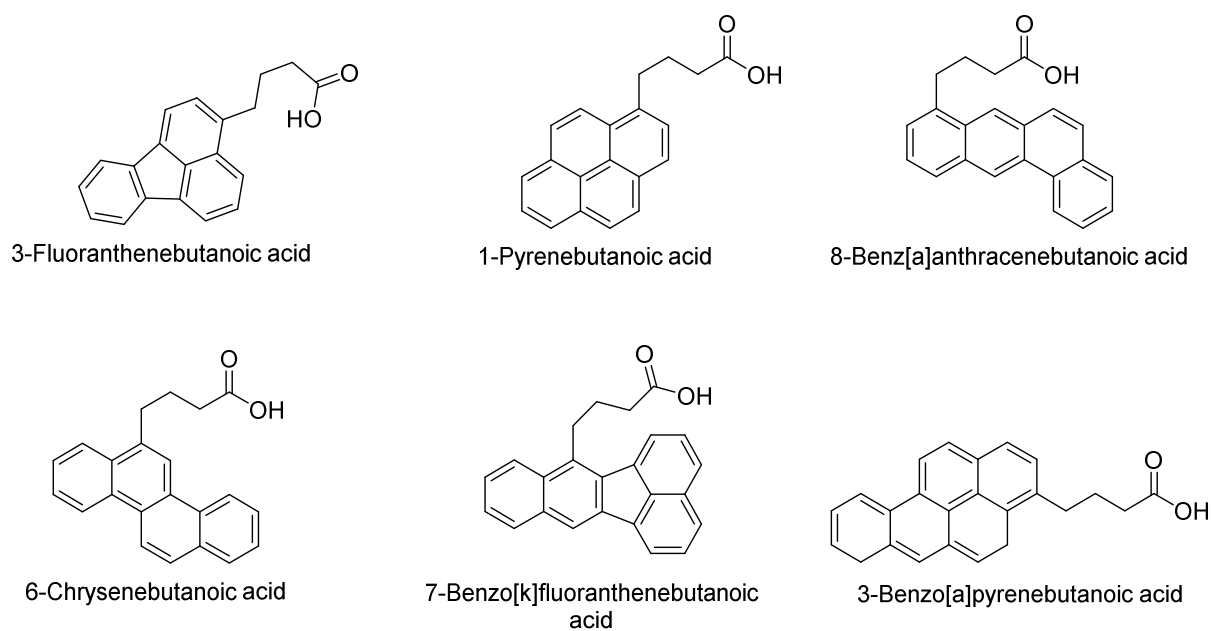
Figure 49: Butyric acid derivatives of PAHs
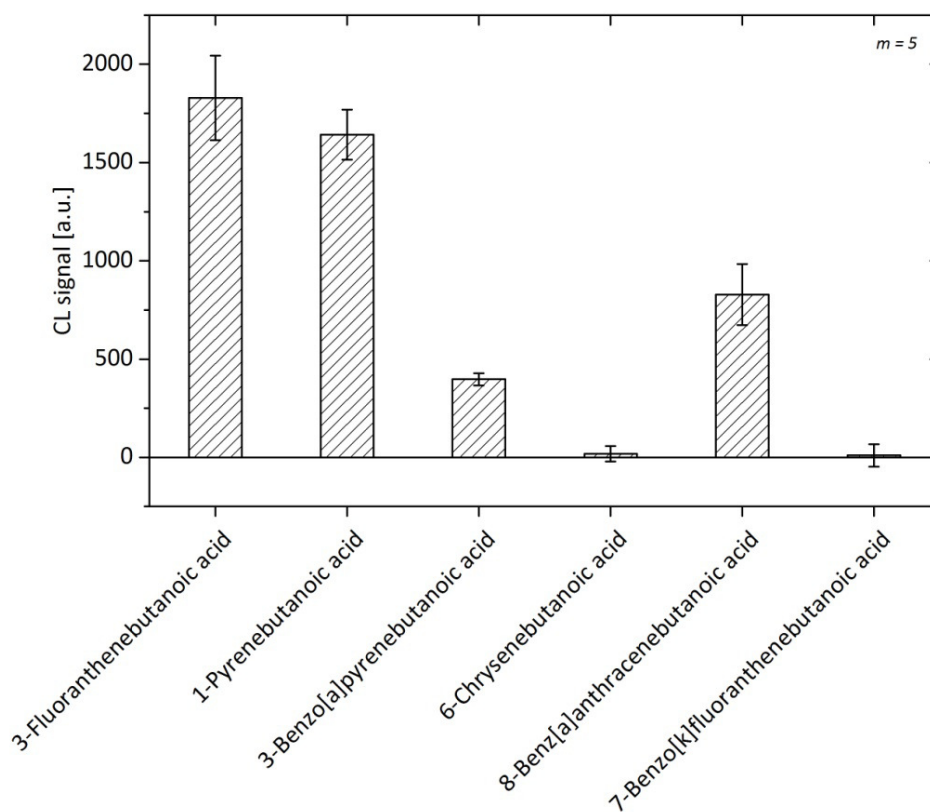
Figure 50: Background subtracted CL signals for different PAH derivatives with mAb 22F12

The PBA microarray was regenerated in 30 cycles (Figure 51). PBA was used with different concentrations for the microspotting method. At a PBA concentration of 1 mM, the signal

could not be raised any further (Table 13). For all spotting concentrations, the signal did not decrease significantly during 30 regeneration cycles. It stayed at 102 – 101 %. Consequently, the microspotting method allowed the preparation of regenerable PBA microarrays.
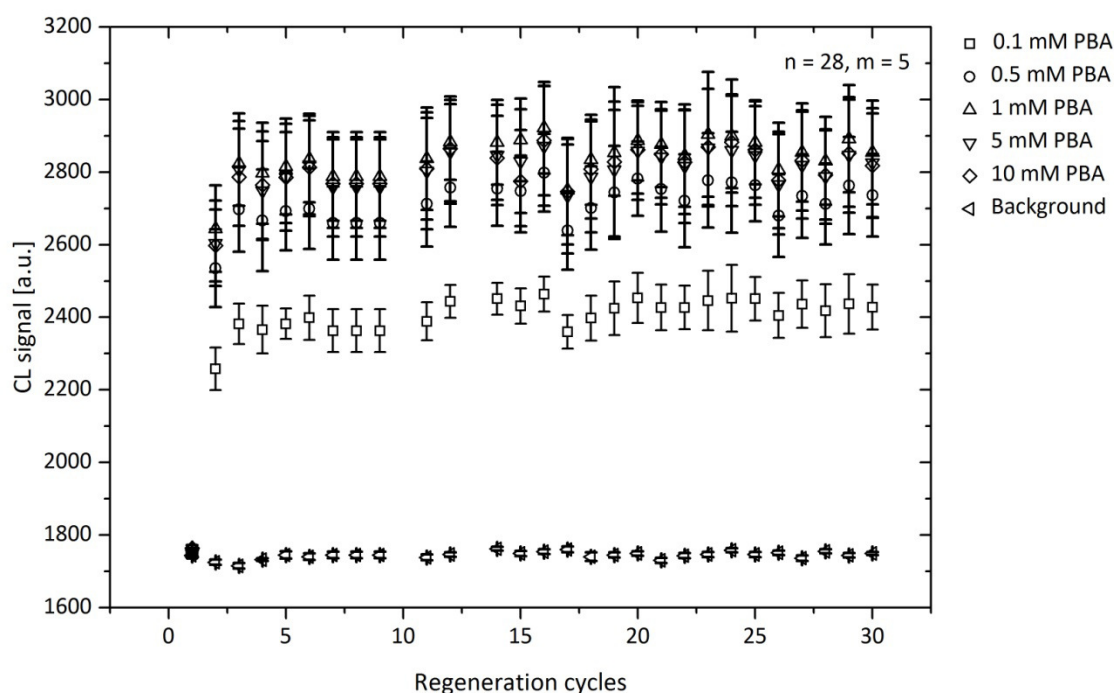
Figure 51: Regeneration of a microarray prepared with different amounts of PBA in the spotting solution and mAb 22F12. Error bars represent standard deviations for 5 different spots on one microarray.

Table 13: Signal intensity and its decrease for different spotting concentrations of PBA.

	c(PBA)	0.1 mM	0.5 mM	1 mM	5 mM	10 mM
Measurements 4-6	Signal in the beginning	2382	2686	2816	2785	2787
Measurements 28-30	Signal at the end	2427	2737	2859	2820	2820
	(Signal at the end)/					
	(Signal in the beginning)					
Signal decrease	× 100 %	102 %	102 %	102 %	101 %	101 %

For calibration experiments with BaP, the same method was used as for DCF and MC-LR. The standards were prepared in 10% of MeOH. The measurement program was used as described in previous works (Sauceda-Friebe, 2010; Oswald, 2013). However, this procedure did not allow any reproducible results. For reasons that had to be identified, the interaction of mAb 22F12 with the sample or the microarray preparation was hampered with this assay

protocol. In Table 22 (Experimental Section), the assay steps are listed. The problems with reproducibility of BaP measurements could be caused by non-specific adsorption of BaP in the tubings, syringes and valves of the instrument.

In order to overcome the problem of non-specific BaP adsorption, the measurements were carried out with a final MeOH content of 25% in the sample/mAb mixture instead of 5%. For this purpose, the MeOH content in the sample was 50%, because the primary mAb solution is mixed with the sample in a ratio of v/v = 1/1. This increase of MeOH lowers non-specific adsorption to the glass surfaces in the sample container, sample syringe or PTFE tubes in the instrument (Qian, 2011; Oliferova ,2007).

For improving the assay sensitivity and reproducibility, the incubation of mAb on the microarray surface was optimized to allow lowest dilutions of mAb 22F12. To optimize the immune recognition in the instrument, 2 program steps were optimized (Table 22 in the Experimental Section):

- Step 3 which includes the mixture of primary antibody with sample and
- Step 4 for interaction of the remaining mAbs with the microarray surface.

The reduction of flow rate by a factor 10 for step 3 did not allow any sensitivity enhancement (Figure 52). The signal for 1 µg/L was 402 ± 100 and 296 ± 50 for 3 different measurements at 60 µL/s and 6 µL/s. Consequently, the signal was not significantly lower at this BaP concentration for a slower mixing step.

In an intra-assay study with 3 injections per standard solution (Figure 54), RSD values were below 7% for the individual calibration points. The assay sensitivity was now in a range that is required for fresh water samples (IC_{50} = 0.15 ± 0.008) µg/L and an LOQ of (0.019± 0.002) µg/L. A recovery experiment with a BaP concentration of 0.50 µg/L in river water (Isar) allowed a recovery rate of 106%. For this measurement, the river water sample was diluted with MeOH in a ratio of v/v = 1/1 and spiked with BaP. The optimized assay conditions were now transferred to multiplex measurements as described in the Chapter 3.

For the optimization of step 4, the flow rate was adjusted from 100 µL/s to 1 µL/s resulting in different times for this incubation step of mAb on the microarray surface (Figure 53). The time for this incubation step is shown in correlation to the CL signal intensity at an antibody concentration of 1/20 000. At a flow rate of 2 µL/s, the CL signal is approaching the

maximum signal intensity. The time for step 4 is still below 10 min (600 s). Therefore, this flow rate was chosen as the optimal flow rate for high CL signal at a given mAb dilution.
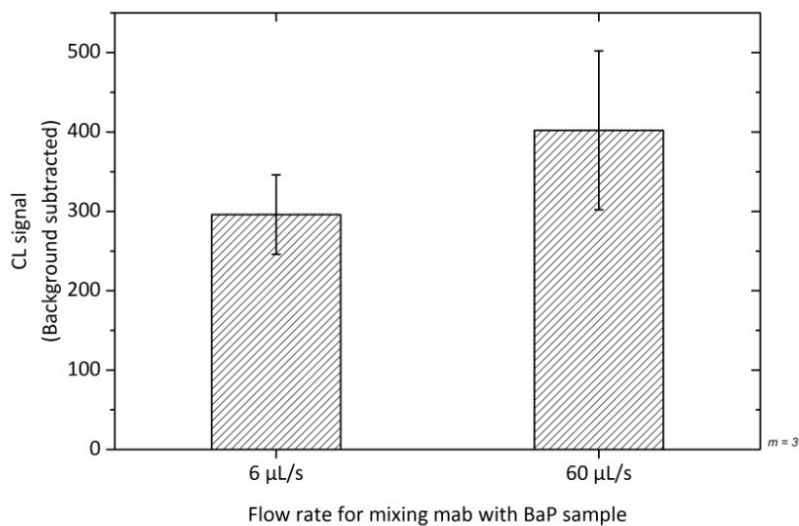
Figure 52: Optimization of the mixing rate of mAb with sample in the MCR 3 (1 µg/L BaP in water/MeOH = 1/1). Error bars represent standard deviations for 3 standard injections.
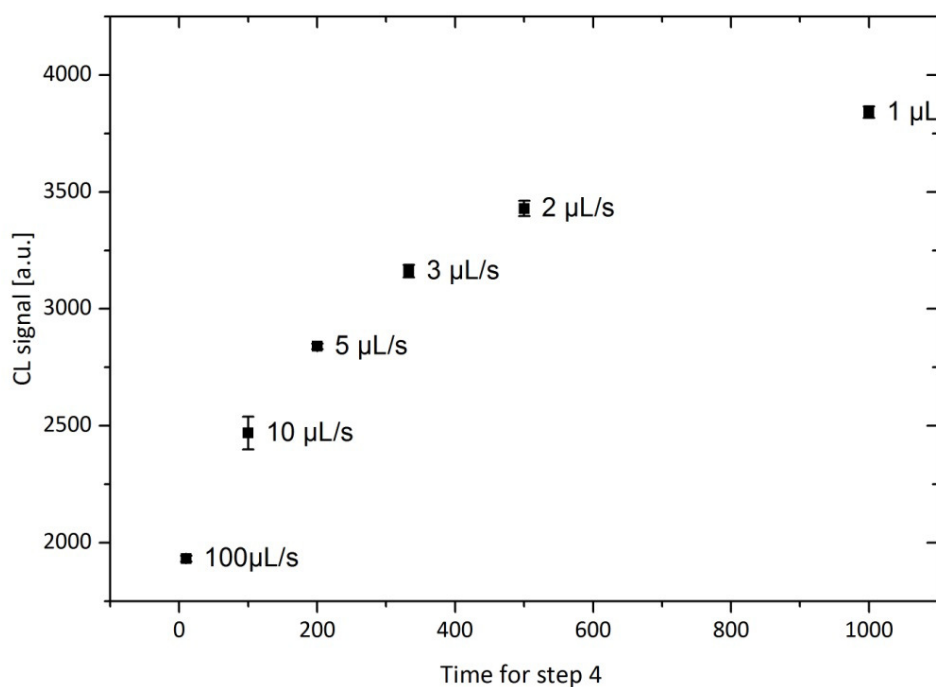
Figure 53: CL signal intensity at different flow rates. Error bars represent standard deviations for 5 different PBA spots on one microarray.

83
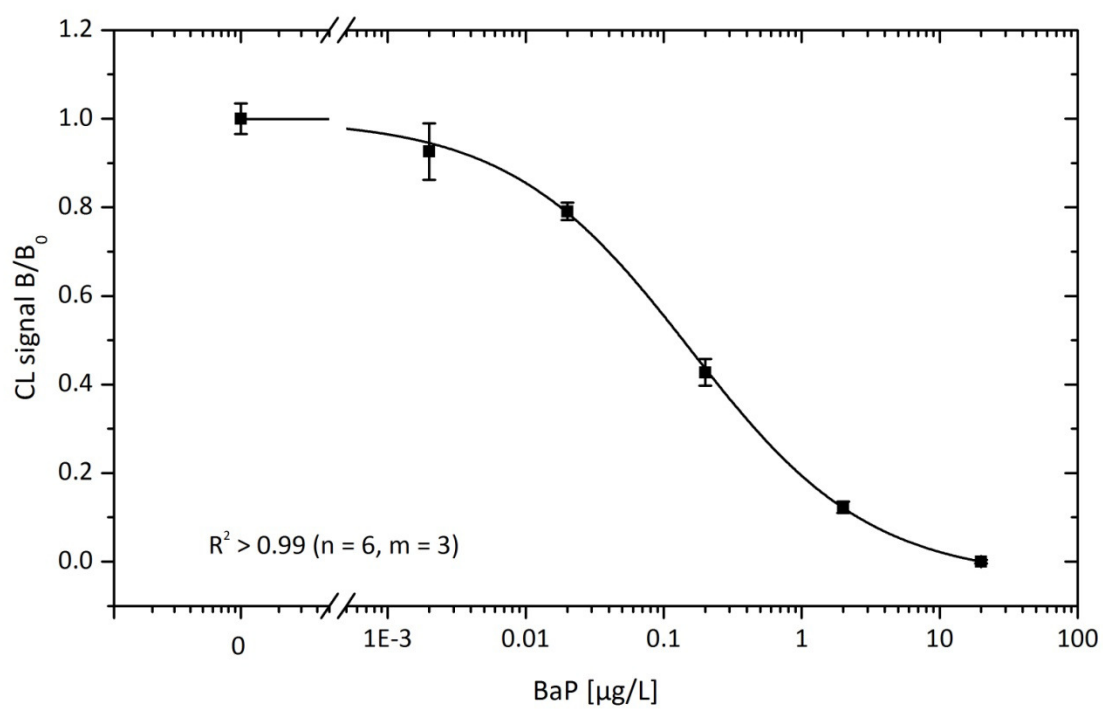
Figure 54: Intra-assay experiment with BaP.

2.3 Surface characterization of a regenerable surface preparation

The surface chemistry for regenerable surface preparations is supposed to allow successive covalent grafting of functionalization layers to the glass surface. This assumption can be investigated by using methods for surface analysis. For using XPS analysis and FT-IR spectroscopy on the surface, the surface chemistry was transferred to Si wafers. They carry a native silica layer like the glass carriers used for microarray preparation.

2.3.1 AFM

In order to investigate the topological structure of the glass slides modified with the PEG layer, 5 x 5-μm images were taken in the peak force mode under air (Figure 55). The root-mean-square (RMS) values are calculated by an algorithm that averages the height deviations taken from the mean image data plane. They indicate the surface roughness. On the silicon wafer, the roughness is 1.6 nm for the DAPEG layer. The surface seems uneven with wholes deeper than 5 nm. These holes are caused by the original rough wafer surface. The 1-μm lateral profiles show that the PEG creates a smooth surface on the silica. After the attachment of DCF from solution in DMF, the RMS value is lowered to 1.3 nm. The holes have disappeared. Consequently, the PEG chains seem to be more evenly distributed after the reaction with activated DCF from DMF solution.

For the glass slide surface, the attachment of DAPEG to the surface results in a RMS of 1.1 nm. The difference to the Si wafer is caused by the initially smoother glass slide. With the microspotting method, the PEG-ylated surface was imprinted with DCF active ester in dioxane/water on distinct spots with an average of 0.5 mm . Their locations were marked on the opposite side of the glass slide directly after the spotting process and before the slides were washed in PBST and water. Around the spots, the RMS was 1.0 nm compared to previously 1.1 nm. Hence, the overall roughness of the DAPEG coating is not significantly influenced by the washing steps of the method. At the DCF spot, the RMS was 1.2 nm. The roughness is increased by the spotting of DCF. This increase is caused by some bulky adducts on the surface with 100 - 200 nm in diameter and 10 - 30 nm in height. They are not present on the silicon wafer, which was incubated with the EDC/NHS activated DCF in DMF solution. So they are possibly created during the microspotting method where the dioxane/water drop with activated DCF is placed on the surface and slowly evaporates over night. The small agglomerates can stem from non-specific deposition of side products of the amide formation

like urea derivatives. The final washing steps in aqueous solutions do not dissolve the agglomerates. However, the lateral profiles in the nm-range show, that the PEG and the DCF are distributed evenly on the glass surface. The final roughness is the same for the glass surface and the silicon wafer modified with DCF.
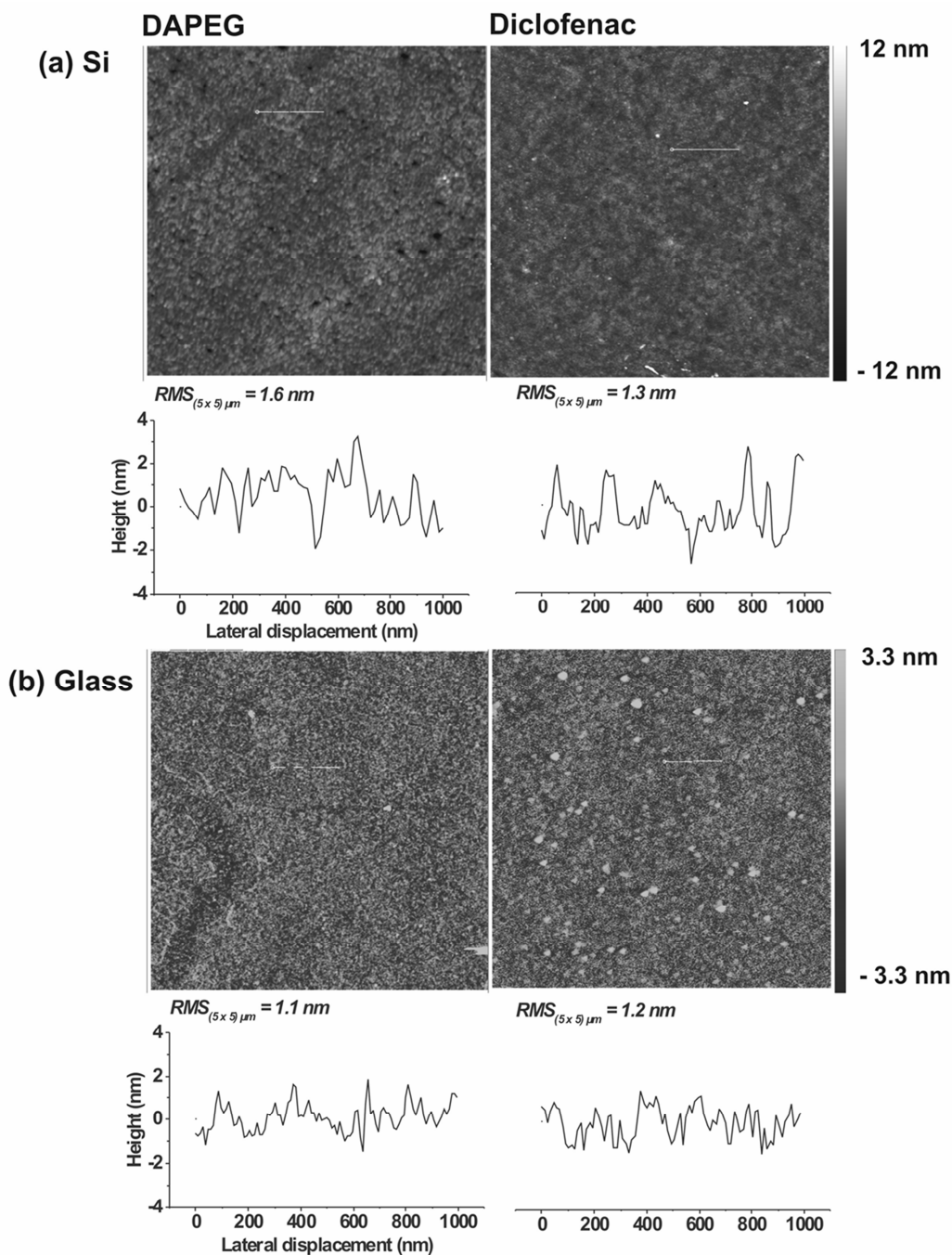
Figure 55: 5 x 5-µm images (peak force QNM mode, air) of silicon wafer (a) and glass slide (b). 1 µm cross sections were taken at the white line

2.3.2 Contact angle measurement

In Figure 56, the water contact angle values for the successive functionalization steps of the surface grafting on glass slides and Si wafer are shown. On the wafer, the contact angle was $(7.5 \pm 3.3)°$ after the oxidation step. This low angle indicates a hydrophilic character of the surface from a high yield of silanol groups on the silica surface. After GOPTS grafting, the mean contact angle was $(50 \pm 1.2)°$ indicating a coverage of the surface with the silane in the range of a monolayer (Tsukruk, 1999). The subsequent steps, DAPEG grafting and coverage of DCF, lowered the contact angle to $(44 \pm 2.7)°$ and $(45 \pm 1.8)°$. This observation indicates that the hydrophilic DAPEG covers the surface densely and allows a moderate wettability of the silicon wafer. The DCF layer has not an apparent influence on the interfacial properties of the PEG-ylated wafer surface.

On the glass slide, the oxidation step creates a mean contact angle of less than 5°. It could not be determined more precisely, because the drops were not stable on the surface. Consequently, the yield of silanol groups on the glass surfaces is also high. After the grafting with GOPTS, the contact angle is raised to $(47 \pm 2.0)°$.

The wettability did not change significantly after adding the DAPEG $(46 \pm 2.5)°$ and after microspotting $(47 \pm 1.8)°$. Apparently, the final water contact angles were comparable between the glass slide microarray and the Si wafer covered with DCF.

2.3.3 XPS

The XPS spectra for the different preparation steps deliver different intensities for each element. The signal intensities are summarized in Table 14. For the GOPTS layer, no nitrogen signal can be observed as expected (Figure 57a). The –CO/–CC ratio is 1.3 according to the data. According to the original molecular structure, the ratio should be 1.8. Accordingly, the decrease of this ratio shows that on average at least two of three methoxy groups have reacted. On the DAPEG surface an amine terminus is present as NH_3^+ as the band at 403 eV indicates. After the reaction with DCF, the band at 403 eV (NH_3^+) has decreased and an increased band at 401 eV can be observed. The band is attributed to NH or NH_2 groups. This shift of the nitrogen band would correspond to a formation of amide bonds on the DAPEG surface.
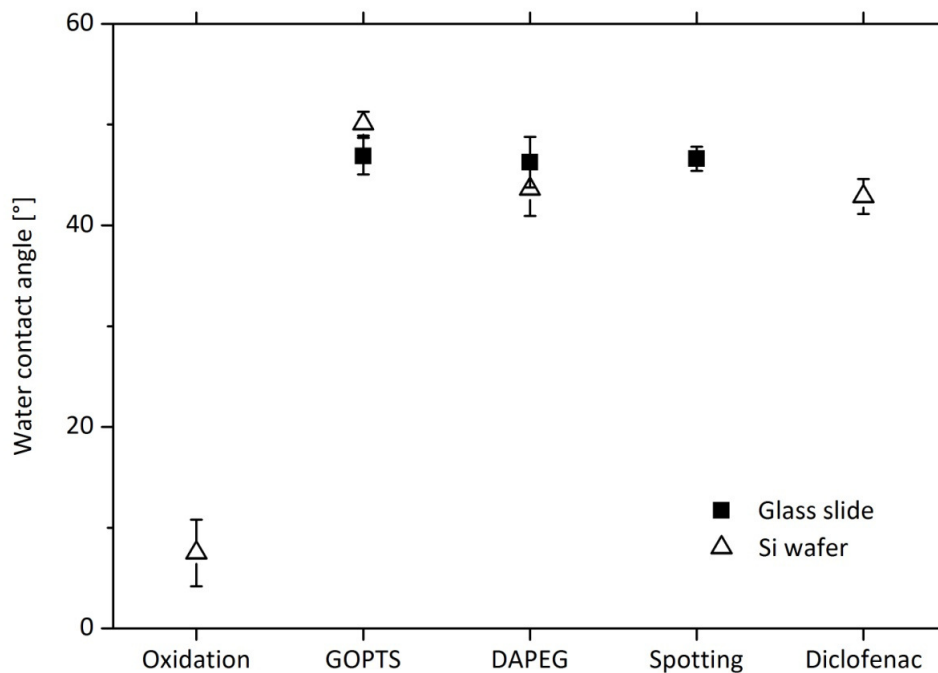
Figure 56: The water contact angle for the different preparation steps. For the oxidation step on the glass slide, a contact angle could not be measured due to the low water drop stability on the surface
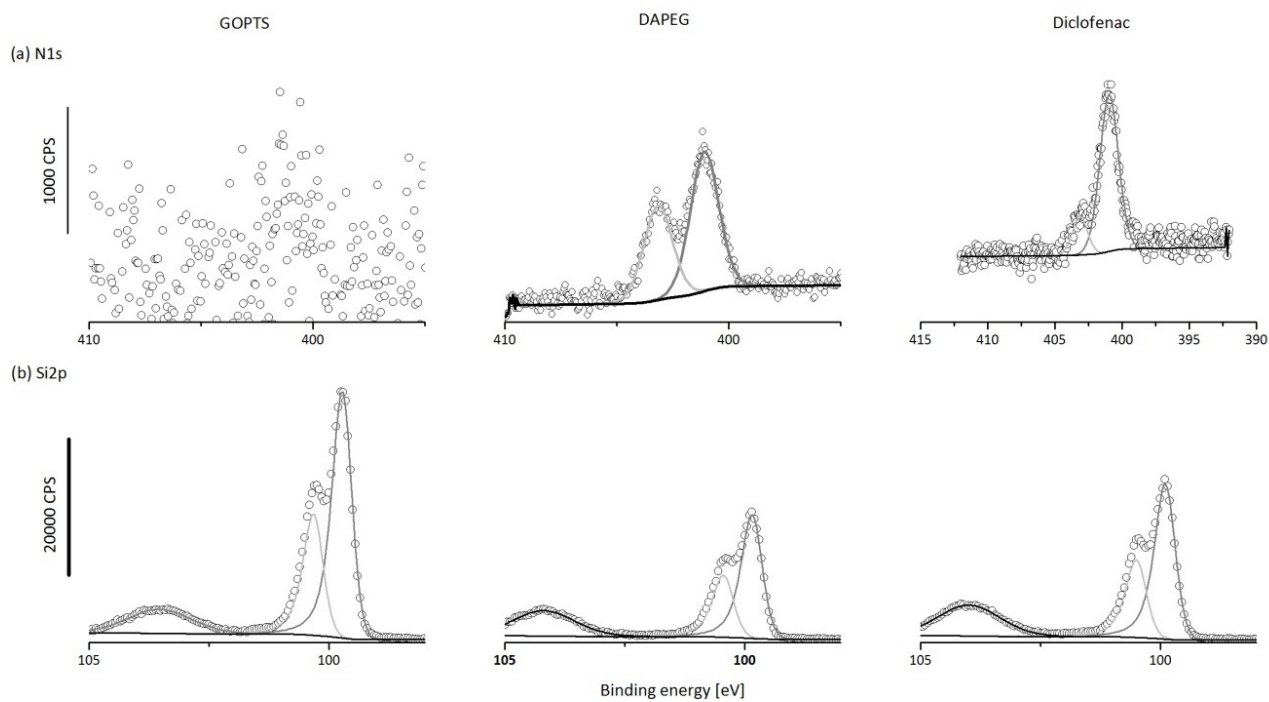
Figure 57: (a) N1s and (b) Si2p XP spectra on Si wafer preparations

The presence of DCF is notified by the chlorine signal which is 0.2% of the overall surface coverage (Figure 58, Table 14). This chlorine content corresponds to 0.8% of DCF on the PEGylated Si wafer.

With the intensities of the Si2p bands (Figure 57b), the layer thickness can be estimated according to Equation 8 (Theoretical Section). The resulting layer thickness is summarized in Table 15. For the GOPTS layer, the calculated thickness of 0.53 nm is below the range of a monolayer. A monolayer would be 0.76 nm (Dinh, 2009). The difference indicates that not the entire surface was covered with the silane. The thickness of the GOPTS–DAPEG layer was 1.7 nm. After the addition of DCF, the thickness was slightly changed to 1.6 nm. This decrease is smaller than the PEG-layer itself. Consequently, it is caused by a reorientation of the PEG chains after the attachment of DCF. This rearrangement was also shown by GA-ATR FT-IR measurements as described in the following section.

Table 14: Atomic composition on the Si wafer surfaces after the different modification steps according to XPS spectra

Binding energy (eV)	Assignment	Peak Area (%)		
		GOPTS	DAPEG	DCF
533	O 1s	22	26	26
403	NH_3^+	-	0.3	0.1
401	NH, NH_2	-	0.5	0.7
290	C 1s	0.8	-	0.7
287	C-O or C-N	9.7	22	21
286	C-C	7.5	15	6.6
274	Cl 2s	-	-	0.2
104	SiO2	6.0	6.4	7.8
101	Si 2p1/2	27	15	18
100	Si 2p3/2	27	15	19
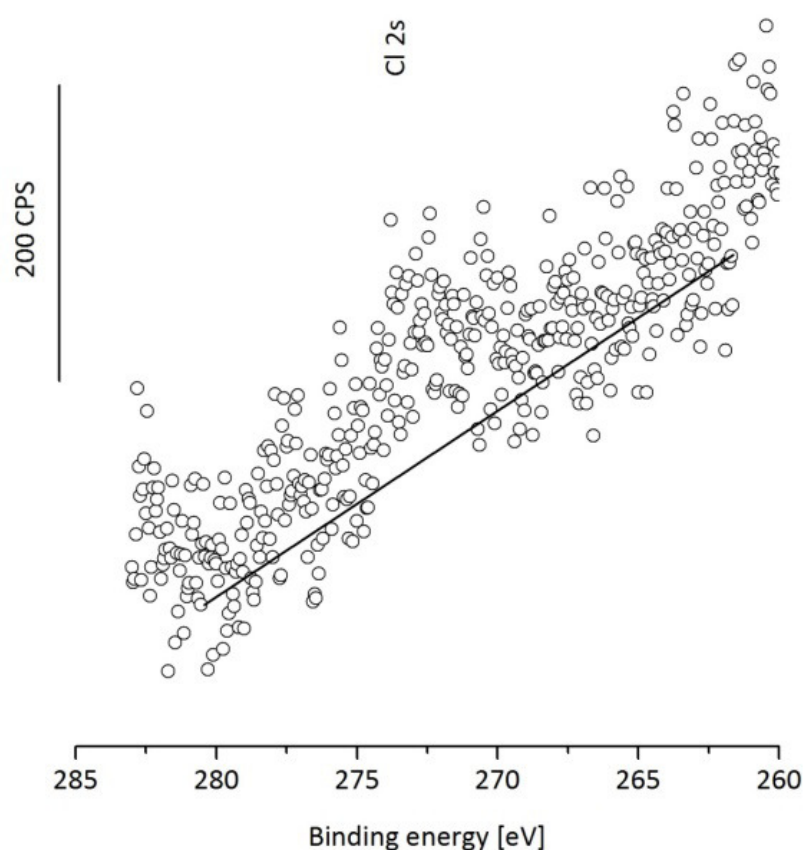
Figure 58: XPS signal for Cl 2s at 274 eV on the DCF covered PEG-layer

Table 15: Intensities of the Si 2p band and estimated layer thickness d from Equation 1

Layer	I (Si 2p) in counts s^{-1}	d [nm]
Si ref	22602	-
GOPTS	18203	0.53
DAPEG	11101	1.7
DCF	11640	1.6

2.3.4 GA-ATR FT-IR

In Figure 59a, the baseline-corrected spectra for a bare Si wafer are shown. They were recorded between the steps of the preparation of the surface for functionalization. The bare silicon wafer was cleaned with ethanol only. It can be observed, that the surface has adsorbed more water (band at 1650 cm^{-1}) after the steps of the cleaning procedure with MeOH/HCl. The bands at 1060 and 1110 cm^{-1} can be assigned to a continuous Si-O-Si layer

(Tian, 2010). The band at 880 cm^{-1} can be assigned to silanol groups (Yim, 2005). After the treatment with concentrated sulfuric acid, the oxidation step, the band at 1060 cm^{-1} of Si-O-Si decreased. In the meantime, the band at 880 cm^{-1} (Si-OH) was raised by the treatment. This shows that the surface structure has changed from a Si-O-Si network to predominantly Si-OH groups. The band at 1650 cm^{-1} has disappeared suggesting the reaction or removal of adsorbed water.

The spectra for the following surface modifications are shown in Figure 59b. After the incubation of the oxidized wafer with GOPTS, an intense band at 1110 cm^{-1} appears. It can be assigned to the C-O-C ether bonds in the silane. The band at 880 cm^{-1} was reduced which indicates a reaction of the silanol groups. On the GOPTS layer, adsorbed water is measured (1650 cm^{-1}). At 1260 cm^{-1}, a weak epoxy band is observed (Yim, 2005). The bands for the DAPEG layer are more intense, because it is a much larger molecule (MW = 1,900 Da) than GOPTS (MW = 236 Da). The bands are the same, because of the ether-type structure of both compounds. However, two additional bands arise at 1260 and 1210 cm^{-1}. The increase of the band at 1650 cm^{-1} can be attributed to the terminal amino groups of the DAPEG and to a higher amount of trapped water, as the PEG is hydrophilic and adsorbs considerable amount of water molecules. The band at 1260 cm^{-1} has disappeared.

For DCF, no specific bands were identified. The concentration is too low for obtaining characteristic bands of this compound on DAPEG. The decrease of the intensity can be explained by a shift of the chain orientation to a parallel alignment of the chains after the coverage with NHS activated DCF (Lummerstorfer, 2007).

Figure 60 shows the CH stretching bands for the different preparation steps. The bands for methyl groups at 2955 and 2966 cm^{-1} arise in the DAPEG-spectrum. The shoulder at 2955 cm^{-1} in the GOPTS spectrum were attributed to a rest of methoxy groups that have not reacted.

For the GOPTS and DAPEG layers, the absorbance intensities do not change considerably. The short GOPTS chains are less oriented than the long PEG chains in general. However, the DAPEG layer is also less organized, because the intensity is still high. This could be caused by hydrogen bridge bonds of the terminal amino groups to other functional groups. After the attachment of DCF, the intensity decreases. This decrease can be attributed to a more

parallel chain orientation of the PEG layer after the attachment of DCF (Lummerstorfer, 2007).
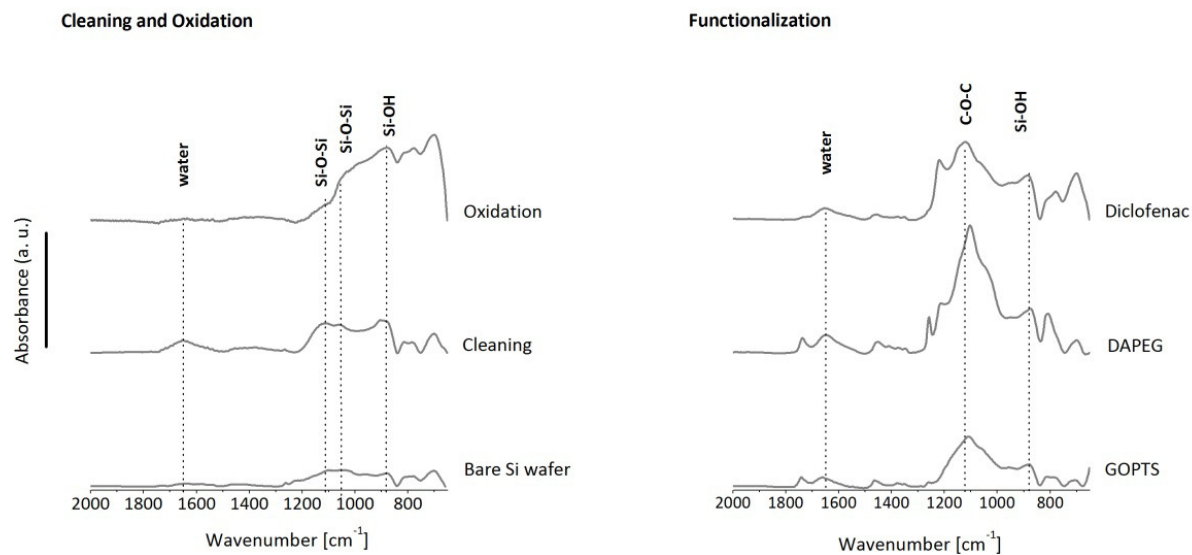
Figure 59: (a) Baseline corrected GA-ATR FT-IR spectra of Si wafers after cleaning and oxidation and (b) after the functionalization steps
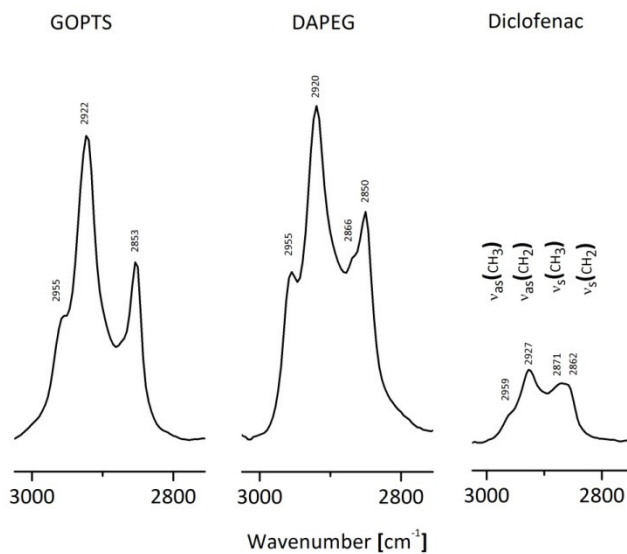
Figure 60: CH stretching absorptions measured by GA-ATR FT-IR with a germanium crystal

2.3.5 Summary of the results of surface analysis

The presented PEG-surface coverage allows preparing homogeneous and stable surfaces for measuring antibody interaction with the corresponding hapten. Every surface preparation step could be analyzed in detail with the described methods (Figure 61).

GA-ATR FT-IR spectra showed that the initial cleaning method allows moistening the Si-O-Si framework on the silica surface. In addition, the oxidation with concentrated sulfuric acid works efficiently and generates a high yield of silanol groups on the silicon and glass slide surfaces. The following application of GOPTS yields a dense surface coverage on both substrates as observed by high contact angles. The XPS data showed that the silane reacts with the oxidized surface and leads to a surface coverage below the monolayer range. However, after the PEG attachment, uneven spots on the silicon wafer have vanished indicating a homogeneous functionalized silica surface which can be observed in AFM images as well. The XPS analysis revealed that the chlorine of DCF can be detected, however, the amount of DCF is only about 0.8% and the layer thickness is not notably changed. Only rearrangements of the PEG chains can be seen in GA-ATR FT-IR as indicated by the decrease of intensity of the bands. The surfaces are densely covered by the DCF coupled to the PEG, because the RMS values (1.2 and 1.1 nm) are smaller than the layer thickness as determined by XPS (1.6 nm). This dense coverage prevents the antibody with a diameter of ~ 10 - 12 nm from non-specific interaction with the silica surface.

The recognition and response measurements by QCM-D showed that the created surface is stable over at least 10 regeneration cycles and all bound protein (antibodies) is removed during a regeneration cycle. Finally, the chemiluminescence measurements of a DCF microarray on a glass slide showed that the antibody binds only to DCF immobilized on the PEG surface. The primary antibody can be detected by a secondary anti-rabbit IgG peroxidase conjugate. One chip can be regenerated for at least 30 regeneration cycles without significant decrease of CL signal intensity. The chip area outside the spotted DCF did not adsorb proteins from the diluted antiserum during the whole measurement time (~ 6 h).

Consequently, a stable and reliable surface for reversible immunorecognition has been created. This surface was also stable for several days when stored in the microflow device in aqueous solution. The model analyte DCF can be replaced by any other hapten or antigen and, the experiments on QCM-D and the MCR 3 show that the surface chemistry can be used

for either label-free or label-based biosensing applications. Therefore, this sensing layer can be used as universal platform for small-sized analyte biosensing. The chip will be tested with real sample applications as described in the following section for mutliplex analysis as described in Chapter 3.
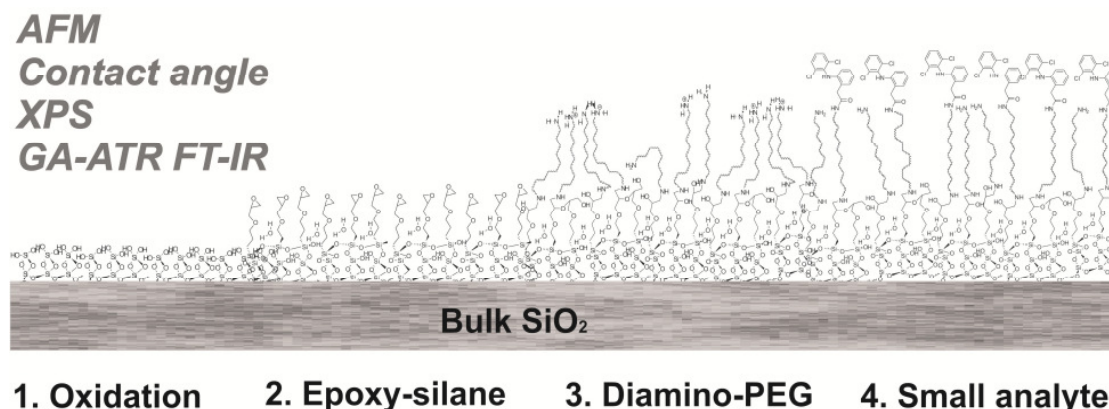
Figure 61: Summary on surface analysis

2.4 Assessment of gold nanoparticle use for chemiluminescence enhancement

For improving the assay sensitivity, gold was used in different ways to enhance the CL signal. Gold nanoparticles (AuNPs) were coupled to the secondary antibodies or grafted on the DAPEG surface by the French project partners (Ben Haddada, 2015). The PMMA slide was also covered with gold for another experiment.

2.4.1 AuNP labelled anti-mouse-HRP antibodies

The signal was compared for anti-mouse-HRP secondary antibodies with and without AuNP label (Figure 62). The CL signal was not increased for the same concentration of anti-mouse-HRP. A calibration experiment was not performed, because of the low quantity of the AuNP labeled anti-mouse-HRP antibodies. This label was also of poor stability due to ageing of the AuNP dispersion. Consequently, this approach was not further developed for the immunoassay application.
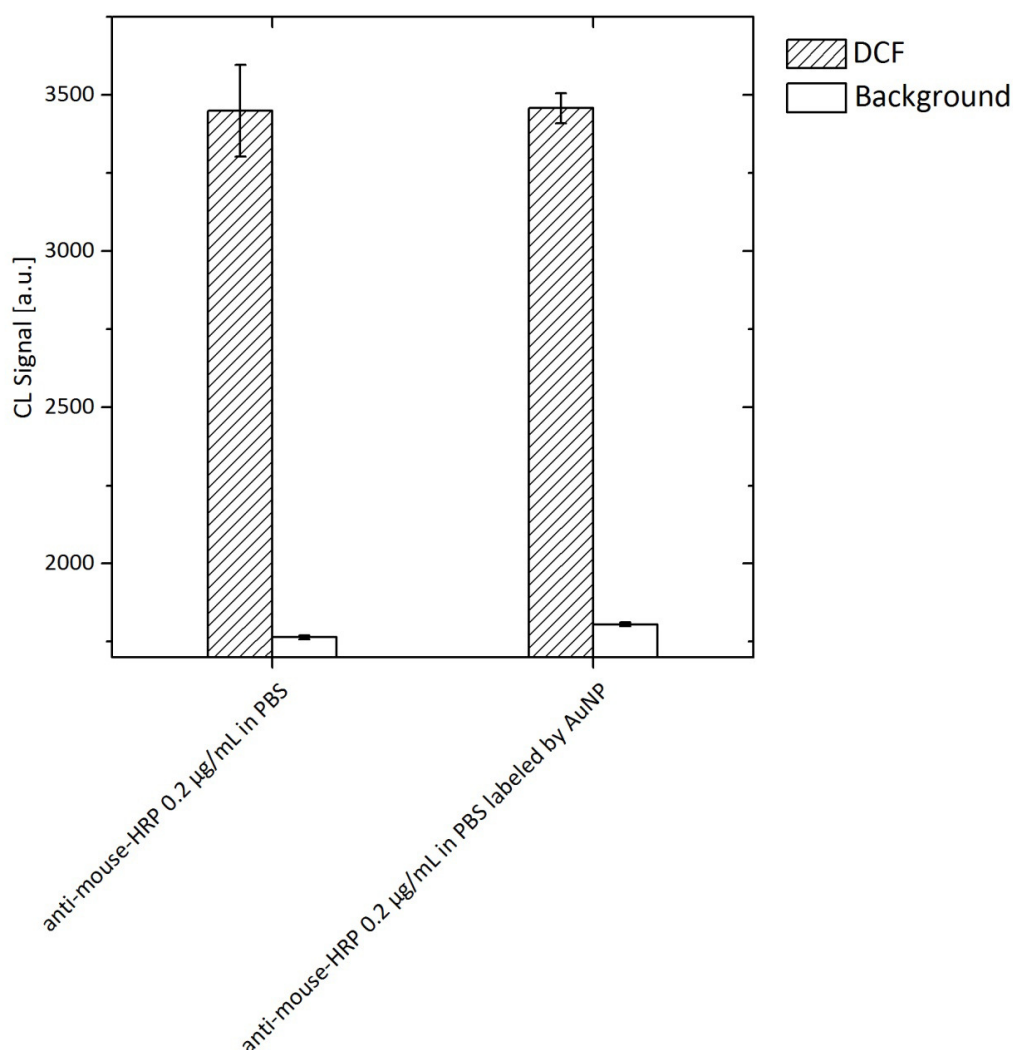
Figure 62: Signal intensities for secondary antibody without and with AuNP label. Error bars represent standard deviations for 5 DCF spots on a microarray chip.

2.4.2 AuNP grafted PEG surface

The AuNP grafted PEG was prepared according to Ben Haddada, 2015. The modified surface was treated by the microspotting method in the same time as the PEG surface preparations. In Figure 63, the resulting signal intensities are shown. For the PEG-based surface the signal is larger than 18 000 a.u. whereas the signal on the AuNP-PEG-surface is below 3 000 a. u. This indicates a lower coupling yield of DCF on the AuNP modified surface.

This lower signal intensity results in lower assay sensitivity as shown in Figure 64. The anti-DCF antibody 12G5 could be diluted by 1/100 000 (v/v) for the PEG surface but only 1/10 000 for the AuNP-PEG surface. The IC_{50} value is 0.11 µg/L for the PEG surface and 0.41 µg/L for the AuNP-PEG surface.
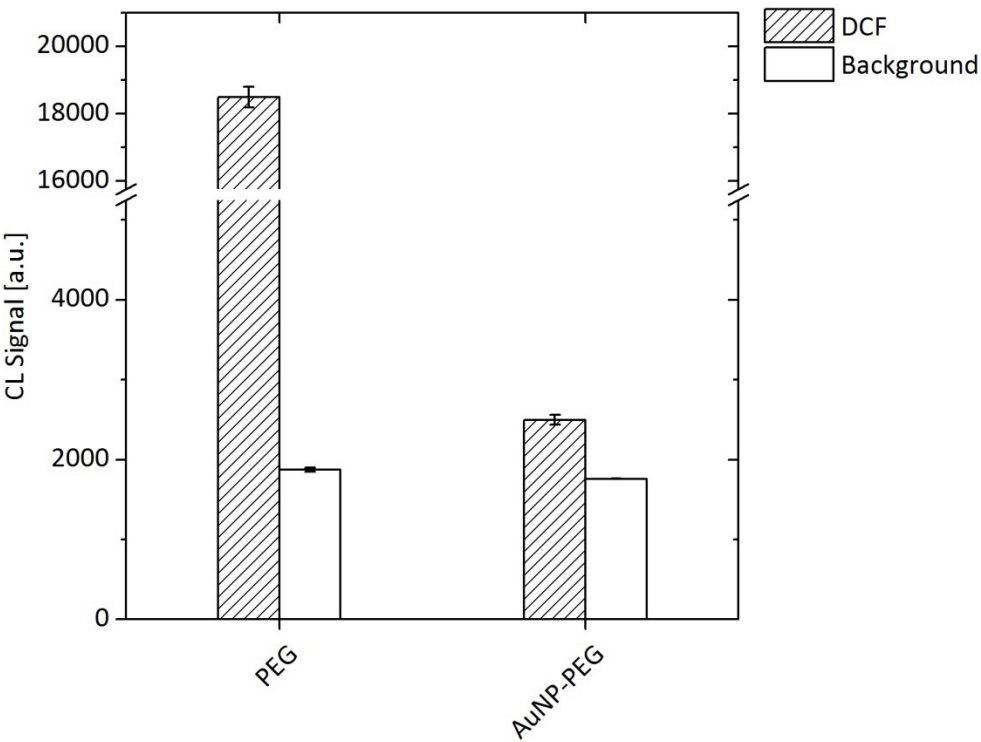
Figure 63: Signal comparison for the same measurement conditions between PEG and AuNP-PEG surface. Error bars represent standard deviations for consecutive measurements on each chip.
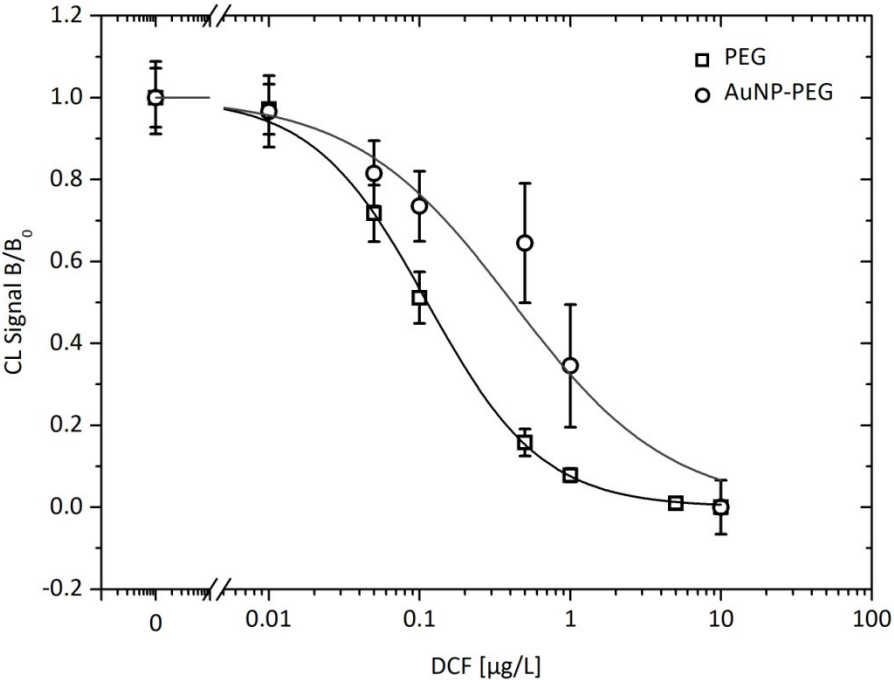
Figure 64: Calibration curves for DCF with antibody 12G5. Error bars represent standard deviations for 5 spots on the same microarray.

2.4.3 Gold covered PMMA slide

The gold covered PMMA carrier (AuPMMA) allowed an increase of the CL signal intensity shown in Figure 65. An increase by the factor 2 was observed for the background corrected CL signal. Therefore, the detection antibody 12G5 could be diluted two times more for the AuPMMA flow cell. In Figure 66, the resulting calibration curves are shown. For the plain PMMA carrier, the IC_{50} value is 0.11 µg/L and for the AuPMMA carrier it is 0.28 µg/L. The sensitivity decreases although the detection antibody was diluted two times higher. In the calibration curve, the difference between 0 µg/L and 0.1 µg/L cannot be seen in the calibration curve. Presumably, the CL signal is not enhanced by the gold layer opposite to the microarray chip in the flow cell. The CL signal is reflected by the AuPMMA carrier. This effect must raise the CL signal independently from mAb concentration on the microarray surface.
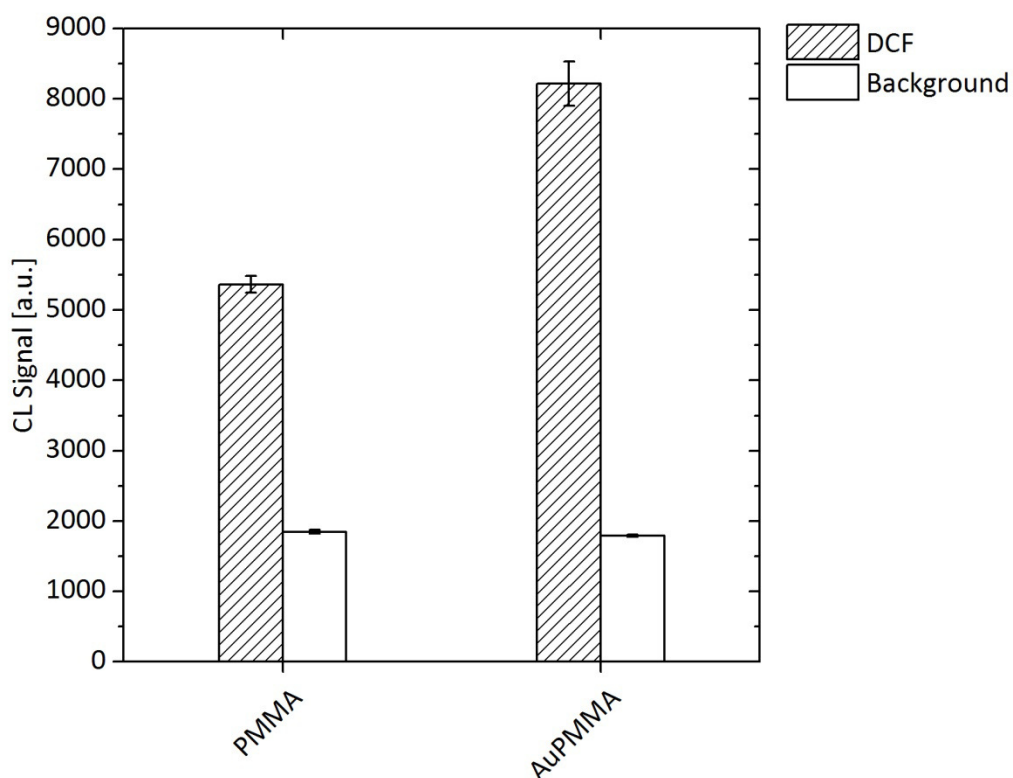
Figure 65: Signal comparison for the PMMA carrier without and with a gold layer attached. Error bars represent standard deviations for 5 spots on the same microarray.
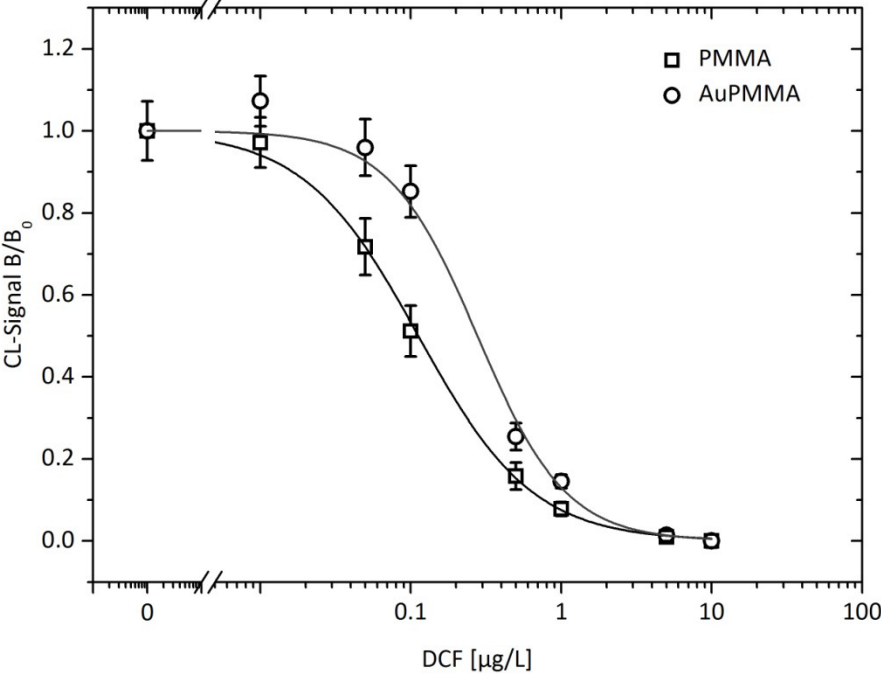
Figure 66: Calibration curves for DCF with antibody 12G5. Error bars represent standard deviations for 5 spots on the same microarray.

3 Preparation of a multi-analyte microarray for the detection of emerging pollutants in fresh water

The described procedure for surface preparation and single-analyte calibrations were combined to develop a multiplex method. This method was further developed and tested with real water samples from wastewater treatment plants and fresh water.

3.1 Microspotting method for multi-analyte microarrays

For the preparation of a multi-analyte microarray, the microspotting was carried out in 2 steps (Figure 67). During the first part, activated esters of DCF and PBA are spotted on a glass slide modified with DAPEG. Then, the microarray is incubated with Traut's reagent to produce thiol groups on the microarray surface. In the second part of the microspotting method, MC-LR is spotted on the surface. The microarrays were stored in an desiccator under vacuum to avoid oxidation of PBA. Figure 68 shows the resulting image of the CCD camera in the MCR 3. The different spots can be seen within the flow-cell of the instrument.
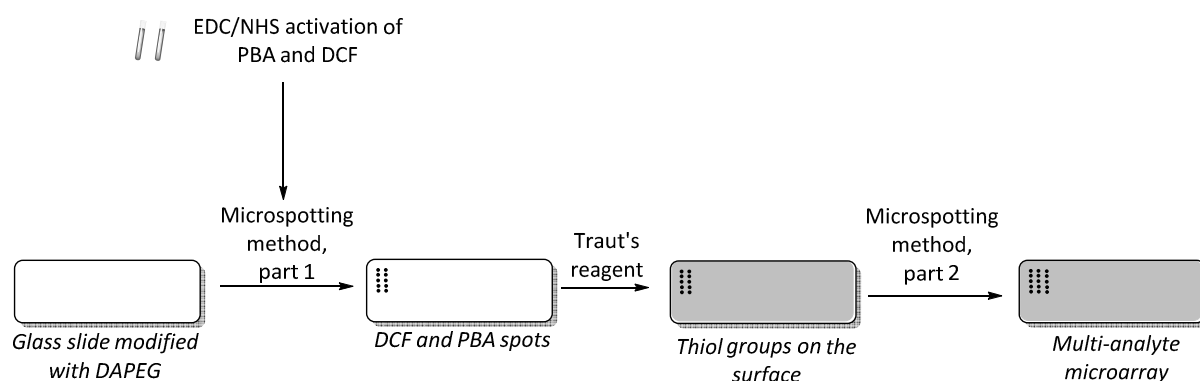
Figure 67: Steps for the preparation of the multiplex microarray on planar glass slides

The prepared microarrays were tested with the different monoclonal antibodies (Figure 69). The CL signals for the target analytes were significantly above the background signal and the signals for non-target analytes were in the range of the background signal. Accordingly, the antibodies did not show CR against non-specific ligands on the surface. For the further calibration and regeneration experiments, mAb 12G5 was also diluted to a signal intensity of about 3000 a.u. to allow high assay sensitivity and satisfactory signal intensity for calibration experiments. One measurement takes 20 min including the regeneration of the chip surface.
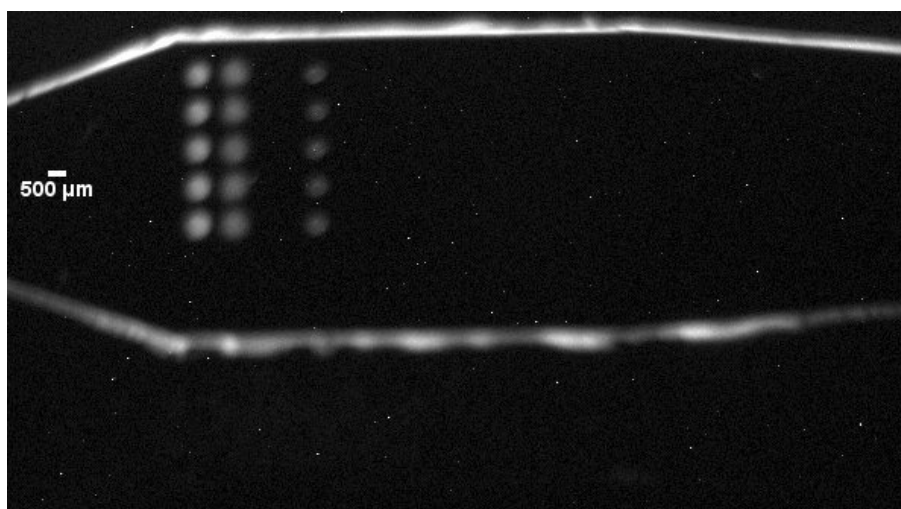
Figure 68: Image of the flow cell with the microarray in the MCR 3. The signals belong to DCF, PBA and MC-LR spots with a blank row in between.
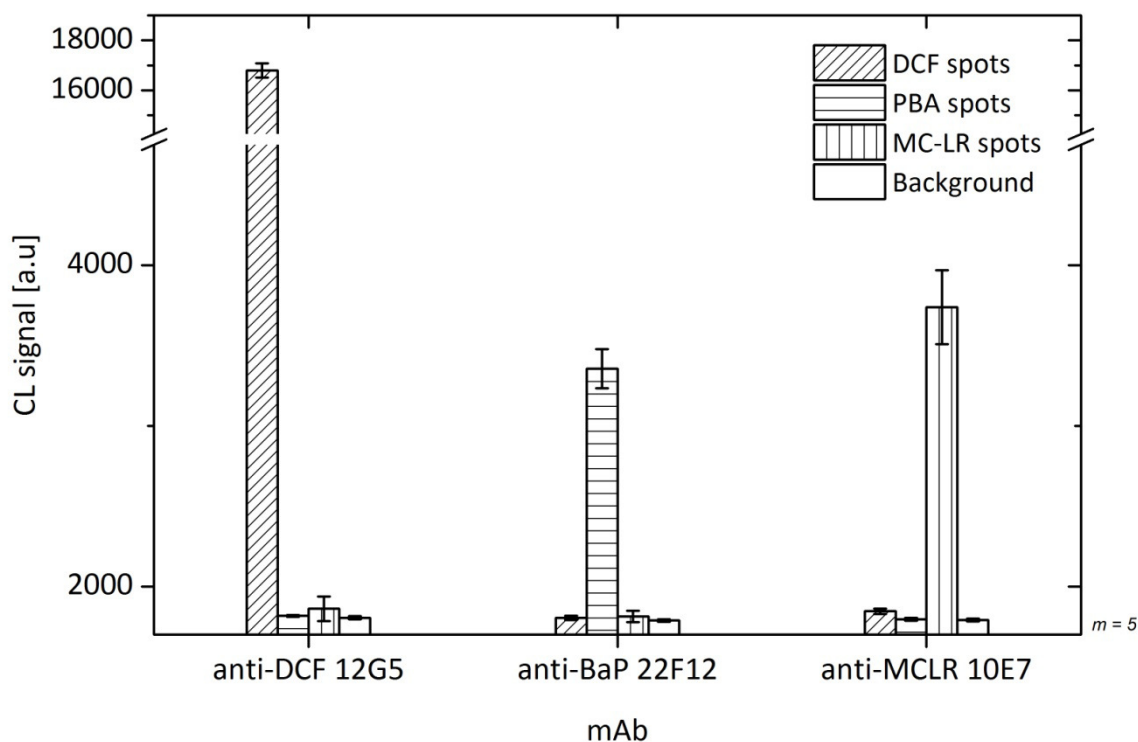
Figure 69: Signal intensities for differend mAbs on a multiplex microarray.

3.2 Regeneration and matrix effects

Since the preparation of the microarrays is labor-intensive (Figure 69), a regenerable multi-analyte surface is economical. In Figure 71, a typical regeneration procedure is shown for more than 20 measurements, which correspond to one day of measurements on the same chip. It can be seen, that the chip is regenerable. After the initial measurement, the signal stays constant for at least 20 more measurements. Consequently, the chip can be used for

one day. For MC-LR, the signal decreases to about 85% in the final measurements of this measurement day. A similar observation was made for DCF in Figure 44. However, the signal decrease could not be observed every day for the two analytes. In order to avoid a high impact of this occasionally occurring signal decrease, the measurements 1-4 were not used for sample or standard measurements. From measurement 5 on, the signal intensities do not fluctuate significantly in regeneration experiments. Consequently, the first measurement of each day was started after regeneration cycle 4.

The regeneration experiment was repeated in pure water, fresh water and different wastewater samples on different days. In this way, the regenerability of different chips and in different matrices was checked. The fresh water and wastewater samples were prepared by filtration and addition of MeOH in a ratio of 1/1 (v/v) as described for the optimized assay protocol (Section 2.2.4). During these regeneration experiments, the signal fluctuation was 7.7 ± 2.5 % in average for different water samples on different microarray chips (Table 17). Thus, the LOD was set at 80% of the initial calibration intensity for this method. This value corresponds to the IC_{20} of the calibration curve, which was also defined as the LOQ for ELISA calibration curves in general.

In Figure 72, the effect of different water samples on the blank signal is presented. The signal was not influenced significantly by the different water samples for the three different analytes. The drinking water sample and fresh water samples were very different in their composition: the Ca^{2+} concentration was 37 - 84 mg/L, Mg^{2+} was 11 - 26 mg/L, DOC was 1.4 - 4.7 mg/L, conductivity 284- 570 µS/cm and pH between 7.8 and 8.2. The individual values are listed in Table 20 in the Experimental Section. The absent influence of the different matrices on the CL signal can be explained be the dilution of sample with MeOH in a ration of 1/1. Furthermore, the mAb is diluted in running buffer (0.5% casein in PBS) during the incubation step. Additionally, the incubation is shorter (< 5 min) than in ELISA experiments on MTP (30 min). Consequently, the immunoassay setup in the MCR 3 allows reproducible measurements which are independent from the water sample

Moreover, wastewater samples were measured on different days on different chips in the MCR 3 (Table 17). Figure 72 shows the CL signals during one of these measurement days. The signals for on PBA spots and MC-LR spots stay constant while the signal on DCF spots decreases to about 20% of the maximum signal intensity. The wastewater samples are polluted by DCF as it was already shown in ELISA experiments in Table 12. Subsequently,

these signal values for DCF were not used for the determination of the signal fluctuation for the LOD determination in Table 17.
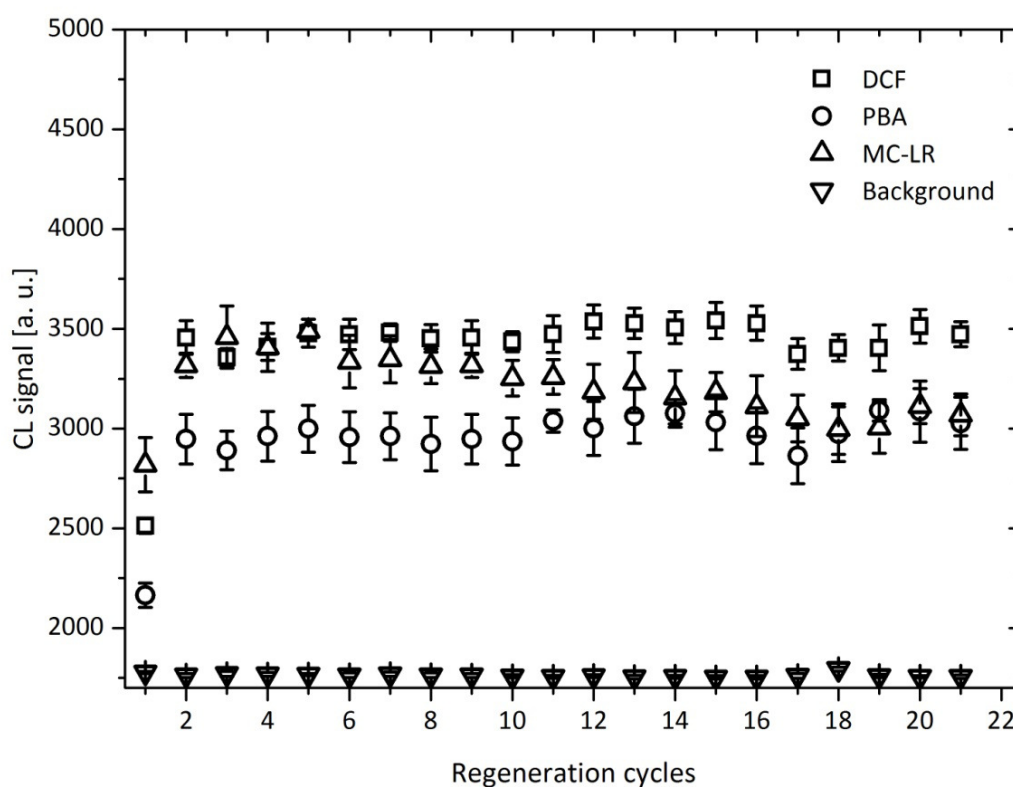
Figure 70: Regeneration of a multiplex chip. Error bars represent signal fluctuations between 5 spots on the microarray

Table 16: Signal fluctuation in % for blank measurements (background corrected)

Microarray spots	Pure water (m = 20)	Fresh water, Wörthsee (m = 17)	Wastewater samples (m = 15, day 1)	Wastewater samples (m = 15, day 2)
DCF	3	5	n. d.	n. d.
PBA	6	9	7	10
MC-LR	10	8	3	10
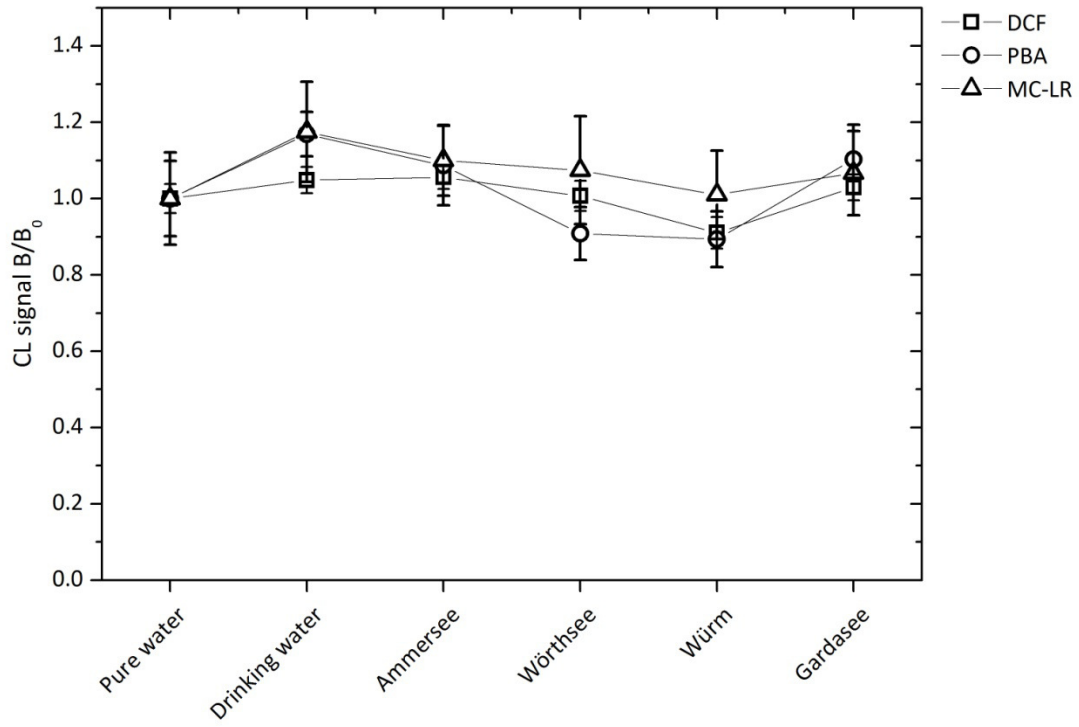
Figure 71: Matrix effect on the blank signal for different water samples in comparison to pure water. Error bars represent signal fluctuations between 5 spots on the microarray.
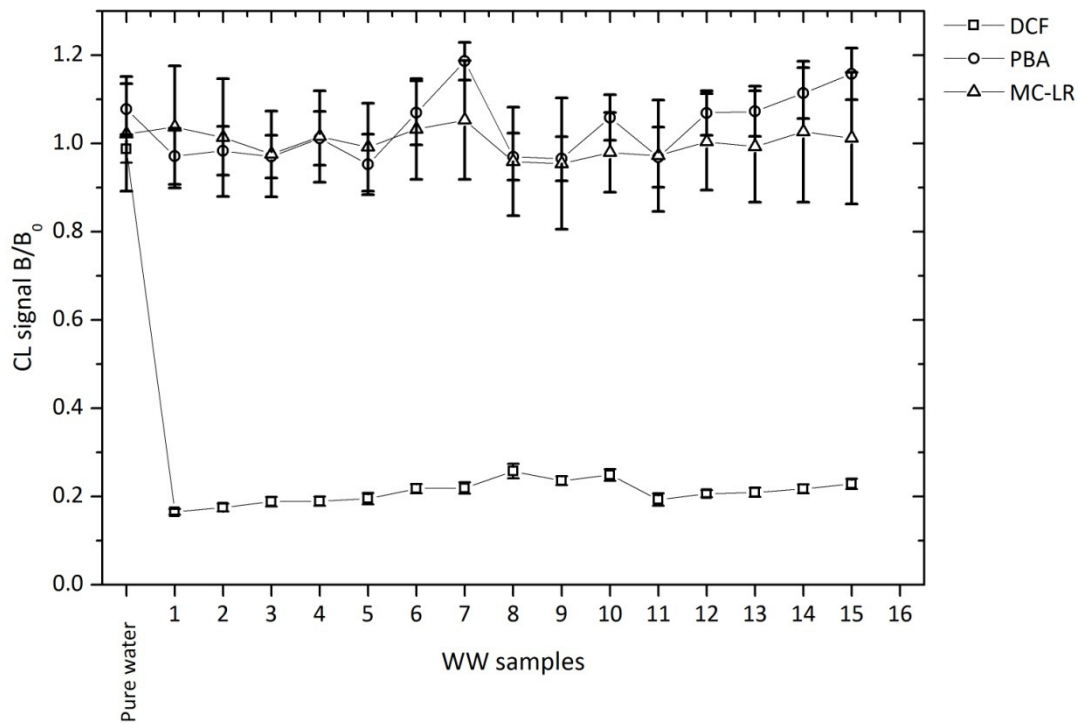
Figure 72: Matrix effect on the blank signal for wastewater samples in comparison to pure water. Error bars represent signal fluctuations between 5 spots on the microarray.

3.3 Calibration and reproducibility

The setup and assay program were now used for the parallel quantification of the three analytes. The RSD for the 5 different spots on one microarray was below 10% for BaP (Figure 74), below 4% for DCF (Figure 75) and below 13% for MC-LR (Figure 76). In an intra-assay study with 3 repeated injections of the standard solutions, the signal intensities fluctuated with RSD values ≤ 6% for the three analyties. Accordingly, the fluctuations between different spots were higher than for different standard injections.

The absolute CL signal was in general the highest for DCF and the lowest for MC-LR. From day to day, the total signal varied with 14% for DCF, 23% for BaP and 18% for MC-LR. This fluctuation can be caused by different chips that were used for each day, new standard solutions and new antibody dilutions for every day. Nevertheless, the measurements were reproducible from day to day as shown in Figures 74 to 76. For an inter-assay comparison, the overall measurement procedure was repeated three times on three different days. The resulting LOD (at 80% signal intensity), assay sensitivities and working ranges are shown in Table 17. They were reproducible from day to day, because the RSD was generally less than 20%. For the LODs of DCF and BaP, they were about 30%, however, the absolute standard deviations were comparable to those of the IC_{50} values.
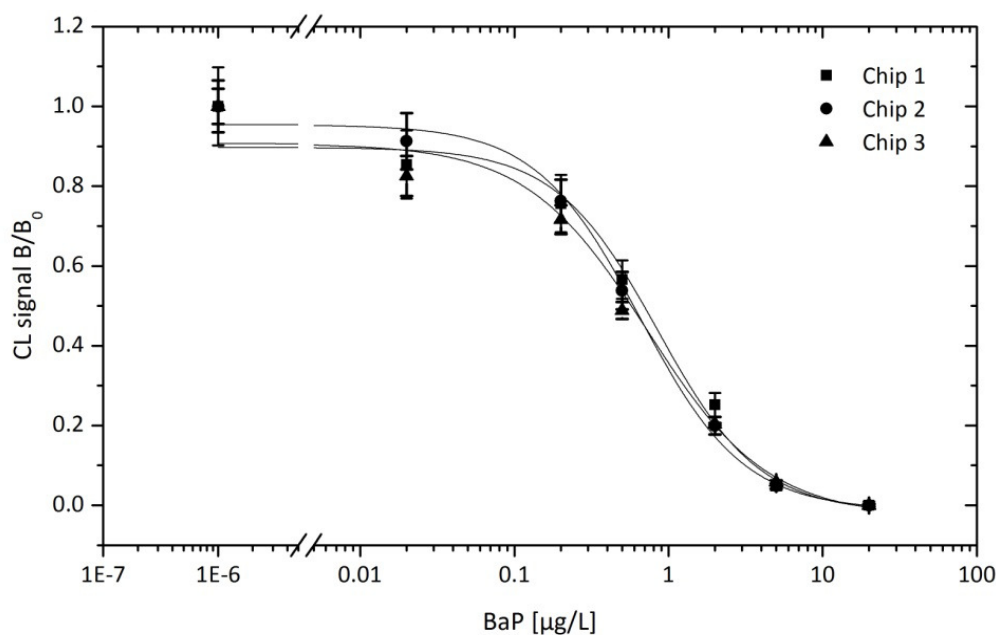
Figure 74: Inter-assay comparison of the multi-analyte microarray for BaP on three different chips on three different measurement days. Error bars represent signal fluctuations between 5 spots of PBA on the microarray.
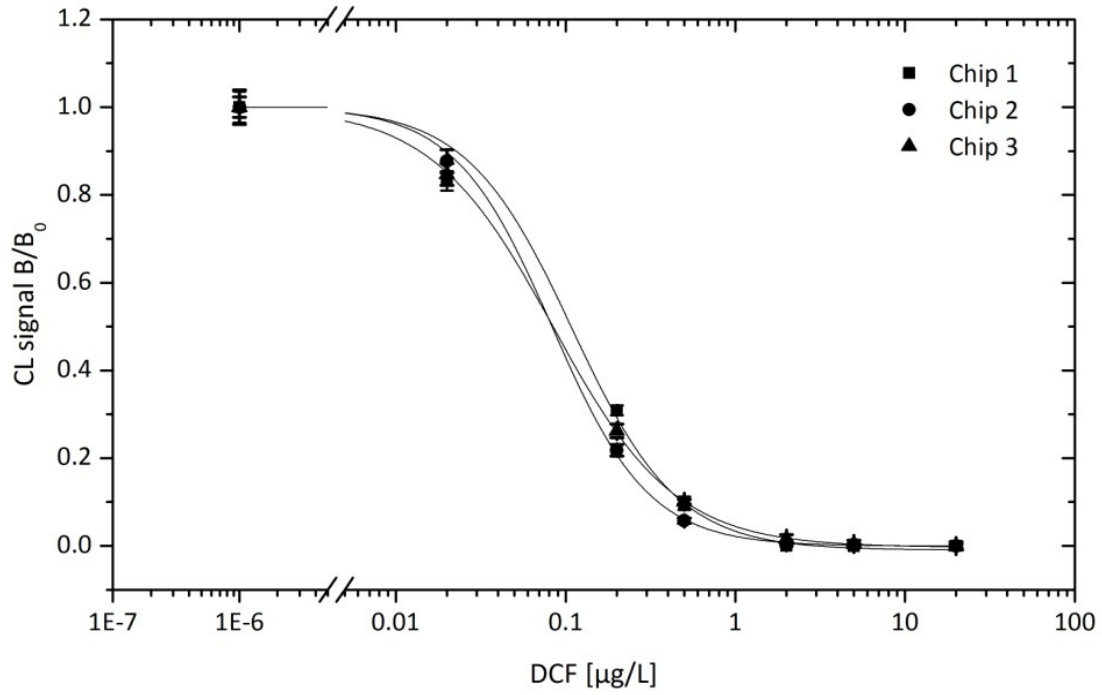
Figure 75: Inter-assay comparison of the multi-analyte microarray for DCF on three different chips on three different measurement days. Error bars represent signal fluctuations between 5 spots of DCF on the microarray.
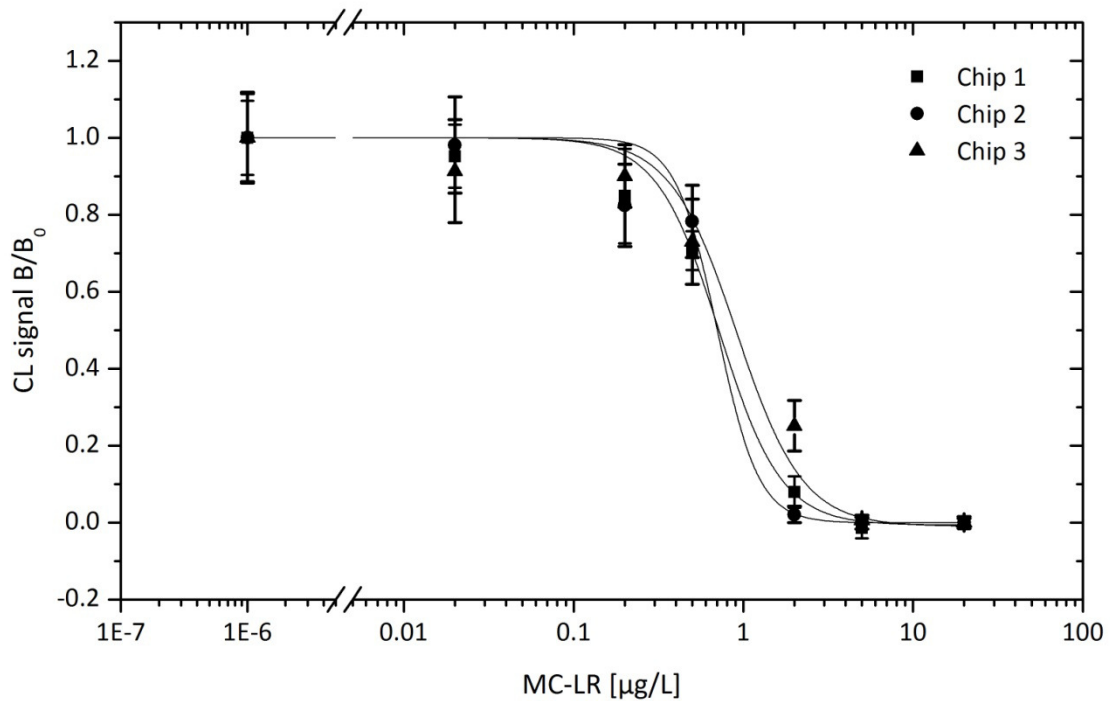
Figure 76: Inter-assay comparison of the multi-analyte microarray for DCF on three different chips on three different measurement days. Error bars represent signal fluctuations between 5 spots of DCF on the microarray

Table 17: Inter-assay study (m = 3)

Analyte	LOD [μg/L]	RSD in %	IC$_{50}$ [μg/L]	RSD in %	Working range of the calibration curves
DCF	0.034 ± 0.010	29	0.092 ± 0.010	11	0.034 – 0.26
BaP	0.22 ± 0.072	33	0.70 ± 0.13	9	0.22 – 2.2
MC-LR	0.58 ± 0.065	11	1.0 ± 0.14	14	0.58 – 1.7

For the Ammersee and Wörthsee samples, enough sample aliquots were available to investigate the real concentration of DCF and BaP in the samples. Moreover, the drinking water sample was analyzed, too. MC-LR was not further investigated, because of the absence of alge in the lakes and in drinking water. The HPLC-MS method was the same as described for ELISA experiments above. The HPLC-FLD method with a previous LLE was carried out as described by Knopp, 2000. The results show that the amount of BaP and DCF is below the LOD in the MCR 3 (see Table 18). Therefore, the detected amounts did not cause a signal decrease in comparison to pure water (Figure 71).

Table 18: LC-based analysis of water samples

Sample	DCF by SPE-HPLC-MS [μg/L]	BaP by LLE-HPLC-MS [μg/L]
Drinking water	n.d.	< LOD
Ammersee	0.0128	< LOD
Wörthsee	< LOD	< LOD
LOD	0.012	0.025

3.4 Recovery in fresh water samples

The optimized calibration method was now used to determine recovery rates with fresh water samples. For the measurements, the analytes were provided in MeOH and then, the filtrated fresh water sample was added in a ratio of v/v = 1/1 for the injection into the MCR 3. In this way, non-specific adsorption of PAHs to the sampling vial or particles in the sample was kept as low as possible.

The recovery was at 116 ± 23 % for DCF, 122 ± 20 % for BaP and 93 ± 9 % for MC-LR in 5 different fresh water samples. These recovery rates are acceptable for immunoassays (Oswald, 2013). They show that the multi-analyte microarray is suitable for the detection of emerging pollutants in fresh water samples. The Windach sample yielded recoveries obf 81% and 80% for DCF and MC-LR. This underestimation may be caused by interference of the matrix which contained more DOC and Ca^{2+} compared to the freshwater samples in Figure 72: 9.7 mg/L and 86 mg/L (see also Table 19).

In addition, a present amount of micropollutant in the water sample can raise the recovery rate. However, according to Table 18, the amounts contribute to an overestimation by 8 % for DCF and <5 % for BaP in the Ammersee sample. For the Wörthsee sample, the amounts account for only 2 % for DCF and < 5%, respectively. Accordingly, the overestimation in the MCR 3 is not uniquely caused by additional amounts of DCF and BaP from the sample. Further effects can arise from similar components within the sample which cross-react with the antibody. Moreover, since the spiked amounts are very low, a systematic error by pipetting these small amounts must not be excluded as an error source. For the samples that were spiked with 1.0 µg/L for BaP and MC-LR, the recovery is in the range between 93 ± 9%.In comparison to the HPLC-MS and HPLC-FLD methods, the MCR 3-based method requires less measurement time, laboratory equipment and simple sample pre-treatment. Sample pre-concentration and extraction by SPE or LLE is not required. Moreover, different instruments are necessary to analyze the same water samples. The sample amount for fresh water analysis is 50 mL for the LC-based methods. In contrast, only 1 mL is sufficient for the analysis by the MCR 3. Consequently, the developed automated immunoassay provides a convenient and promising alternative to the usually applied instruments based on chromatography.

Table 19: Recovery in fresh water samples

	DCF [µg/L]	rec. in %	BaP [µg/L]	rec. in %	MC-LR [µg/L]	rec. in %
Spiked concentration	0.17		0.50		1.0	
Ammersee	0.20	117	0.65	130	0.96	96
Wörthsee	0.19	111	0.56	111	1.02	102
Gardasee	0.23	133	0.93[2]	93	0.97	97
Windach	0.14	81	0.66	132	0.80	80
Donau	0.24	140	0.73	146	0.88	88
Average recovery (m = 5)		116		122		93
Deviation		23		20		9

---

[2] For this measurement, 1.0 µ/L BaP were spiked to the sample.

IV Summary and Outlook

The aim of this work was to elaborate immunological methods for the detection of micropollutants in water samples. These pollutants are highly variable regarding their origin and molecular structures. By using monoclonal antibodies (mAbs), highly specific and sensitive immunoassays can be provided as recently shown for benzo[a]pyrene and microcystin-LR. Another class of emerging pollutants are pharmaceuticals like the non-steroidal anti-inflammatory drug (NSAID) diclofenac. It is found worldwide in the aqueous environment and therefore, has raised increased public concern on potential long-term impact on human health and wildlife. The importance of DCF has been emphasized by the European Union by including this pharmaceutical in the first watch list of priority hazardous substances in order to gather EU-wide monitoring data recently. Rapid and cheap methods of analysis are therefore required for fresh and wastewater monitoring with high sample load. In this work, for the first time, well-characterized mAbs against DCF were generated and a highly sensitive ELISA developed. The best antibody (mAb 12G5) was screened by testing 4 promising mAbs regarding affinity, specificity towards similar pharmaceuticals and DCF metabolites as well as matrix effects in fresh water samples.

Mab 12G5 has turned out to be highly affine (K_D = 1.5 x 10^{-10} M), stable to potential matrix interferences such as pH value (pH range 5.2-9.2), calcium ion concentration (up to 75 mg/L) and humic acid content (up to 20 mg/L). The LOD (S/N = 3) and IC_{50} of the ELISA calibration curve were 7.8 ng/L and 44 ng/L, respectively. The working range was defined between 11-180 ng/L. On average, an about 5% cross reactivity was found for DCF metabolites 5-OH-DCF, 4'-OH-DCF and DCF-acyl glucuronide by using an optimized ELISA protocol. Other structurally related NSAIDs showed binding ≤ 5% compared to the parent compound. While DCF concentrations at the low ppt-range were measured in river and lake water, higher values of 2.9 µg/L and 2.1 µg/L were found in wastewater influents and effluents, respectively. The results could be confirmed by SPE combined with HPLC-MS.

In order to allow the parallel detection of micropollutants in water samples, the mAbs were used to developed a microarray-based competitive ELISA with chemiluminescence (CL) detection in a flow-through device called MCR 3. This device was previously developed at the TU München (Kloth, 2009 a). The microarray chips are prepared on glass carriers, which are modified with a PEG layer that carries terminal amino groups. These glass carriers are glued to a PMMA carrier. On the PEGylated glass slides, an immobilization strategy had to be developed for the different analytes BaP, DCF and MC-LR as model analytes. The

immobilization should not require laborious derivatization of the immobilized hapten and should allow sensitive mAb detection by a high coupling density of the ligand on the microarray surface. In this work, a dioxane based microspotting method was developed that allows the immobilization of hydrophobic 1-pyrenebutanoic acid – a suitable surrogate for BaP – next to DCF and MC-LR. In comparison to previously developed methods (Oswald, 2013), signal intensities were higher and small amounts of hapten (≤ 1 mM in 100 µL) were needed for the microspotting method based on dioxane. The high yield of immobilzation is caused by the absence of salts and the basic character of dioxane to acitvate the terminal amino groups on the DAPEG modified glass carrier. Additionally, the water/dioxane mixture used to the microspotting method (v/v = 1/1) is coating the PEG surface with a lower contact angle than pure water (15° in contrast to 40°). For MC-LR, the same microspotting method could be applied after using Traut's reagent for generating terminal thiol groups on the surface. The developed method allowed the regenerable detection of anti-target analyte antibodies on the microarray chip with low signal fluctuations (< 10%).

This promising surface preparation was further investigated by using the surface analysis methods provied by the French project partners. The strategy for preparing PEG coatings for subsequent hapten immobilization on glass-type silica surfaces was transferred to QCM-D chips and Si wafer. In this way, it could be characterized in detail. The substrates - glass slide and silicon wafers - are bearing terminal silanol groups. For the functionalization, surfaces were first thoroughly cleaned and pretreated to generate additional silanol groups. Then, a silane layer with terminal epoxy groups was created using 3-glycidyloxypropyltrimethoxysilane (GOPTS). Epoxy groups were used to bind a layer of diamino-poly(ethylene glycol) (DAPEG) with terminal amino groups. Finally, the low molecular weight compound diclofenac was bound to the surface to be used as model ligand for competitive biosensing of haptens. The elementary steps were characterized using Atomic Force Microscopy (AFM), Water Contact Angle measurements, Grazing-Angle Attenuated Total Reflection (GA-ATR) FT-IR spectroscopy, and X-Ray Photoelectron Spectroscopy (XPS). The data collected using these techniques have confirmed the successive grafting of the molecular species, evidencing, that homogeneous monolayers were created on the silica surfaces and validated the proposed mechanism of functionalization. The resulting surfaces were used to investigate polyclonal anti-diclofenac antibodies recognition and reversibility using QCM-D measurements or on the MCR 3. For

both techniques, recognition and reversibility of the antibody binding were observed. MAb 12G5 was identified as reliable for surface interaction by using QCM-D, too. The stability of sensors over time was also assessed and no decrease in CL response was observed over 14 days in aqueous solution. The herein presented strategy for surface functionalization can be used in the future as reproducible and reusable universal biosensor platform for small molecules.

In order to further raise the sensitivity of the CL read-out immunoassay on the MCR 3, different ways to incorporate AuNPs or Au enhancement into the flow cells were tested. AuNPs were grafted on the surface or coupled to the anti-mouse-HRP secondary antibody. Moreover, the PMMA carrier was covered with gold. However, none of these methods allowed to further increase the CL signal. Therefore, no sensitivity enhancement of the flow-through assay could be achieved.

For multi-analyte detection of emerging pollutants, the assay protocol was optimized to allow reproducible calibration experiments. For the detection of BaP, 50% of MeOH had to be added to the sample in order to avoid non-specific adsorption to the flow-through capillaries and channels of the MCR 3. This increase of organic solvent was also tolerated by the anti-DCF and anti-MC-LR mAbs 12G5 and 10E7. The maximum CL signal intensity was achieved by using a flow rate of 2 µL/min for the mAb binding step to the microarray surface. The measurements based on this optimized assay program were also reproducible in fresh water and wastewater samples with RSD < 10% for blank measurements in the different matrices. In calibration experiments, the LOD was 34 ng/L for DCF, 220 ng/L for BaP and 580 ng/L for MC-LR. The inter-assay RSD was in general below 20% for the three analytes on three different measurement days on three different microarray chips. Subsequently, the developed assay allows sensitive and reproducible calibration curves for the three different emerging pollutants. Finally, the recoveries in fresh water were tested and they were on average between 93 and 122 % for the three different analytes in 5 different fresh water samples. False positive results were not found in different fresh water samples. These results show the general applicability of the method for fresh water analysis. In comparison to chromatography-based methods, this analysis requires less sample pre-treatment and less laboratory equipment. The monoclonal antibodies are robust and reliable detection reagents for the three different target analytes from different chemical classes.

In the future, additional priority pollutants can be added to the microarray like E2 and EE2 or antibiotics for screening applications. The presented coupling strategy can be transferred to other haptens that were coupled to proteins *via* amino groups for immunization. For the reliable detection of these haptens, however, it is crucial to have access to well characterized and highly reproducible antibodies like mAbs. Therefore, a standardized antibody preparation and characterization will be required to raise the acceptance of the immunological methods for analytical chemistry in general.

For the high-throughput analysis of fresh water analysis, another important development will be the implementation of standardized reference materials for this matrix including PAHs as well as pharmaceuticals, pesticides and toxins. (Elordui-Zapatarietxe, 2015)

V Experiments

1 Instruments and materials

1.1 Instruments

ELISA

Reader Synergy HT (BioTek, Bad Friedrichshall)

Shaker Easyshaker EAS 2/4 (SLT, Crailsheim)

Washing automat ELx 405 Select (BioTek, Bad Friedrichshall)

HPLC-FLD

Column thermostat (Model CTO-20A, Shimadzu, Kyoto, Japan)

High pressure pump (Model LC-20AT, Shimadzu, Kyoto, Japan)

Variable wavelength fluorescence detector (Model RF 10-AXL, Shimadzu, Kyoto, Japan)

HPLC-MS

Column oven HotDog 5090 (ProLab, Reinach, Switzerland)

Exactive – Orbitrap Mass Spectrometer (Thermo Scientific, Bremen)

Hamilton syringe pump (Fusion HT, Thermo Fisher Scientific, Bremen)

Surveyor Autosampler PlusLite (Finnigan, Bremen)

Surveyor MS PumpPlus (Finnigan, Bremen)

Syringe pump Fusion HT (ThermoScientific, Bremen)

MALDI-TOF

Ultraflex TOF/TOF, N_2-Laser, 337 nm (Bruker-Daltonics, Bremen)

Microarray preparation and read-out

Double-sided adhesive foil (ARcare 90106)

Glass syringe SGE, 1 mL, Luer Lock (SGE, Melbourne, Australia)

Microarray spotter BioOdyssey Calligrapher Mini Arrayer (Bio-Rad, München)

Munich Chip Reader 3 (GWK Präzisionstechnik, München)

Spotting pin SNS 12 (ArrayIt, Sunnyvale, USA)

UV Star® 384 well plate (Greiner Bio-one GmbH, Frickenhausen)

Surface Plasmon Resonance measurements

Biacore X100 (GE Healthcare, Freiburg)

Surface analysis

Contact angle measurement device(Krüss GmbH, Hamburg)

MultiMode 8 atomic force microscope (Bruker, Santa Barbara, CA, USA)

Argus X-ray photoelectron spectrometer (Omicron, Taunusstein-Neuhof)

VariGATR-FTIR spectrometer (Harrick Scientific, Pleasantville, NY, USA)

Miscellaneous

Balance Mettler AT261 Delta Range (Mettler-Toledo, Giessen)

Balance Mettler PM4600 Delta Range (Mettler-Toledo, Giessen)

Centrifuge Universal 320R(Hettich, Tuttlingen)

Drying oven 20 – 250 °C (Memmert, Büchenbach)

Engraving pen MICROMOT 50/E (Proxxon, Niersbach)

Lyophilization Alpha 1-4 LSC (Christ, Osterode am Harz)

Magnetic stirrer with heating function (MR 3002 S, Heidolph, Kelheim)

Mixer T25 basic (IKA Labortechnik, Staufen)

pH / conductivity cell Multi 3401 (WTW, Weilheim)

Ultrapure water facility Milli-Q plus 185 (Millipore, Schwalbach)

Ultrasonic bath Sonorex Super RK106 (Bandelin, Berlin)

UV/Vis spectrometer DU 650 (Beckman, Fullerton, USA)

Vortexer TopMix FB1 5024 (Fisher Scientific, Schwerte)

1.2 Software

AVIS V.F. (MSB di F. Cavicchio, Ravenna, Italien)

Biacore X100 Control Software 1.1 and Evaluation Software 1.1 (GE Healthcare, Freiburg)

ChemBioDraw Ultra 14.0 (Perkin Elmer, Waltham, MA, USA)

Exactive Tune (ThermoScientific, Bremen)

Excel (Micosoft, Redmond, USA)

Fusion Instrument Control (Perkin Elmer, Waltham, USA)

Gen5 (BioTek, Bad Friedrichshall)

LabView 8.2 (National Instruments, Austin, USA)

LC solution (Shimadzu, Kyoto, Japan)

MCR ImageAnalyzer Ver. 03.2.1 (GWK, München)

Origin 9.1G (OriginLab Corporation, Northampton, USA)

SIP 0.4 (Karsunke Softwarebüro, Wolnzach)

Xcalibur (ThermoScientific, Bremen)

1.3 Material and chemicals

Antibodies and antigens

Horse Anti-Maus antibodies IgG, HRP labelled, affinity purified (Axxora, Lörrach)

Monoclonal antibody anti-Benzo[a]pyrene 22F12 (Institute of Hydrochemistry, München)

Monoclonal antibody anti-MC-LR 10E7 (Squarix, Marl)

Polyclonal anti-DCF antiserum (Institute of Hydrochemistry, München)

Material

AuNP-coupled anti-mouse IgG labeled with HRP (Laboratory for Surface Reactivity, UPMC, Paris, France)

AuNP-PEG covered glass slides (Laboratory for Surface Reactivity, UPMC, Paris, France)

Adhesive foil, ARcare 90106, Akryl Hybrid, double-sided (Adhesive Research, Limerick, Irland; laser cut by IWC, München)

Biacore X100: BIA Maintenance Kit (BR-1006-66, GE Healthcare, Freiburg)

HBS EP+ buffer (BR-1008-26, GE Healthcare, Freiburg)

PP vials 1.5 mL (BR-1002-87, GE Healthcare, Freiburg)

Sensor chip CM5 (BR-1000-14, GE Healthcare, Freiburg)

Rubber caps (BR-1004-11, GE Healthcare, Freiburg)

Carrier for staining microscopy carriers PP (2291.1, Carl Roth, Karlsruhe)

Centrifugation tubes PP, 15 mL, non-sterile (AN76.1, Carl Roth, Karlsruhe)

Centrifugation tubes PP, 50 mL, non-sterile (AN78.1, Carl Roth, Karlsruhe)

Eppendorf pipettes (0,5 – 10 µL, 10 – 100 µL, 100 – 1000 µL, 1 – 5 mL, multi-channel pipette 20 – 300 µL) (Eppendorf, Hamburg)

Folded filter 210 mm (531 – 021, Macherey-Nagel, Düren)

Glass microfibre filters GF/C, 47 mm in diameter (1822047, Whatman, UK)

Gloves, nitrile (P778.1, Carl Roth, Karlsruhe)

HEPES (Carl Carl Roth, Karlsruhe)

IsoQuick™ Kit for Mouse Monoclonal Isotyping (ISOQ, Sigma-Aldrich, Steinheim)

Low-IgG fetal calf serum (Invitrogen, Carlsbad, USA)

Microtiter plate, 384-well, flat bottom, UV Star® (Greiner, Frickenhausen)

Microtiter plate, 96-well, flat bottom, high binding capacity (655061, Greiner, Frickenhausen)

Multi-reaction flasks 0.65 mL (7060.1, Carl Roth, Karlsruhe)

Oasis HLB 1cc (Waters, Eschborn)

Parafilm (H666.1, Carl Roth, Karlsruhe)

Pasteur pipette (4522, Carl Roth, Karlsruhe)

Petri dish (0690.1, Carl Roth, Karlsruhe)

Pipette tips: 0.1 – 10 µL (K138.1, Carl Roth, Karlsruhe, Deutschland)

0.5 – 5 mL (Brand, Wertheim)

100 – 1000 µL (2679.1, Carl Roth, Karlsruhe, Deutschland)

1 – 200 µL (B007.1, Carl Roth, Karlsruhe)

PMMA carrier (Sahlberg, Feldkirchen; milled at IWC, München)

Reaction flask 10 mL (X655.1, Carl Roth, Karlsruhe)

Reaction flask 1.5 mL (4190.1, Carl Roth, Karlsruhe)

Rubber cap (BR-1004-11, GE Healthcare, Freiburg)

Sealing foils for microtiter plates (EN76.1, Carl Roth, Karlsruhe)

(Silicon wafers <100> (Sigma-Aldrich, France)

Single-use canola, 0.80 x 120 mm (C630.1, Carl Roth, Karlsruhe)

Single-use canola, 0.90 x 40 mm (C721.1, Carl Roth, Karlsruhe)

Single-use syringe, 1 mL (H.999.1, Carl Roth, Karlsruhe)

Single-use syringe, 10 mL (0058.1, Carl Roth, Karlsruhe)

Single-use syringe, 5 mL (0057.1, Carl Roth, Karlsruhe)

Single-use syringe filter, reg. cellulose, pore size 0.20 µm (5824.2, Carl Roth, Karlsruhe)

Staining shell TPX (2290.1, Carl Roth, Karlsruhe)

Vials PP, 1.5 mL (BR-1002-87, GE Healthcare, Freiburg)

ZipTipC4 pipette tips (Merck Millipore, Darmstadt)

Chemicals

1 -Fluoranthenebutanoic acid, solid (PAH Research Institute, Greifenberg)

1,1`-Carbonyldiimidazole (21860, Sigma-Aldrich, Steinheim)

1-Hydroxybenzo triazole (54802, Sigma-Aldrich, Steinheim)

1-Pyrenebutanoic acid, solid (257354, Sigma-Aldrich, Steinheim)

2,2'-azino-bis(3-ethylbenzothiazoline-6-sulphonic acid) (Roche, Mannheim)

2,4-Dihydroxybenzoic acid (37530, Fluka, Buchs)

2-Iminothiolane hydrochloride (I6256, Sigma-Aldrich, Steinheim)

2-Mercaptoethanol (Serva, Heidelberg, Germany),

3,3`,5,5`-Tetramethylbenzidine, (T2885, Sigma-Aldrich, Steinheim)

3-Benzo[a]pyrenebutanoic acid, solid (PAH Research Institute, Greifenberg)

3-Glycidyloxypropyltrimethoxysilane (50040, Sigma-Aldrich, Steinheim)

4'-Hydroxydiclofenac, solid (University of Connecticut, Storrs, USA)

5-Hydroxydiclofenac, solid (Sandford Burnham Medical Research Institute, Orlando, USA)

6-Chrysenebutanoic acid, solid (PAH Research Institute, Greifenberg)

7-Benzo[k]fluoranthenebutanoic acid, solid (PAH Research Institute, Greifenberg)

8-Benzo[a]anthracenebutanoic acid, solid (PAH Research Institute, Greifenberg)

Acetic acid (320099, Sigma-Aldrich, Steinheim)

Aceton, laboratory reagent (179973, Sigma-Aldrich, Steinheim)

Acetonitrile, HPLC-MS grade (34967, Sigma-Aldrich, Steinheim)

Acylglucuronide of diclofenac, solid (University of Connecticut, Storrs, USA)

Ammonium hydroxide, 28% NH3 in water (338818, Sigma-Aldrich, Steinheim)

Benzo[a]pyrene, solid (Dr. Ehrnstorfer, Augsburg)

Bovine insulin (Roche, Mannheim, Germany)

Bovine serum albumin (A3059, Sigma-Aldrich, Steinheim)

Calcium chloride (C1016, Sigma-Aldrich, Steinheim)

Carboxymethoxylaminhydrochloride (C13408-IG, Sigma-Aldrich, Steinheim)

Casein (C5890, Sigma-Aldrich, Steinheim)

Diaminopolyethylenglycol DAPEG, M~2000 g/mol (XTJ 502, Huntsman, Rotterdam, Netherlands)

Diclofenac (D-6899, Sigma-Alrdich, Steinheim)

Dimethyl sulfoxide (41647, Sigma-Aldrich, Steinheim)

Dioxane, (296309, Sigma-Aldrich, Steinheim)

Dipotassium hydrogen phosphate (60220, Sigma-Aldrich, Steinheim)

Ethylendiamindihydrochloride (195804, Sigma-Aldrich, Steinheim)

Fenoprofen (F-1517, Sigma-Aldrich, Steinheim)

Formic acid, p.a. for MS (94318, Sigma-Aldrich, Steinheim)

Gentamycin (Serva, Heidelberg)

Glucose (Merck, Darmstadt, Germany),

Glycine (33226, Sigma-Aldrich, Steinheim)

Horserasish peroxidase (Dianova, Hamburg)

Hydrochloric acid ~ 4.0 M (84435, Fluka, Buchs)

Hydrochloric acid 37 % (84422, Sigma-Aldrich, Steinheim)

Hydrogen peroxide solution for chemiluminescence assay (1859679, Pierce, Rockford)

Hydrogen peroxide solution, 30 % (95321, Sigma-Aldrich, Steinheim)

Ibuprofen (I-4883, Sigma-Aldrich, Steinheim)

Ketoprofen (K-1751, Sigma-Aldrich, Steinheim)

L-glutamine (Invitrogen, Carlsbad, CA, USA)

Luminol solution for chemiluminescence assay (1859678, Pierce, Rockford)

Magnesium chloride hexahydrat (1.05832, Merck, Darmstadt)

Meclofenamic acid(M-4531, Sigma-Aldrich, Steinheim)

Mefenamic acid (M-4267, Sigma-Aldrich, Steinheim)

Methanol (65548, Sigma-Aldrich, Steinheim)

Methanol, HPLC-MS grade (34966, Sigma-Aldrich, Steinheim)

Microcystin-LR (ALX-350-012-M001, Enzo Life Sciences, Lörrach)

N,N`-Diisopropylethylamine (496219, Sigma-Aldrich, Steinheim)

N,N´-Dimethylformamide, for analysis (1.0650.2500, Merck, Darmstadt)

N-Hydroxysuccinimide (56480, Sigma-Aldrich, Steinheim)

Nitrogen 5.0 (Air Liquide, München)

Ovalbumin (A5503, Sigma-Aldrich , Steinheim)

Polyethylen glycoldiamine 2000 Da Fa. (XTJ-502, Huntsman, Deggendorf)

Polyethylene glycol 1500 (Boehringer, Mannheim)

Potassium dihydrogen phosphate (04248, Sigma-Aldrich, Steinheim)

Potassium dihydrogencitrate hydrate (44415, Alfa Aesar, Karlsruhe)

Potassium sorbate (85520, Sigma-Aldrich, Steinheim)

Sodium dodecylsulfate (71728, Fluka, Buchs)

Sodium azide (S2002, Sigma-Aldrich, Steinheim)

Sodium carbonate (71628, Sigma-Aldrich, Steinheim)

Sodium chloride (13565, Sigma-Aldrich, Steinheim)

Sodium hydrogencarbonate (K28996729, Merck, Darmstadt)

Sulfuric acid 95 – 98 % (435589, Sigma-Aldrich, Steinheim)

Tergazyme, enzyme detergent (Z273287-1EA, Sigma-Aldrich, Steinheim)

Tolfenamic acid (T-0535, Sigma-Aldrich, Steinheim)

Triethylamine (90340, Fluka, Steinheim)

Tween 20 (8.17072, Merck, Darmstadt)

α-Cyano-4-hydroxycinnamic acid (C8982, Sigma-Aldrich, Steinheim)

1.4 Buffers and preparations

All solutions were prepared using purified water from a MilliQplus 185 system.

Blocking solution for ELISA (1 % Casein)

1 g Casein

PBS, ad 100 mL

Heated to 90 °C for dissolution of casein and filtrated through a folded filter

Coating buffer for ELISA (pH 9.6)

Na_2CO_3, 1.59 g

$NaHCO_3$, 2.93 g

NaN_3, 0.2 g

Water, ad 1000 mL

Flushing buffer

KH_2PO_4, 1.36 g

K_2HPO_4, 12.2 g

NaCl, 8.5 g

MeOH, ad 200 mL

Water, ad 800 mL

Phosphate buffer (PBS, pH 7.6)

KH_2PO_4, 1.36 g

K_2HPO_4, 12.2 g

NaCl, 8.5 g

Water, ad 1000 mL

Regeneration buffer

Glycine, 15.01 g

NaCl, 11.7 g

Sodium dodecyl sulphate (SDS), 2 g

Water, ad 2000 mL, pH = 3.0 (H_2SO_4)

Running buffer for MCR 3 measurements

0.5 g casein

PBS, ad 100 mL

Heated to 90 °C for dilution of casein

Stopp solution for ELISA (5 % H2SO4)

98 % H_2SO_4, 50 mL

Water, ad 1000 mL

Substrate solution for ELISA

Substrate buffer, 25 mL

TMB stock solution, 500 μL

H_2O_2 (1%), 100 μL

Substrate buffer for ELISA (pH 3.8)

Potassium dihydrogencitrate, 46.04 g

Potassium sorbate, 0.10 g

Water, ad 1000 mL

Cleaning mixture (MCR 3)

Tergazyme, 4 g

Water, ad 200 mL

Triethylamine buffer (TEA, 50 m, pH = 9.5 / HCl)

Triethylamine, 695 μL

Water, ad 100 mL

TMB stock solution for ELISA

3,3',5,5'-Tetramethylbenzidine, 375 mg

DMSO, 30 mL

Washing buffer, concentrated for ELISA

KH_2PO_4, 8.17 g

K_2HPO_4, 73.16 g

124

NaCl, 52.6 g

Tween 20, 30 mL

Water, ad 1000 mL

Washing buffer for ELISA (pH 7.6)

Washing buffer concentrate, 42 mL

Water, ad 2500 mL

1.5 Samples

1.5.1 WWTP samples for ELISA measurements

The WWTPs were sampled for 24 h at the influent and at the effluent in glass bottles (500 mL, Schott).

WWTP 1: München I

WWTP 2: München II

WWTP 3: Mittleres Isartor, Mittenwald

1.5.2 Fresh water samples

Fresh water samples were taken in glass bottles which were rinsed with ultrapure water before. The fresh water samples were analyzed at the IWC as described in Table 19 regarding different parameters.

Table 20: Fresh water samples

Sample	Date	c(Ca) [mg/L]	c(Mg) [mg/L]	DOC = TOC [mg/L]	Conductivity [µS/cm] comp. to 25 ^{o}C	pH
Isar, Scharnitz	28.08.2014	37.3 ± 0.20	8.44 ± 0.005			
Isar, München (Flaucher)	28.08.2014	56.7 ± 0.05	14.4 ± 0.00			
Isar, Freising	28.08.2014	60.6 ± 0.00	17.0 ± 0.00			

Isar, Marzling	28.08.2014	61.4 ± 0.30	16.5 ± 0.00			
Wörthsee	03.09.2014	39.7 ± 0.28	14.0 ± 0.00			
Ammersee	17.03.2015	59.5 ± 0.09	23.,2 ± 0.06	3.69 ± 0.09	515 ± 0.00	8.02 ± 0.03
Wörthsee	17.03.2015	37.3 ± 0.16	15.1 ± 0.06	4.67 ± 0.03	335 ± 0.00	8.19 ± 0.02
Würm	17.03.2015	45.5 ± 0.09	15.6 ± 0.06	4.63 ± 0.01	397 ± 0.00	8.07 ± 0.01
Drinking water	17.03.2015	84.1 ± 0,21	25.6 ± 0,10	1.43 ± 0,15	570 ± 0,00	7,87 ± 0,01
Gardasee	03.05.2015	37.3 ± 0.09	10.8 ± 0.06	2.80 ± 0.09	284 ± 0.00	7.77 ± 0.01
Donau	25.05.2015	66.7 ± 0.15	15.6 ± 0.00	4.65 ± 0.02	459 ± 0.00	7.92 ± 0.01
Windach	26.05.2015	86.1 ± 0.11	22.7 ± 0.14	9.72 ± 0.07	550 ± 0.00	8.17 ± 0.00

2 Preparation of stock and standard solutions

DCF was diluted in MeOH and stored at 4°C in the dark. Benzo[a]pyrene was diluted in ACN and stored at 4°C in the dark. MC-LR was delivered in aliquots of 1.0 mg. It was diluted in 90 µL DMSO and further diluted to 1.0 mg/mL with 910 µL ACN. The MC-LR stock solution was stored at -20°C in the dark. These stock solutions were used for dilution series for calibration experiments with ELISA, the MCR 3 or HPLC-MS.

3 Preparation of monoclonal anti-DCF antibodies

Dr. E. Weber from the University of Halle-Wittenberg accomplished the immunization and generation of hybridoma cells from mice. The procedure is described in Chapters 3.2 to 3.4. Conjugate synthsis for immunization, screening cell culture supernatatns, characterization of mAbs and developing an indirect competitive ELISA for the analysis of fresh water was performed at the IWC.

3.1 Preparation of DCF protein conjugates

For immunization, TG was used as carrier protein for DCF. The synthesis was carried out as described previously. (Deng, 2003) For the coating of microtiter plates, OVA and BSA conjugates were synthesized by the DCC-NHS method. DCF (33.33 mM) was activated in dry dioxane by 1.05 eq. NHS and 1.3 eq. DCC for 20 h under shaking at 100 rpm. The side product N,N'-dicyclohexylurea was separated by centrifugation at 2550G for 2 min. Then, 1.00 mL of this solution was added to 40 mg OVA dissolved in 4.66 mL coupling buffer (0.13 M $NaHCO_3$, pH 7.8). The coupling reaction was carried out in the dark for 2 h. Non-reacted reagents were separated by dialysis against water. The final conjugate was lyophilized to yield a colorless solid and stored at -20°C.

3.2 Immunization and generation of hybridomas

A modified version of the Koehler and Milstein protocol was used for the generation of the monoclonal antibodies. Twelve three-month-old Balb/c mice were immunized with 25 µg of conjugate of either DCF-BSA or DCF-TG dissolved in carbonate buffer (Na_2CO_3 15 mM; $NaHCO_3$ 35 mM; pH 9.6) and emulsified in 300 µL of complete Freund´s adjuvant. Immunization was continued with 25 µg of the conjugates emulsified in incomplete Freund´s adjuvant three and five weeks after priming. Four days and 24 h before hybridization on day 56 of the immunization protocol mice received another 25 µg of the conjugates but without any adjuvant. Titer determination revealed that only the mice immunized with DCF-TG-conjugate showed an immune response and the splenocytes of those mice (4) were further used for the fusion process.

Mouse spleen cells (1×10^8) and cells (8×10^7) of the mouse myeloma cell line P3X63Ag8.653 were thoroughly mixed and cell fusion was mediated by polyethylene glycol 1500. Fused cells were cultured in RPMI-based HAT selection medium (100 µM hypoxanthine, 4 mM aminopterine, 160 µM thymidine) for 3 weeks and another two weeks in HT-medium. Surviving hybridomas were grown in RPMI 1640 medium supplemented with 10% of a low-IgG fetal calf serum, HEPES (4.77 g/L, acidic), glucose (2.5 g/L), 2-mercaptoethanol (1 mM), L-glutamine (2 mM), bovine insulin (5 mg/L) and gentamycine (80 mg/L).

3.3 ELISA for the detection of mAbs to DCF (primary screening)

Costar high-binding immunoplates (96 wells) were coated overnight with 50 µL of DCF-OVA conjugate in order to avoid isolation of clones which produce antibodies cross-reacting with TG protein. After blocking non-specific binding sites with blocking buffer (Roche) for 2 h, wells were washed three times with NaCl (0.154 M) containing Tween 20 (0.05%). Fifty µL of hybridoma supernatant were then added to each well and incubated for 2 h. After extensive washing antigen-bound antibodies were detected by incubating the plates with a goat anti-mouse IgG, F_c-specific and conjugated to HRP at a dilution of 1/10,000. Plates were read 10 - 15 min after adding the HRP substrate 2,2'-azino-bis(3-ethylbenzothiazoline-6-sulphonic acid. Approximately 3000 of the obtained clones were tested and 46 were identified to produce specific monoclonal antibodies against DCF. These clones were isolated and rendered monoclonal by limited dilution.

3.4 Indirect ELISA screening for highly affine mAbs in hybridoma supernatant (secondary screening)

Microtiter plates were coated with DCF-OVA conjugate (1 µg/mL) dissolved in coating buffer (200 µL/well) and incubated at 4°C overnight. The microtiter plates were automatically washed three times with washing buffer (300 µL/well) and blocked with blocking reagent (300 µL/well) for 1 h at room temperature with slight horizontal shaking at 100 rpm. After another washing step, cell culture supernatants (CCS) were added (200 µL/well) in different dilutions starting from 1/50 and incubated for 1 h at 100 rpm. Then, the plate was washed automatically again. The HRP-labeled secondary anti-mouse antibody was diluted in PBS to 0.2 µg/mL and incubated on the plate for 1 h at 100 rpm. After the last washing step, substrate solution (200 µL/well) was added and the plate was incubated at 100 rpm at room temperature. The dilution of every CCS was optimized to give ~1.0 absorbance at 450 nm after 15 min of incubation and then the enzymatic reaction was stopped with stop solution.

In order to screen for high affinity supernatants, the supernatant was used in the optimized dilution (100 µL/well) and incubated with 0 and 10 µg/L of DCF (100 µL/well) by using the same protocol. Thereafter, most promising CCS were further tested with dilution series of DCF (0 – 100 µg/L in 10% MeOH in water) in order to construct a calibration curve. Eleven out of 46 CCS showed IC_{50} values below 10 µg/L. The antibodies of the five most sensitive clones were affinity purified and their affinities were determined by SPR spectroscopy.

3.5 MALDI-TOF-MS analysis of purified mAbs

For the determination of kinetic parameters by SPR, purified antibodies were analyzed by MALDI-TOF-MS to determine their molecular weight. The PBS was removed by dialysis against water and the antibody was lyophilized and re-dissolved in coating buffer (5 mg/mL). They were desalted by using ZipTipC4, washed with ultrapure water and then eluted with a saturated solution of the matrix: a saturated solution of α-cyano-4-hydroxy-cinnamic acid in 45% ACN, 0.1% TFA and ultrapure water. The eluate was dispensed on a steel target and dried at room temperature. IgG subtypes were determined by determined with IsoQuick[TM] Kit for Mouse Monoclonal Isotyping from Sigma-Aldrich.

3.6 Determination of kinetic parameters by SPR measurements

SPR measurements were carried out in the indirect format using the Biacore X100 system and sensor chip CM5 at 25°C. For the immobilization procedure, the running buffer was HBS EP+ and flow rate adjusted to 10 µL /min. The sensor chip surface was activated by an aqueous solution of EDC (0.4 M) and NHS (0.1 M) for 7 min. Then, DCF-OVA (0.01 mg/mL) was dissolved in 10 mM NaOAc buffer at an optimized pH value of 4.5 (set up with HCl) and flown for 9 min and 5 min, successively. The surface was blocked by ethanolamine (1 M, pH = 8.0/HCl) for 4 min.

The kinetic constants were determined in single cycles with consecutive injections of 5 dilutions of IgG solutions in running buffer, starting with the lowest. On average, the maximum binding capacity of the CM5 chip covered with R_{max} was determined to be 72 ± 3.5 resonance units (RU). Running buffer was used as storage buffer in order to avoid the so bulk effects. For regeneration, the surface was flown with regeneration buffer and re-equilibrated in running buffer. The rate constants were determined by a bivalent binding model by the BiacoreX100 evaluation software.

4 Preparation of microarrays and QCM-D quartz

4.1 PEG-ylation

The glass slides were previously marked with numbers by using a diamond cutter. For the functionalization, the opposite side of the slide was used.

4.1.1 Cleaning and oxidation

To remove impurities, the glass slides, silicon wafers or quartz slides were cleaned in 200 mL of 2% *Hellmanex* solution for 1 h by sonication, for 15 h under mild shaking and for 1 h by sonication. After thoroughly rinsing with 5 × 200 mL of water, the slides were dried in nitrogen flow. For etching the silica surface, the slides or wafers were shaken for 1 h in 200 mL of a mixture of 37% hydrochloric acid and methanol (v/v = 1/1) rinsed with 5 × 200 mL of water and shaken in 200 mL of concentrated sulfuric acid for 1 h. After rinsing with 5 × 200 mL water and drying them with nitrogen, they were immediately used for silanization or measurements with XPS, GA-ATR FT-IR or Water Contact Angle measurement device.

4.1.2 Grafting with GOPTS

One half of the number of activated slides or wafers was spread with 600 µL GOPTS and then covered with the remaining slides or wafers in a "sandwich" format. These sandwiches were incubated for 3 h. Afterwards, they were separated and sonicated successively in ethanol, methanol and again ethanol for 5 min. Finally, they were dried under nitrogen flow for 5 min at 85°C and used for the DAPEG functionalization or were immediately submitted to measurements with XPS, GA-ATR FT-IR or Water Contact Angle measurement device.

4.1.3 DAPEG functionalization

The slides or wafers were incubated with 600 µL molten DAPEG in the sandwich format (see 2.2.2) for 12 h at 98°C. The sandwiches were separated and sonicated in water for 2 × 15 min. After rinsing them thoroughly with water and drying them under nitrogen flow, they were stored in desiccators, used for GA-ATR FT-IR, XPS and water contact angle measurements or used for the immobilization of DCF.

4.2 Microspotting method

4.2.1 Activation of DCF and PBA

The solution of DCF or PBA in dioxane/water (v/v = 1/1; 2 mM) was activated by adding 1.2 eq N-hydroxysuccinimide (NHS) in dioxane and N-(3-dimethylaminopropyl)-N'-ethylcarbodiimide in water hydrochloride (EDC). The reaction flask was shaken over night at

room temperature. Then, the solution was added in a cavity of a Greiner UV Star® 384 well plate.

4.2.2 Microspotting of DCF, PBA and MC-LR

This UV Star MTP was placed into the BioOdyssey Calligrapher MiniArrayer. During the printing process, the air humidity was set to 50% and the temperature of the plates was 20 - 22 °C. The spotting pin SNS 12 places approximately 5 nL of the solution on the surface. For statistical purpose, 5 spots of the same composition were placed in one row. Finally, the glass surfaces were incubated at 25°C for 15 h, washed for 15 min in water and dried under nitrogen flow. The prepared chips were stored in a desiccator under reduced pressure.

The DAPEG surface was then modified with Traut's reagent (2-iminothiolane, 2.35 mg/mL) diluted in TEA buffer (50 mM, pH= 9.5, HCl). The microarray slides were incubated with this reagent for 4 h at room temperature under shaking (100 rpm). Then, the slides were rinsed with water several times and dried in nitrogen flow. Microcystin-LR was diluted in dioxane/water (2 µL stock solution in 100 µL, v/v = 1/1) and spotted like DCF and PBA as described above. The multianalyte microarrays were stored in a desiccator in the dark.

4.2.3 Flow-cell assembly for MCR 3 measurements

The microarray surface is glued towards a black polymethylmethylacrylate slide (PMMA) with a double-sided adhesive foil. This foil was laser-cut to build up two flow-through channels. (Kloth, 2009 a) For the assembly, a special roller was used. It was fabricated by an in-house workshop. The flow cells were connected to the MCR 3 by inlet and outlet ports on the PMMA carrier. The height of 142 µm constitutes a volume of 43.3 µL in one flow cell and allows a laminar flow over the microarray surface. The detectable area of one microarray is about 12 mm × 8 mm.

4.3 Attachment of DCF from solution phase

Alternatively to the microspotting method, the whole silicon wafer and quartz slide for the QCM experiments were functionalized with DCF. The solution of DCF sodium salt was activated in dry DMF (10 mM) by adding 1.2 eq. NHS and 1.2 eq. EDC. The reaction flask was shaken for 150 min at room temperature. Then, the silicon wafers and quartz slides were put

into the solution. They were shaken over night at room temperature and washed for 15 min in 100 mL H_2O. They were stored in a desiccator.

5 Surface characterization techniques

5.1 AFM

The MultiMode 8 atomic force microscope was equipped with a 150 × 150 × 5 µm J-scanner. The AFM cantilevers were ScanAsyst-Air probes (Bruker). The radius of the tips was approximately 2 nm according to the provider. The coated silicon wafers were measured by using PeakForce *QNM®* (Quantitative Nanomechanical Property Mapping) mode under air at room temperature. The data of the images were flattened for the presentation by using a 3rd order polynomial function.

5.2 Contact Angle

The instrument is using a charge coupled device (CCD) camera and an image analysis processor (Krüss GmbH, Hamburg). Static contact angles were measured at room temperature using the sessile water drop method and image analysis of the drop profile. The droplet volume was 1 µL, and the contact angle was measured 3 s after the drop was deposited on the sample. For each step, the water contact angle was determined by three different calculation methods (tangent method 1 and 2, circle fitting) on three different spots on the surface preparation (n = 9), if not stated differently.

Interfacial tension (IFT) of single water drops with different organic solvent contens were measured by the hanging drop method. The drop was hanging from the capillary and its surface extension was measured by extending the drop volume automatically in the same image analysis processor from Krüss.

5.3 GA-ATR FT-IR spectroscopy

The Si wafers were used for GA-ATR FT-IRmeasurements directly after their preparation. The IR spectra were obtained with a VariGATR equipped with a horizontal reflection GA-ATR accessory on a germanium crystal. The detector of the spectrometer was a nitrogen-cooled mercury-cadmium-telluride wide-band detector. The silicon wafer sample were pressed towards the germanium crystal. The angle of incidence was fixed at 64.5°. IR spectra were recorded in a wavelength range from 650 to 4000 cm^{-1}. For each spectrum, 256 scans were

collected with a nominal resolution of 8 cm^{-1}. The background was recorded without any substrate pressed against the crystal.

5.4 XPS

XPS analyses were performed on an Omicron Argus X-ray photoelectron spectrometer, using a monochromated AlK$_\alpha$ (hv = 1486.6 eV) radiation source having a 300 W electron beam power. The emission of photoelectrons from the sample was analyzed at a takeoff angle of 45° under ultra-high vacuum conditions (1 x 10^{-8} Pa). XP spectra were collected at pass energy of 100 eV for the survey scan and 10 eV for the C1s, O1s and N1s core XPS levels. The peak areas were determined after subtraction of a Shirley background. The spectra were fitted using Casa XPS software and applying a Gaussian/Lorentzian ratio (G/L) equal to 70:30.

The comparison of the intensity of the Si 2p peaks of a clean silicon substrate and the one with the layers allows the estimation of their thicknesses. Assuming a homogeneous layer, the thickness *d* was estimated using the Equation 8.

6 QCM-D and automated flow-through ELISA

6.1 QCM-D measurements

Piezoelectric measurements were performed on AT-cut quartz silica-coated quartz crystals with nominal frequency F of 5 MHz. The QCM-D (E1 model) was operated in flow-through mode at 22 ± 0.1°C. The flow rate was adjusted by using a peristaltic pump. For the antiserum injections diluted 1/1 000 in PBS/EtOH (9/1 = v/v) and signal stabilization, it was 25 μL/min. The signal stabilization was carried out for 20 min in degassed PBS containing 10% EtOH. For the regeneration procedure, the flow rate was adjusted to 50 μL/min. The regeneration buffer was a solution of 2 w% SDS in water/ethanol (9/1 = v/v) with pH = 2 (HCl). The measurement procedure is described in Table 19.

Table 21: Protocol for the injection of diluted antiserum and regeneration of the surface.

Measurement protocol	Injection time [min]	Flow rate [μL/min]
Injection of diluted polyclonal anti-DCF serum	5-10	25.0
Signal stabilization in degassed PBS containing 10% EtOH	7-10	25.0
Injection of regeneration buffer (2 w% SDS, pH = 2 (HCl),	5-10	50.0

10% EtOH)		
Washing with degassed PBS containing 10% EtOH	5	50.0
Signal stabilization in degassed PBS containing 10% EtOH	5	25.0

6.2 Automated Flow-through ELISA by using the MCR 3

6.2.1 Single analyte measurements of DCF and MC-LR

The overall measurement procedure was carried out based on the existing method described previously (Sauceda-Friebe, 2011; Oswald, 2013). The standard and samples preparations were prepared in glass vials with 10 % MeOH. Before starting the measurements, 3×1 mL casein/PBS was pumped with 200 µL/s through the flow cell. The program for the automated CL immunoassay on the chip is summarized in Table 22. In the first step, 1 mL of the running buffer is submitted to the chip with a flow speed of 500 µL/s. Afterwards, 500 µL of sample and same volume of the mixture of primary antibodies solutions in running buffer were pumped simultaneously into an incubation loop at a flow rate of 60 µL/s. The detection antibodies were used as follows:

- pAb anti-DCF 1/10 000
- mAb 12G5 (anti-DCF, 0.55 mg/mL) 1/100 000
- mAb 10E7 (anti-MC-LR, 1 mg/mL) 1/2 000

The sample/antibodies mixture was pushed over the chip with 1 mL of running buffer at a flow rate of 100 µL/s. After a washing step with 2 mL of running buffer at a flow rate of 500 µL/s, the chip was incubated with 1 mL of HRP-labeled secondary antibody (200 µL at a flow rate of 100 µL/s and followed by 800 µL at a flow rate of 10 µL/s. The chip was washed again with 2 mL of running buffer at a flow rate of 500 µL/s. Then, 400 µL of luminol/H_2O_2 (v/v = 1/1) was sent over the chip at a flow rate of 150 µL/s. Afterwards, the flow was stopped, and an image was taken for 60 s by the CCD camera. After the recording, the chip was regenerated by using a total volume of 22.5 mL of regeneration buffer at a flow rate of 100 µL/s. The overall assay time was 20 min. The text files generated by the CCD camera were automatically evaluated with MCR Image analyzer software.

6.2.2 Measurements with BaP and multi-analyte experiments

The method was further developed for reproducible BaP measurements- The standard and samples preparations were prepared in glass vials with 50 % MeOH to reduce non-specific

adsorption of BaP to the vial, syringes and tubes in the instrument. The detection antibodies were used as follows:

- mAb 12G5 (anti-DCF, 0.55 mg/mL) 1/100 000
- mAb 22F12 (anti-BaP, 1 mg/mL) 1/30 000
- mAb 10E7 (anti-MC-LR, 1 mg/mL) 1/2 000

The sample/antibodies mixture was pushed over the chip with 1 mL of running buffer at a flow rate of 2 µL/s. All further steps were the same as described above.

6.2.3 Sample preparation for recovery experiments

Fresh water and wastewater samples were filtrated by a GF/C filter (0.2 µm) and mixed with MeOH (v/v = 1/1) and directly injected into the MCR 3. For recovery determinations, the analytes were added to MeOH and then the fresh water sample was added in a ratio v/v = 1/1.

Table 22: MCR 3 program

Step	Flow cell	Pump and velocity
1)	1 mL running buffer	500 µL/s P4
2)	200 µL sample	100 µL/s P2
3)	500 µL sample + 500 µL detection mAbs	60 µL/s P2, P1
4)	1 mL running buffer	100 or 2 µL/s P2
5)	2 mL running buffer	500 µL/s P4
6)	200 µL sec. ab	100 µL/s P0
7)	800 µL sec. ab.	10 µL/s P0
8)	2 mL running buffer	500 µL/s P4
9)	400 µL luminol + H_2O_2	150 µL/s P3
10)	2 x 1mL flushing buffer	250 µL/s P2
11)	2 x 1mL store buffer	250 µL/s P2
12)	2 x 1mL flushing buffer	250 µL/s P2
13)	5 x 2 x 60 µL regeneration buffer	10 µL/s P5
14)	3 x 2 x 60 µL regeneration buffer	10 µL/s P5
15)	5 x 300 µL regeneration buffer	500 µL/s P5
	(5 x 100 µL back and forth)	100µ/l/s P5
16)	3 x 500 µL flushing buffer	500 µL/s P5
17)	1.5 mL store buffer	500 µL/s P5
18)	2 x 1.5 mL flushing buffer	500 µL/s P5

7 HPLC-MS

7.1 SPE

A generic SPE was carried out. Surface and wastewater samples were collected in amber glass bottles pre-rinsed with deionized water. The samples were immediately transported to the laboratory and filtered prior to analysis, in order to eliminate suspended solid matter. Afterwards, the samples were stored in the dark at 4 °C and submitted to SPE within 36 h. Analytes were extracted with offline SPE using Oasis HLB (divinylbenzene/N-vinylpyrrolidone copolymer−1cc) and no pH adjustment of the samples was chosen as reported in literature (Gros, 2006; Kosma, 2014). The cartridges were preconditioned with 5 mL of MeOH and 5 mL of ultrapure water by using a SPE manifold. The sample aliquots of 15 mL for waste

water and 50 mL for fresh water were loaded onto the cartridge at a flow rate of 1 mL/min, followed by washing with 1 mL of ultrapure water. The cartridges were dried under vacuum for 15 min. The analytes were eluted with 3 x 0.5 mL of methanol by gravity flow. The extracts were dried under a gentle stream of nitrogen until dryness. Then, the wastewater and fresh water residues were reconstituted with 150 μL and 100 μL of water (HPLC-MS grade), respectively. Finally, they were stored in glass vials at -20 °C until being analyzed by HPLC-MS.

7.2 HPLC-MS analysis

The sample extracts were analyzed by using HPLC-MS method. The autosampler collected 10 μL of the extract. Chromatographic separation was performed using a Hypersil GOLD column (100 nm x 2.1 mm, 1.9 μm particle size) in a column oven at 30°C with a guard column of Phenomenex (C12, 4 mm x 2.0 mm) and using a gradient solvent program: The initial composition of the mobile phase was 90% HPLC-MS grade water and 10% ACN; both solvents contained 0.1% NH_4OH. The initial mobile phase composition of 10% ACN was increased to 90% in 12 min. To clean the column, the amount of ACN was kept for 2 min and then decreased to 50% and kept constant for 3 min. The initial mobile phase composition was restored, and then the column was equilibrated for 5 min.

For the detection, an Orbitrap-based Exactive^{TM} benchtop mass spectrometer equipped with an electrospray source (ESI) operated in negative ionization mode. It was operated at resolution of 50,000 (2 Hz). The scan range covered was m/z 200.0-400.0. The automatic gain control (AGC) target was set at ultimate accuracy (5 · 10^5 ions) and the maximum injection was 50.0 ms. Initial instrument calibration was done by infusing calibration mixtures in both positive and negative ion. The calibration mixture was composed of caffeine, MRFA peptide, SDS, sodium taurocholate, and Ultramark® 1621 in water and methanol (v/v = 1/1) as described by Thermo Fisher Scientific. It was injected in the ESI probe by using a Hamilton syringe pump. The all-ion fragmentation using the High Energy Collision Dissociation (HCD) cell was turned off. The fore-vacum, high vacuum and ultra high vacuum were maintained at about 1 mbar, from 3 ·10^{-5} and below 3 ·10^{-10} mbar, respectively. Instrument control and data processing were carried out by using Xcalibur 2.1 software. DCF was identified by its retention time of 7.6 ± 0.1 min and its exact mass [M-H]$^-$ = 294.00941. An accuracy ± 5.0 ppm was accepted.

Calibration of the HPLC-MS method was repeated before every extract measurement with DCF standards in pure water from 5 to 500 µg/L. Measurements were carried out in triplicate. Blank values were determined before, during and after the calibration measurements. A linear correlation was determined and the resulting equation (correlation coefficient $R^2 = 0.99$, m = 3, n = 5) was used to determine sample concentrations.

For the determination of recoveries in fresh water samples, three different aliquots of each sample with a volume of 50 mL were fortified at 0.05 µg/L and 0.1 µg/L. Recovery was 70 ± 13% in fresh water samples from lake and river (m = 8 in 4 different samples). Wastewater samples were quantified spiked with 0.27 or 0.13 µg/L for recovery rate determinations and obtained recovery was 97 ± 3.3% (m = 5 in different samples).

8 HPLC-FLD

8.1 LLE

To 50 mL of filtered (GF/C, 0.2 µm) water sample were added 5 g of NaCl and 10 mL of cyclohexane. After stirring for 1 h with a magnetic stirrer a volume of 5 mL of the organic phase was separated and evaporated under nitrogen. The residue dissolved with 500 µL ACN.

8.2 HPLC-FLD analysis

The analysis for BaP was carried out on a modular liquid chromatography setup consisting of a high pressure pump (Mocel LC-20AT), a column thermostat (Model CTO-20A), a variable wavelength fluorescence detector (Model RF-10-AXL) (all from Shimadzu, Kyoto, Japan), and evaluated by the LC solution software.

Freshwater Extracts were analyzed by using the column from Restek (Pinnacle II, PAH, 4 µm, 150 × 3.2 mm). For the elution of the analyte mixture, a gradient was applied with a flow of 0.5 mL/min: Starting with 60% ACN in water for 3.0 min and increasing to 100% in 12 min. The final ACN content was kept constant for 17.5 min. The total analysis time was 32.5 min. A volume of 20 µL was injected. The retention time of BaP was 19.7 min.

Calibration of the HPLC-FLD method was carried out with BaP standards in ACN from 20 to 20 000 ng/L. Measurements were carried out in triplicate. Blank values were determined before, during and after the calibration measurements. A linear correlation was determined

and the resulting equation (correlation coefficient $R^2 > 0.99$ (m = 3, n = 6) was used to determine sample concentrations.

For the determination of recoveries in fresh water samples, three different aliquots of drinking water, Ammersee and Wörthsee samples with a volume of 50 mL were fortified at 0.4 µg/L. Recovery was 109 ± 7% for the three water samples.

VI Abbreviations

4'-OH-DCF	4'-Hydroxydiclofenac
4-PL	4-Parameter logistic
5-OH-DCF	5-Hydroxydiclofenac
a. u.	Arbitrary units
Ab	Antibody
Ag	Antigen
ACN	Acetonitrile
AFM	Atomic force microscopy
AuNP	Goldnanoparticles
AuPMMA	Gold covered PMMA carrier
BaP	Benzo[a]pyrene
BSA	Bovine serum albumin
CCD	Charge coupled device
CCS	Cell culture supernatant
CL	Chemiluminescence
CR	Cross reactivity
D	Dissipation
Da	Dalton
DAPEG	Diamino-poly(ethylene glycol)
DCC	*N.N'*-Dicyclohexylcarbodiimide
DCF	Diclofenac
DCF-GLU	Diclofenac-glucuronide
DMF	Dimethylformamide
DMSO	Dimethylsulfoxide
DOC	Diluted organic carbon

E2	17β-estradiol
EDC	1-Ethyl-3-(3-dimethylaminopropyl)carbodiimid
EE2	17α-ethinylestradiol
EIA	Enzyme immunoassay
ELISA	Enzyme-linked immunosorbent assay
eq.	Equivalent
ESI	Elecrospray ionization
EU	European Union
F	Frequency
FBS	Fetal bovine serum
FLD	Fluorescence detectors
GA-ATR FT-IR	Grazing-angle attentuated total reflection fourier-transformed infrared spectroscopy
GC	Gas chromatography
GOPTS	3-Glycidyloxypropyltrimethoxysilane
h	Hour
HAT	Hypoxanthine/ aminopterine/ thymidine medium
HEIA	Homogenous immunoassay
HPLC	High-performance liquid chromatography
HRP	Horseradish peroxidase
IC_{50}	Half maximal inhibitory concentration
IFT	Interfacial tension
Ig	Immune globulins
IUPAC	Union of Pure and Applied Chemistry
IWC	Institute of Hydrochemistry, TU München

LBA	Ligand binding assay
LC	Liquid chromatography
LLE	Liquid liquid extraction
LOD	Limit of detection
LOQ	Limit of quantification
m	Number of repetitions
M	molar (mol/L)
mAb	Monoclonal antibody
MALDI	Matrix assisted Laser Desorption/Ionization
MC-LR	Microcystin-LR
MCR 3	Microarray Chip Reader of the 3rd generation
MeOH	Methanol
min	Minute
MIP	Molecular imprinted polymer
MS	Mass spectrometry
MTP	Microtiter plate
MW	Molecular weight
n	Number of concentrations
n. d.	not determined
NHS	*N*-Hydroxysuccinimide
NSAID	Non-steroidal anti-inflammatory drug
OVA	Ovalbumin
pAb	Polyclonal antibodies
PAH	Polycyclic aromatic hydrocarbon
PBA	1-Pyrenebutanoic acid

PBS	Phosphate buffered saline
PEG	Polyethylene glycol
PHS	Priority hazardous substances
PMMA	Polymethylmethacrylate
PS	Priority substances
QCM	Quartz crystal microbalance
QCM-D	Quartz-crystal microbalance with dissipation measurement
rpm	Rounds per minute
rec.	Recovery
R_{max}	Maximum SPR respnse
r.t.	Room temperature
RSD	Relative standard deviation
RU	Refractive units
SDS	Sodium dodecyl sulfate
SPE	Solid phase extraction
SPR	Surface Plasmon resonance
TEA	Triethylamine
TG	Thyreoglobulin
TMB	3.3',5,5'-Tetramethylbenzidine
TOC	Total organic carbon
TOF	Time of flight
UV	Ultraviolet
v/v	Ratio of volumes
w%	Percentage of weight
WFD	Water framework directive

WHO	World Health Organization
WR	Working range of the sigmoidal calibration curve
WWTP	Wastewater treatment plant
XPS	X-ray photoelectron Spectroscopy

VII Literature

Aissaoui N., Bergaoui L., Landoulsi J., Lambert J.-F., Boujday S., Silane layers on silicon surfaces: mechanism of interaction, stability and influence on protein adsorption, *Langmuir* **2012**, *28*, 656-665.

Anderson A. S., Dattelbaum A. M., Montano G. A., Price D. N., Schmidt J. G., Martinez J. S., Grace K. W., Grace K. M., Swanson B. I., Functional PEG-modified thin films for biological detection. *Langmuir* **2008**, *24*, 2240-2247.

Bahlmann A., Carvalho J. J., Weller M. G., Panne U., Schneider R. J., Immunoassays as high-throughput tools: monitoring spatial and temporal variations of carbamazepine, caffeine and cetirizine in surface and wastewaters. *Chemosphere* **2012**, *89*, 1278-1286.

Barco-Bonilla N., Martínez Vidal J. L., Garrido Frenich A., Romero-González R., Comparison of ultrasonic and pressurized liquid extraction for the analysis of polycyclic aromatic compounds in soil samples by gas chromatography coupled to tandem mass spectrometry. *Talanta* **2009**, *78*, 156-164.

Barnes A. J., Young S., Spinelli E., Martin T. M., Klette K. K., Huestis M. A., Evaluation of a homogenous enzyme immunoassay for the detection of synthetic cannabinoids in urine. *Forensic Sci. Int.* **2014**, *241*, 27-34.

Ben Haddada M., Blanchard J., Casale S., Krafft J.-M., Vallée A., Méthivier C., Boujday S., Optimizing the immobilization of gold nanoparticles on functionalized silicon surfaces: amine- vs thiol-terminated silane. *Gold Bull.* **2015**, *46*, 335-341.

Benner J., Helbling D. E., Kohler H.-P. E., Wittebol J., Kaiser E., Prasse C., Ternes T. A., Albers C. N., Aamand J., Horemans B., Springael D., Walravens E., Boon N., Is biological treatment a viable alternative for micropollutant removal in drinking water treatment processes? *Water Res.* **2013**, *47*, 5955-5976.

Berg J. M, Tymoczko J. L., Stryer L., Biochemie, 6th edition, Spektrum Akademischer Verlag, Heidelberg, **2010**.

Bouissou-Schurtz C., Houeto P., Guerbet M., Bachelot M., Casellas C., Mauclaire A. C., Panetier P., Delval C., Masset D., Ecological risk assessment of the presence of pharmaceutical residues in a French national water survey. *Regul. Toxicol. Pharmacol*.

2014, *69*, 8.

Boujday S., Briandet R., Salmain M., Herry J. M., Marnet P. G., Gautier M., Pradier, C. M., Detection of pathogenic *Staphylococcus aureus* bacteria by gold based immunosensors. *Microchim. Acta* **2008**, *163*, 203-209.

Boujday S., Gu C., Girardot M., Salmain M., Pradier C.-M., Surface IR applied to rapid and direct immunosensing of environmental pollutants. *Talanta* **2009 a**, *78*, 165-170.

Boujday S., Methivier C., Beccard B., Pradier C.-M., Innovative surface characterization techniques applied to immunosensor elaboration and test: comparing the efficiency of Fourier transform-surface plasmon resonance, quartz crystal microbalance with dissipation measurements, and polarization modulation-reflection absorption infrared spectroscopy. *Anal. Biochem*. **2009 b**, *387*, 194-201.

Boujday S., Nasri S., Salmain M., Pradier C.-M., Surface IR immunosensors for label-free detection of benzo[a]pyrene. *Biosens. Bioelectron.* **2010**, *26*, 1750-1754.

Brennan J., Dillon P., O'Kennedy R., Production, purification and characterisation of genetically derived scFv and bifunctional antibody fragments capable of detecting illicit drug residues. *J. Chromatogr. B* **2003**, *786*, 327-342.

Camman K., Instrumentelle Analytische Chemie. Spektrum Akademischer Verlag, Heidelberg, **2001**.

Corgier B. P., Li F., Blum L. J., Marquette C. A., On-chip chemiluminescent signal enhancement using nanostructured gold-modified carbon microarrays. *Langmuir* **2007**, *23*, 8619-8623.

Cras J. J., Rowe-Taitt C. A., Niven D. A., Ligler F. S., Comparison of chemical cleaning methods of glass in preparation for silanization. *Biosens. Bioelectron.* **1999**, *14*, 683-688.

Croué J.-P., Benedetti M. F., Violleau D., Leenheer J. A., Characterization and copper binding of humic and nonhumic organic matter isolated from the South Platte River: evidence for the presence of nitrogenous binding site. *Environ. Sci. Technol.* **2003**, *37*, 328-336.

De la Cruz A., Trevor J., Dionysiou D., The effects of sample matrices on immunoassay to

detect microcystin-LR in water. *J. Environ. Prot.* **2012**, *3*, 1275-1285.

Dekeyser C. M., Buron C. C., Mc Evoy K., Dupont-Gillain C. C., Marchand-Brynaert J., Jonas A. M., Rouxhet P. G., Oligo(ethylene glycol) monolayers by silanization of silicon wafers: real nature and stability. *J. Colloid Interface Sci.* **2008**, *324*, 118-126.

Deng A. P., Himmelsbach M., Qing-Zhi Z., Frey S., Sengl M., Buchberger W., Niessner R., Knopp D., Residue analysis of the pharmaceutical diclofenac in different water types using ELISA and GC-MS. *Environ. Sci. Technol.* **2003**, *37*, 3422-3429.

Desmet C., Blum L. J., Marquette C. A., High-throughput multiplexed competitive immunoassay for pollutants sensing in water. *Anal. Chem*. **2012**, *84*, 10267-10276.

Ding X., Wang X.-M., Xie Z.-Q-, Xiang C.-H., Mai B.-X., Sun L.-G., Zheng M., Sheng G.-Y., Fu J.-M., Pöschel U., Atmospheric polycyclic aromatic hydrocarbons observed over the North Pacific Ocean and the Arctic area: Spatial distribution and source identification. *Atmos. Environ.* **2007**, *41*, 2061-2072.

Dinh D. H., Vellutini L., Bennetau B., Dejous C., Rebière D., Pascal E. M., Moynet D., Belin C., Desbat B., Labrugère C., Pillot J.-P., Route to smooth silica-based surfaces decorated with novel self-assembled monolayers (SAMs) containing glycidyl-terminated very long hydrocarbon chains. *Langmuir* **2009**, *25*, 5526-5535.

Directive 98/83/EC of the European Parliament and of the Council of 3 November 1998 on the quality of water intended for human consumption.

Directive 2000/60/EC of the European Parliament and of the Council of 23 October 2000 establishing a framework for the Community action in the field of water policy.

Directive 2008/105/EC of the European Parliament and of the Council of 16th December 2008 on environmental quality standards in the field of water policy, amending and subsequently repealing Council Directives 82/176/EEC, 83/513/EEC, 84/156/EEC, 84/491/EEC, 86/280/EEC and amending Directive 2000/60/EC of the European Parliament and of the Council.

Directive 2013/39/EU of the European Parliament and of the Council of 12th August 2013

amending Directives 2000/60/EC and 2008/105/EC as regards priority substances in the field of water policy with EEA relevance.

Elordui-Zapatarietxe S., Fettig I., Philipp R., Gantois F., Lalère B., Swart C., Petrov P., Goenaga-Infante H., Vanermen G., Boom G., Emteborg H., Novel concepts for preparation of reference materials as whole water samples for priority substances at nanogram-per-liter level using model suspended particulate matter and humic acids. *Anal. Bioanal. Chem.* **2015**, *11*, 3055-3067.

Fadley C.S., Braid R. J., Siekhaus W., Novakov T., Bergström S. A. L., Surface analysis and angular distributions in x-ray photoelectron spectroscopy. J*. Electron Spectrosc. Relat. Phenom.* **1974**, *4*, 93-137.

Fang S., Zhang B., Ren K.-W., Cao M.-M., Shi H.-Y., Wang M.-H., Development of a sensitive indirect competitive enzyme-linked immunosorbent assay (ic-ELISA) based on the monoclonal antibody for the detection of the imidaclothiz residue. *J. Agric. Food Chem.* **2011**, *59*, 1594-1597.

Farré M., Brix R., Kuster M., Rubio F., Goda Y., López de Alda M. J., Barceló D., Evaluation of commercial immunoassays for the detection of estrogens in water by comparison with high-performance liquid chromatography tandem mass spectrometry HPLC–MS/MS (QqQ). *Anal. Bioanal. Chem.* **2006**, *385*, 1001-1011.

Feng L., He M., Zhu A., Baodong S., Jianwu S., Shi H., Compact quantitative optic fiber-based immunoarray biosensor for rapid detection of small analytes. *Biosens. Bioelectron.* **2010**, *26*, 16-22.

Fernández F., Hegnerová K., Piliarik M., Sanchez-Baeza F., Homola J., Marco M.-P., A label-free and portable multichannel surface plasmon resonance immunosensor for on site analysis of antibiotics in milk samples. *Biosens. Bioelectron.* **2010**, *26*, 1231-1238.

Findlay J. W. A., Dillard R. F., Appropriate Calibration Curve Fitting in Ligand Binding Assays. *AAPS J.* **2007**, *9*, E260-E267.

Frostell A., Vinterbaeck L., Sjoebom H., Protein-ligand interactions using SPR systems. *Methods in Molecular Biology*, Springer Science+Business Media: New York, **2013**, *1008*,

139-165.

Goetz T., Hillenbrand T., Marschneider-Weidemann F., Fuchs S., Scherer U., Abschätzung der Einträge von polyzyklischen aromatischen Kohlenwasserstoffen in deutsche Gewässer / Aktuelle Datengrundlage. *Umweltwiss. Schadst. Forsch.* **2009**, *21*, 433–442.

Gooding J. J., Ciampi S., The molecular level modification of surfaces: from self-assembled monolayers to complex molecular assemblies. *Chem. Soc. Rev.* **2011**, *40*, 2704-2718.

Gros M., Petrović M., Barceló D., Development of a multi-residue analytical methodology based on liquid chromatography–tandem mass spectrometry (LC–MS/MS) for screening and trace level determination of pharmaceuticals in surface and wastewaters. *Talanta* **2006**, *70*, 678-690.

Gui W.-J., Wang S.-T., Guo Y.-R.; Zhu G.-N., Development of a one-step strip for the detection of triazophos residues in environmental samples. *Anal. Biochem.* **2008**, *377*, (2), 202-208.

Han K. N., Li C. A., Seong G. H., Microfluidic chips for immunoassays. *Annu. Rev. Anal. Chem.* **2013**, *6*, 119-141.

Helfrich J., Armstrong D. E., Polycyclic aromatic hydrocarbons in sediments of the southern basin of Lake Michigan. *J. Great Lakes Res.* **1986**, *12*, 192-199.

Hoeger B., Kölnner B., Dietrich D. R., Hitzfeld B., Water-borne diclofenac affects kidney and gill integrity and selected immune parameters in brown trout (Salmo trutta f. fario). *Aquat. Toxicol.* **2005**, *75*, 53-64.

Huebner M., Wutz K., Szkola A., Niessner R., Seidel M., A glyco-chip for the detection of ricin by an automated chemiluminescence read-out system. *Anal. Sci.* **2013**, *29*, 461-466.

Huntscha S., Singer H. P., McArdell C. S., Frank C. E., Hollender J., Multiresidue analysis of 88 polar organic micropollutants in ground, surface and wastewater using online mixed-bed multilayer solid-phase extraction coupled to high performance liquid chromatography-tandem mass spectrometry. *J. Chromatogr. A* **2012**, *1268*, 74-83.

IUPAC, Glossary for chemists of terms used in biotechnology, IUPAC Recommendations.

1992, *64*, 148.

Jiang X., Li D., Xu X., Ying Y., Li Y., Ye Z., Wang J., Immunosensors for detection of pesticide residues. *Biosens. Bioelectron.* **2008**, *23*, 1577-1587.

Joeng C.B., Niazi J.H., Lee S.J., Gu M.B., SsDNA aptamers that recognize diclofenac and 2-anilinophenylacetic acid. *Bioorg. Med. Chem.* **2009**, *17*, 5380–5387.

Kaiser T., Gudat P., Stock W., Pappert G., Grol M., Neumeier D., Luppa P.B., Biotinylated steroid derivatives as ligands for biospecific interaction analysis with monoclonal antibodies using immunosensor devices. *Anal. Biochem.* **2000**, *282*, 173-185.

Kanso H., Barthelmebs L., Inguimbert N., Noguer T., Immunosensors for estradiol and ethinylestradiol based on new synthetic estrogen derivatives: application to wastewater analysis. *Anal. Chem.* **2013**, *85*, 2397-2404.

Karaseva N. A., Ermolaeva T. N., Piezoelectric immunosensors for the detection of individual antibiotics and the total content of penicillin antibiotics in foodstuffs., *Talanta* **2014**, 120, 312-317.

Karsunke X, Pschenitza M., Rieger M., Weber E., Niessner R., Knopp D., Screening and characterization of new monoclonal anti-benzo[a]pyrene antibodies using automated flow-through microarray technology. *J. Immunol. Meth.* **2011**, *31*, 81-90.

Kenny J., Maggs J., Meng X., Sinnott D., Clarke S., Park B., Stachulski A., Syntheses and characterization of the acyl glucuronide and hydroxy metabolites of Diclofenac. *J. Med. Chem.* **2004**, *47*, 2816-2825.

Kloth K., Niessner R., Seidel M., Development of an open stand-alone platform for regenerable automated microarrays. *Biosens. Bioelectron.* **2009 a**, *24*, 2106-2112.

Kloth K., Rye-Johnsen M., Didier A., Dietrich R., Märtlbauer E., Niessner R., Seidel M. A regenerable immunochip for the rapid determination of 13 different antibiotics in raw milk. *Analyst* **2009 b**, *34*, 1433 - 1439.

Knopp D., Seifert M., Väänänen V. Niessner R., Determination of polycyclic aromatic hydrocarbons in contaminated water and soil samples by immunological and

chromatographic methods**.** *Enviiron. Sci. Technol.* **2000**, *34*, 2035-2041.

Knopp D., Deng A., Letzel M., Himmelsbach M., Zhu Q.-Z., Peröbner I., Kudlak B., Frey S., Sengl M., Buchberger W., Taggart M., Hutchinson C., Cunningham A., Pain D., Cuthbert R., Raab A., Meharg A., Swan G., Jhala Y., Prakash V., Rahmani A., Quervedo M., Niessner R., Immunological determination of the pharmaceutical diclofenac in environmental and biological samples. *Rational Environmental Management of Agrochemicals: Risk Assessment, Monitoring, and Remedial Action.* ACS Symp. Ser., ACS Washington **2007**, *966*, 203-226.

Knopp D., Immunoassay development for environmental analysis. *Anal. Bioanal. Chem.* **2006**, 425-427.

Koehler G., Milstein C., Continuous cultures of fused cells secreting antibody of predefined specificity. *Nature* **1975**, *256*, 495-497.

Kosma C. I., Lambropoulou D. A., Albanis T. A., Investigation of PPCPs in wastewater treatment plants in Greece: Occurrence, removal and environmental risk assessment. *Sci. Total Environ.* **2014**, *466-467*, 421-438.

Krämer P. M., Martens D., Forster S., Ipolyi I., Brunori C., Morabito R., How can immunochemical methods contribute to the implementation of the Water Framework Directive? *Anal. Bioanal. Chem.* **2007**, *387*, 1435-1448.

Kunz P. Y., Kienle C., Carere M., Homazava N., Kase R., In vitro bioassays to screen for endocrine active pharmaceuticals in surface and waste waters. *J. Pharm. Biomed. Anal.* **2015**, *106*, 107-115.

Kwok D. Y., Neumann A. W., Contact angle measurement and contact angle interpretation. *Adv. Colloid Interface Sci.* **1999**, *81*, 167-249.

Li D., Wei S., Yang H., Li Y., Deng A., A sensitive immunochromatographic assay using colloidal gold-antibody probe for rapid detection of pharmaceutical indomethacin in water samples. *Biosens. Bioelectron.* **2009**, *24*, 2277-2280.

Liebes Y., Amir L., Marks R. S., Banai M., Immobilization strategies of brucella particles on

optical fibers for use in chemiluminescence immunosensors. *Talanta* **2009**, *80*, 338-345.

Lin Z., Sauceda-Friebe J. C., Lin J.-M., Niessner R., Knopp D., Double-codified nanogold particles based automated flow-through CLEIA for 2,4-dinitrotoluene. Anal. Methods, **2010**, *2*, 824–830.

Lindner P., Molz R., Yacoub-George E., Wolf H., Rapid chemiluminescence biosensing of microcystin-LR. *Anal. Chim. Acta* **2009**, *636*, 218-223.

Long F., He M., Zhu A. N., Shi H. C., Protable optical immunosensor for highly sensitive detection of microcystin-LR in water samples. *Biosens. Bioelectron.* **2009**, *24*, 2346-2351.

Lummerstorfer T., Hoffmann H., IR reflection spectra of monolayer films sandwiched between two high refractive index materials. *Langmuir* **2004**, *20*, 6542-6545.

Lummerstorfer T., Kattner J., Hoffmann H., Monolayers at solid–solid interfaces probed with infrared spectroscopy. *Anal. Bioanal. Chem.* **2007**, *388*, 55-64.

Luo Y., Guo W., Ngo H. H., Nghiem L. D., Hai F. I., Zhang J., Liang S. Wang X. C., A review on the occurence of micropollutants in the aquatic environment and their fate and removal during wastewater treatment. *Sci. Total Environ.* **2014**, 619-641.

Luppa P. B., Sokoll L. J., Chan D. W., Immunosensors – Principles and applications to clinical chemistry. *Clin. Chim. Acta* **2001**, *314*, 1-26.

Lux G., Langer A., Pschenitza M., Karsunke X., Strasser R., Niessner R., Knopp D., Rant U., Detection of the carcinogenic water pollutant benzo[a]pyrene with an electro-switchable biosurface. *Anal. Chem.* **2015**, *87*, 4538–4545.

March C., Manclús J. J., Jiménez Y., Arnau A., Montoya A., A piezoelectric immunosensor for the determination of pesticide residues and metabolites in fruit juices. *Talanta* **2009**, *78*, 827-833.

Marquette C. A., Blum L. J., Chemiluminescent enzyme immunoassays: a review of bioanalytical applications. *Bioanalysis* **2009**, *1*, 1259-1269.

Matschulat D., Deng A. P., Niessner R., Knopp D., Development of a highly sensitive

monoclonal antibody based ELISA for detection of benzo[a]pyrene in potable water. *Analyst* **2005**, *130*, 1078-1086.

McEneff G., Barron L., Brian K., Brett P., Quinn B., A year-long study of the spatial occurrence and relative distribution of pharmaceutical residues in sewage effluent, receiving marine waters and marine bivalves. *Sci. Total Environ.* **2014**, *476-477*, 317-326.

Mehinto A. C., Hill E. M., Tyler C. R., Uptake and biological effects of environmentally relevant concentrations of the nonsteroidal anti-inflammatory pharmaceutical diclofenac in Rainbow Trout (*Oncorhynchus mykiss*). *Environ. Sci. Technol.* **2010**, *44*, 2176-2182.

Mehne J., Markovic G., Pröll F., Schweizer N., Zorn S., Schreiber F., Gauglitz G., Characterisation of morphology of self-assembled PEG monolayers: a comparison of mixed and pure coatings optimised for biosensor applications. *Anal. Bioanal. Chem.* **2008**, *391*, 1783-1791.

Memmert U., Peither A., Burri R., Weber K., Schmidt T., Sumpter J. P., Hartmann A., Diclofenac: New data on chronic toxicity and bioconcentration in fish. *Environ. Toxicol. Chem.* **2013**, *32*, 442-452.

Mercier D., Boujday S., Annabi C., Villanneau R., Pradier C.-M., Proust A., Bifunctional polyoxometalates for planar gold surface nanostructuration and protein immobilization. *J. Phys. Chem. C* **2012**, *116*, 13217-13224.

Meulenberg E. P., Peelen G. O. H., Lukkien E., Koopal K., Immunochemical detection methods for bioactive pollutants. *Int. J. Environ. Anal. Chem.* **2005**, *85*, 861-870.

Mirasoli M., Guardigli M., Michelini E., Roda A., Recent advancements in chemical luminescence-based lab-on-chip and microfluidic platforms for bioanalysis. *J. Pharm. Biomed. Anal.* **2014**, *87*, 36-52.

Mohammed M.-I., Desmulliez M. P. Y., Lab-on-a-chip based immunosensor principles and technologies for the detection of cardiac biomarkers: a review. *Lab Chip* **2011**, *11*, 569-595.

Morais S., Tortajada-Genaro L. A., Arnandis-Chover T., Puchades R., Maquierira A.,

Multiplexed microimmunoassay on a digital versatile disk. *Anal. Chem.* **2009**, *81*, 5646-5654.

Nagaraj V. J., Jacobs M., Vattipalli K. M., Annam V. P., Prasad S., Nanochannel-based electrochemical sensors for the detection of pharmaceutical contaminants in water. *Environ. Sci.: Processes Impacts* **2014**, *16*, 135-140.

Ng A., Chinnappan R., Eissa S., Liu H., Tlili C., Zourob M., Selection, characterization, and biosensing application of high affinity congener-specific microcystin-targeting aptamers. *Environ. Sci. Technol.* **2012**, *46*, 10697-10703.

Niessner R. (ed.), Höll: Wasser - Nutzung im Kreislauf: Hygiene, Analyse und Bewertung, 9th edition, Walter de Gruyter Verlag, Berlin/New York, **2010**.

Oaks J. L., Gilbert M., Virani M. Z., Watson R. T., Meteyer C. U., Rideout B. A., Shivaprasad H. L., Ahmed S., Chaudry M. J. I., Arshad M., Mahmood S., Ali A., Khan A. A., Diclofenac residues as a cause of vulture population decline in Pakistan. *Nature* **2004**, *427*, 630-633.

Oliferova L., Statkus M., Tsysin G., Zolotov Y., On-line solid-phase extraction and high performance liquid chromatography determination of polycyclic aromatic hydrocarbons in water using polytetrafluoroethylene capillary. *Talanta* **2007**, *72*, 1386-1391.

Osorio V., Imbert-Bouchard M., Zonja B., Abad J.-L., Pérez S., Barceló D., Simultaneous determination of diclofenac, its human metabolites and microbial nitration/nitrosation transformation products in wastewaters by liquid chromatography/quadrupole-linear ion trap mass spectrometry. *J. Chromatogr. A* **2014**, *1347*, 63-71.

Oswald S., Karsunke X. Y. Z., Dietrich R., Märtlbauer E., Niessner R., Knopp D., Automated regenerable microarray-based immunoassay for rapid parallel quantification of mycotoxins in cereals. *Anal. Bioanal. Chem.* **2013**, *405*, 6405-6414.

Pandey M. K., Mishra K. K., Khanna S. K., Das M., Detection of polycyclic aromatic hydrocarbons in commonly consumed edible oils and their likely intake in the Indian population. *J. Am. Oil Chem. Soc.* **2004**, *81*, 1130-1136.

Paerl H. W., Otten T. G., Harmful cyanobacterial blooms: Causes, consequences and

controls. *Microb. Ecol.* **2013**, *65*, 995-1010.

Petrie B., Barden R., Kasprzyk-Hordern B., A review on emerging contaminants in wastewaters and the environment: Current knowledge, understudied areas and recommendations for future monitoring. *Water Res.* **2015**, *72*, 3-27.

Piazza R., Gambaro A., Argiriadis E., Vecchiato M., Zambon S., Cescon P., Barbante C., Development of a method for simultaneous analysis of PCDDs, PCDFs, PCBs, PBDEs, PCNs and PAHs in Antarctic air. *Anal. Bioanal. Chem.* **2013**, *405*, 917-931.

Piehler J., Brecht A., Valiokas R., Liedberg B., Gauglitz G., A high-density poly(ethylene glycol) polymer brush for immobilization on glass-type surfaces. *Biosens. Bioelectron.* **2000**, *15*, 473-481.

Prieto-Simón B., Campàs M., Immunochemical tools for mycotoxin detection in food. *Monatsh. Chem.* **2009**, *140*, 915-920.

Pschenitza M., Hackenberg R., Niessner R., Knopp D., Analysis of benzo[a]pyrene in vegetable oils using molecularly imprinted solid phase extraction (MISPE) coupled with enzyme-linked immunosorbent assay (ELISA). *Sensors* **2014**, *14*, 9720-9737.

Qian Y., Posch T., Schmidt T. C., Sorption of polycyclic aromatic hydrocarbons (PAHs) on glass surfaces. *Chemosphere* **2011**, *82*, 859-865.

Ramin S., Weller M. G., Extremely sensitive and selective antibodies against the explosive 2,4,6-trinitrotoluene by rational design of a structurally optimized hapten. *J. Mol. Recognit.* **2012**, *25*, 89-97.

Rau S., Hilbig U., Gauglitz G., Label-free optical biosensor for detection and quantification of the non-steroidal anti-inflammatory drug diclofenac in milk without any sample pretreatment. *Anal. Bioanal. Chem.* **2014**, *406*, 3377-3386.

Ravindra K., Sokhi R., Van Grieken R., Atmospheric polycyclic aromatic hydrocarbons: Source attribution, emission factors and regulation. *Atmos. Environ.* **2008 a**, *42*, 2895-2921.

Ravindra K., Wauters E., Van Grieken R., Variation in particulate PAHs levels and their relation with the transboundary movement of the air masses. *Sci. Total Environ.* **2008 b**,

396, 100-110.

Reemtsma T., Weiss S., Mueller J., Petrovic M., González S., Barcelo D., Ventura F., Knepper T. P., Polar pollutants entry into the water cycle by municipal wastewater: a European perspective. *Environ. Sci. Technol.* **2006**, *40*, 5451-5458.

Renneberg R., Bioanalytik für Einsteiger: Diabetes, Drogen und DNA. Spektrum Akademischer Verlag, Heidelberg, **2009.**

Rodahl M., Höök F., Krozer A., Brzezinski P., Kasemo B., Quartz crystal microbalance setup for frequency and Q-factor measurements in gaseous and liquid environments. *Rev. Sci. Instrum.* **1995**, *66*, 3924-3930.

Sachera F. L., Frank T., Brauch H.-L., Blankenhorn I., Pharmaceuticals in groundwaters: Analytical methods and results of a monitoring program in Baden-Wuerttemberg, Germany. *J. Chromatogr. A* **2001**, *938*, 199-210.

Saini M., Taggart M. A., Knopp D., Upreti S., Swarup D., Das A., Gupta P. K., Niessner R., Prakash V., Mateo R., Cuthbert R. J., Detecting diclofenac in livestock carcasses in India with an ELISA: a tool to prevent widespread vulture poisoning. *Environ. Pollut.* **2012**, *160*, 11-16.

Salmain M., Ghasemi M., Boujday S., Pradier C.-M., Elaboration of a reusable immunosensor for the detection of staphylococcal enterotoxin A (SEA) in milk with a quartz crystal microbalance. *Sens. Actuators B* **2012**, *173*, 148-156.

Sauceda-Friebe J. C., Karsunke X. Y. Z., Vazac S., Biselli S., Niessner R., Knopp D., Regenerable immuno-biochip for screening ochratoxin A in green coffee extract using an automated microarray chip reader with chemiluminescence detection. *Anal. Chim. Acta* **2011**, *689*, 234-242.

Sauerbrey, G., Verwendung von Schwingquarzen zur Waegung duenner Schichten und zur Mikrowaegung. *Zeitschrift für Physik* **1959**, *155*, 206-222.

Schwaiger J., Ferling H., Mallow U., Wintermayr H., Negele R. D., Toxic effects of the non-steroidal anti-inflammatory drug diclofenac part I: histopathological alterations and

bioaccumulation in rainbow trout. *Aquat. Toxicol.* **2004**, *68*, 141-150.

Schwarzenbach R. P., Escher B., Fenner K., Hofstetter T. B., Johnson C. A., von Gunten U., Wehrli B., The challenge of micropollutants in aquatic systems. *Science* **2006**, *313*, 1072-1077.

Shankarana D. R., Gobi K. V., Miura, N., Recent advancements in surface plasmon resonance immunosensors for detection of small molecules of biomedical, food and environmental interest. *Sens. Actuators B* **2007**, *121*, 158-177.

Sharma A. K., Saini M., Sing S. D., Prakash V., Das A., Bharathi Dasan R., Pandey S., Bohara D., Galligan T. H., Green R. E., Knopp D., Cuthbert R. J., Diclofenac is toxic to the Steppe Eagle Aquila nipalensis: widening the diversity of raptors threatened by NSAID misuse in South Asia. *Bird Conserv. Intern.* **2014**, *24*, 282-286.

Shi H.-C., Song B.-D., Long F., Zhou X.-H., He M., LV Q., Yang H.-Y., Automated online optical biosensing system for continuous real-time determination of microcystin-LR with high sensitivity and specificity: early warning for cyanotoxin risk in drinking water sources. *Environ. Sci. Technol.* **2013**, *47*, 4434-4441.

Shiddiky M. J. A., Kithva P. H., Kozak D., Trau M., An electrochemical immunosensor to minimize the nonspecific adsorption and to improve sensitivity of protein assays in human serum. *Biosens. Bioelectron.* **2012**, *38*, 132-137.

Silva C. P., Lima D. L. D., Schneider R. J., Otero M., Esteves V. I., Development of ELISA methodologies for the direct determination of 17β-estradiol and 17α-ethinylestradiol in complex aqueous matrices. *J. Environ. Manage.* **2013**, *124*, 121-127.

Smith J., Sammons D., Robertson S., Biagini R., Snawder J., Measurement of multiple drugs in urine, water, and on surfaces using fluorescence covalent microbead immunosorbent assay. *Toxicol. Mech. Method*. **2010**, *20*, 587-593.

Spadavecchia J., Boujday S., Landlousi J., Pradier C.-M., nPEG-TiO2 Nanoparticles: A facile route to elaborate nanostructured surfaces for biological applications. *ACS Appl. Mater. Interfaces* **2011**, *3*, 2637-2642.

Su X., Chew F. T., Li S. F. Y., Design and application of piezoelectric quartz crystal-based immunoassay. *Anal. Sci.* **2000**, *16*, 107-114.

Tanamua S., Powell C. J., Penn D. R., Calculations of electron inelastic mean free paths. V. Data for 14 organic compounds over the 50-2000 eV range. *Surf. Interface Anal.* **1994**, *21*, 165-176.

Ternes T. A., Occurenece of drugs in German sewage. *Water Res.* **1998**, *32*, 3245-3260.

Tian R., Seitz O., Li M., Hu W., Chabal Y. J., Gao J., Infrared characterization of interfacial Si−O bond formation on silanized flat SiO 2 /Si Surfaces. *Langmuir* **2010**, *26*, 4563-4566.

Tort N., Salvador J.-P., Marco M.-P., Multiplexed immunoassay to detect anabolic androgenic steroids in human serum. *Anal. Bioanal. Chem.* **2012**, *403*, 1361-1371.

Triebskorn R., Casper H., Heyd A., Eikemper R., Köhler H.-R., Schwaiger J., Toxic effects of the non-steroidal anti-inflammatory drug diclofenac Part II. Cytological effects in liver, kidney, gills and intestine of rainbow trout (Oncorhynchus mykiss). *Aquat. Toxicol.* **2004**, 151-166.

Tschmelak J., Proll G., Riedt J., Kaiser J., Kraemmer P., Bárzaga L., Wilkinson J. S., Hua P.,Hole J. P., Nudd R., Jackson M., Abuknesha R., Barceló D., Rodriguez-Mozaz S., López de Alda M. J., Sacher F., Stienh J., Slobodník J., Oswald P., Kozmenko H., Korenková E., Tóthová L., Krascsenits Z., Gauglitz G., Automated Water Analyser Computer Supported System (AWACSS) Part I: Project objectives, basic technology, immunoassay development, software design and networking. *Biosens. Bioelectron.* **2005 a**, 1499-1508.

Tschmelak J., Proll G., Riedt J., Kaiser J., Kraemmer P., Bárzaga L., Wilkinson J. S., Hua P.,Hole J. P., Nudd R., Jackson M., Abuknesha R., Barceló D., Rodriguez-Mozaz S., López de Alda M. J., Sacher F., Stienh J., Slobodník J., Oswald P., Kozmenko H., Korenková E., Tóthová L., Krascsenits Z., Gauglitz G., Automated Water Analyser Computer Supported System (AWACSS) Part II: Intelligent, remote-controlled, cost-effective, on-line, water-monitoring measurement system. *Biosens. Bioelectron.* **2005 b**, 1509-1519.

Tschmelak J., Kumpf M., Proll G., Gauglitz G., Biosensor for seven sulphonamides in drinking,

ground, and fresh water with different matrices. *Anal. Lett.* **2004**, *37*, 1701-1718.

Tschmelak J., Proll G., Gauglitz G., Improved strategy for biosensor-based monitoring of water bodies with diverse organic carbon levels. *Biosens. Bioelectron*. **2005 c**, *21*, 979-983.

Tsukruk V. V., Luzinov I., Julthongpiput D., Sticky molecular surfaces: epoxysilane self-assembled monolayers. *Langmuir* **1999**, *15*, 3029-3032.

Ulman A., Formation and structure of self-assembled monolayers. *Chem. Rev.* **1996**, *96*, 1533-1554.

Umweltbundesamt, Polyzyklische Aromatische Kohlenwasserstoffe – Umweltschädlich! Giftig! Vermeidbar? , **2012**, https://www.umweltbundesamt.de/sites/default/files/medien/publikation/long/4372.pdf (14.04.2015).

Vo-Dinh T., Fetzer J., Campiglia A. D., Monitoring and characterization of polyaromatic compounds in the environment, *Talanta* **1998**, *47*, 943-969.

Wang X., Niessner R., Knopp D., Magnetic bead-based colorimetric immunoassay for aflatoxin B1 using gold nanoparticles. *Sens. Actuators B* **2014**, *14*, 1-15.

Weller M., Zeck A., Eikenberg A., Nagata S., Ueno Y., Niessner R., Development of a Direct competitive microcystin immunoassay of broad specificity. *Anal. Sci.* **2001**, *17*, 1445-1448.

Weller M., Immunoassays and biosensors for the detection of cyanobacterial toxins in water. *Sensors* **2013**, *13*, 15085-15112.

Weller M., Schuetz A. J., Winklmair M., Niessner R., Highly parallel affinity sensor for the detection of environmental contaminants in water. *Anal. Chim. Acta* **1999**, *393*, 29-41.

Wolter A., Niessner R., Seidel M., Preparation and characterization of functional poly(ethylene glycol) surfaces for the use of antibody microarrays. *Anal. Chem.* **2007**, *79*, 4529-4537.

Wutz K., Niessner R., Seidel M., Simultaneous determination of four different antibiotic

residues in honey by chemiluminescence multianalyte chip immunoassays. *Microchim. Acta* **2010**, *173*, 1-9.

Xu T., Gong Xu Q., Li H., Wang J., Li Q. X., Shelver W. L., Li J., Strip-based immunoassay for the simultaneous detection of the neonicotinoid insecticides imidacloprid and thiamethoxam in agricultural products. *Talanta* **2012**, *101*, 85-90.

Xu Z.-L., Wang Q., Lei H.-T., Eremin S. A., Shen Y.-D., Wang H., Beier R. C., Yang J.-Y., Maksimova K. A., Sun Y.-M., A simple, rapid and high-throughput fluorescence polarization immunoassay for simultaneous detection of organophosphorus pesticides in vegetable and environmental water samples. *Anal. Chim. Acta* **2011**, *708*, 123-129.

Yim H., Kent M. S., Tallant D. R., Garcia M. J., Majewski J., Hygrothermal degradation of (3-glycidoxypropyl)trimethoxysilane films studied by neutron and X-ray reflectivity and attenuated total reflection infrared spectroscopy. *Langmuir* **2005**, *21*, 4382-4392.

Zeck A., Eikenberg A., Weller M. G., Niessner R., Highly sensitive immunoassay based on a monoclonal antibody specific for [4-arginine]microcystins. *Anal. Chim. Acta* **2001 a**, *441*, 1-13.

Zeck A., Weller M. G., Bursill D., Niessner R., Generic microcystin immunoassay based on monoclonal antibodies against ADDA. *Analyst* **2001 b**, *126*, 2002-2007.

Zeck A., Weller M. G., Niessner R., Multidimensional biochemical detection of microcystins in liquid chromatography. *Anal. Chem.* **2001 c**, *73*, 5509-5517.